REPORT DOCUMENTATION PAGE

Form Approved
OMB No. 0704-0188

PLEASE DO NOT RETURN YOUR FORM TO THE ABOVE ADDRESS.

1. REPORT DATE *(DD-MM-YYYY)*	2. REPORT TYPE	3. DATES COVERED *(From - To)*
10/Aug/2001	THESIS	

4. TITLE AND SUBTITLE
NUCLEAR RADIATION-INDUCED DIMENSIONAL CHANGES IN BOROSILICATE GLASS SUBSTRATES

5a. CONTRACT NUMBER

5b. GRANT NUMBER

5c. PROGRAM ELEMENT NUMBER

6. AUTHOR(S)
CAPT ALLRED CLARK L

5d. PROJECT NUMBER

5e. TASK NUMBER

5f. WORK UNIT NUMBER

7. PERFORMING ORGANIZATION NAME(S) AND ADDRESS(ES)
MASSACHUSETTS INSTITUTE OF TECHNOLOGY

8. PERFORMING ORGANIZATION REPORT NUMBER
CI01-188

9. SPONSORING/MONITORING AGENCY NAME(S) AND ADDRESS(ES)
THE DEPARTMENT OF THE AIR FORCE
AFIT/CIA, BLDG 125
2950 P STREET
WPAFB OH 45433

10. SPONSOR/MONITOR'S ACRONYM(S)

11. SPONSOR/MONITOR'S REPORT NUMBER(S)

12. DISTRIBUTION/AVAILABILITY STATEMENT
Unlimited distribution
In Accordance With AFI 35-205/AFIT Sup 1

13. SUPPLEMENTARY NOTES

14. ABSTRACT

15. SUBJECT TERMS

16. SECURITY CLASSIFICATION OF:			17. LIMITATION OF ABSTRACT	18. NUMBER OF PAGES	19a. NAME OF RESPONSIBLE PERSON
a. REPORT	b. ABSTRACT	c. THIS PAGE		104	19b. TELEPHONE NUMBER *(Include area code)*

Nuclear Radiation-Induced Dimensional Changes in Borosilicate Glass Substrates Used for MEMS Oscillators

by

Clark L. Allred

B.S. Physics
Rochester Institute of Technology, 1996

SUBMITTED TO THE DEPARTMENT OF MATERIALS SCIENCE AND ENGINEERING IN PARTIAL FULFILLMENT OF THE REQUIREMENTS FOR THE DEGREE OF

MASTER OF SCIENCE IN MATERIALS SCIENCE AND ENGINEERING
AT THE
MASSACHUSETTS INSTITUTE OF TECHNOLOGY

September 2000

Signature of Author _____
Department of Materials Science and Engineering
August 4, 2000

Certified by _____
Jeffrey T. Borenstein
Charles Stark Draper Laboratory
Thesis Supervisor

Certified by _____
Linn W. Hobbs
Professor of Materials Science
Thesis Advisor

Accepted by _____
Carl V. Thompson
Stavros Salapatas Professor of Materials Science and Engineering
Chair, Departmental Committee on Graduate Students

Nuclear Radiation-Induced Dimensional Changes in Borosilicate Glass Substrates Used for MEMS Oscillators

by

Clark L. Allred

Submitted to the Department of Materials Science and Engineering of the Massachusetts Institute of Technology on August 4, 2000 in partial fulfillment of the requirements for the Degree of Master of Science in Materials Science and Engineering

ABSTRACT

A study was made of radiation-induced dimensional changes in Pyrex® and Hoya SD-2® glasses. These glasses are used as substrates for MEMS devices employing silicon oscillating beams, and changes in substrate dimension can compromise device performance. Silicon MEMS strain gauges mounted on glass substrates were exposed to gamma doses up to 385 Mrad. The device-substrate differential strain thus measured corresponds to an expansion in the glass following a linear trend with dose of about 5 (± 4) $\times 10^{-15}$ /rad and 4.5 (± 0.2) $\times 10^{-14}$ /rad for Pyrex and Hoya SD-2, respectively. Separate glass samples were irradiated with a neutron fluence composed primarily of thermal neutrons, and a floatation technique was employed to measure the resulting density changes in the glasses alone. Transport of Ions in Matter (TRIM) calculations were performed to relate fast (~1MeV) neutron atomic displacement damage to that from boron thermal neutron capture events, and measured density changes in the glass samples were thus proportionally attributed to thermal and fast neutron fluences. Maximum neutron fluences received by glass samples were estimated at 4×10^{16} n/cm^2 thermal and 6×10^{14} n/cm^2 fast. The glasses irradiated with thermal neutrons were found to exhibit linear compaction at a rate of -2.8×10^{-20} per n/cm^2 for Pyrex and -1.0×10^{-21} per n/cm^2 for Hoya SD-2. For fast neutron fluence, strain rate (per n/cm^2) was also linear: -6.1×10^{-21} for Pyrex and -7.9×10^{-22} for Hoya SD-2. The gamma irradiation strain gauge results cannot be explained by the radiation-induced compaction previously reported for Pyrex, and are thought to result from either changes in glass radiation response caused by the anodic bonding process used to make the MEMS strain gauges or from radiation-assisted creep of the strain gauge anchors. The neutron irradiation results for Pyrex show good agreement with those of previous studies.

Technical Supervisor: Dr. Jeffrey Borenstein
Title: Principal Member of the Technical Staff

Thesis Advisor: Professor Linn W. Hobbs
Title: Professor of Materials Science

Nuclear Radiation-Induced Dimensional Changes in Borosilicate Glass Substrates Used for MEMS Oscillators

by

Clark L. Allred
Captain, United States Air Force

Master of Science Thesis
Materials Science and Engineering
Massachusetts Institute of Technology
2000
104 pages

ABSTRACT

A study was made of radiation-induced dimensional changes in Pyrex® and Hoya SD-2® glasses. These glasses are used as substrates for MEMS devices employing silicon oscillating beams, and changes in substrate dimension can compromise device performance. Silicon MEMS strain gauges mounted on glass substrates were exposed to gamma doses up to 385 Mrad. The device-substrate differential strain thus measured corresponds to an expansion in the glass following a linear trend with dose of about 5 (± 4) $\times 10^{-15}$ /rad and 4.5 (± 0.2) $\times 10^{-14}$ /rad for Pyrex and Hoya SD-2, respectively. Separate glass samples were irradiated with a neutron fluence composed primarily of thermal neutrons, and a floatation technique was employed to measure the resulting density changes in the glasses alone. Transport of Ions in Matter (TRIM) calculations were performed to relate fast (~1MeV) neutron atomic displacement damage to that from boron thermal neutron capture events, and measured density changes in the glass samples were thus proportionally attributed to thermal and fast neutron fluences. Maximum neutron fluences received by glass samples were estimated at 4×10^{16} n/cm^2 thermal and 6×10^{14} n/cm^2 fast. The glasses irradiated with thermal neutrons were found to exhibit linear compaction at a rate of -2.8×10^{-20} per n/cm^2 for Pyrex and -1.0×10^{-21} per n/cm^2 for Hoya SD-2. For fast neutron fluence, strain rate (per n/cm^2) was also linear: -6.1×10^{-21} for Pyrex and -7.9×10^{-22} for Hoya SD-2.

Bibliography

J.B. Bates et al., Journal of Chemical Physics, **61**, 1974, p. 4163

P.R. Bevington, *Data Reduction and Error Analysis in the Physical Sciences*, McGraw-Hill Book Company, New York, 1969, p.313

Y.-M. Chiang, D.P. Birnie III, and W.D. Kingery, *Physical Ceramics*, John Wiley & Sons, Inc., 1997, p. 89

S.L. Conners, "Effects of Gamma Radiation on the Structure and Properties of Borosilicate Glasses", M.S. Thesis, 1992, Alfred University, Alfred, New York

Corning Incorporated, Corning, NY, 14831

A. Cozma and B. Puers, "Characterization of the electrostatic bonding of silicon and Pyrex glass," Journal of Micromechanical Microengineering, **5** (1995), p. 98-102

J.H. Crawford, Jr., "Radiation Damage in Solids: A Survey," Ceramic Bulletin, **44** (12), 1965

H.A. El-Batal, "Effect of Thermal Neutrons on Thermal Expansion of some Ternary Borate Glasses," Nuclear Instruments and Methods in Physics Research, **B88**, 1994, p.411-417

Evans East, 104 Windsor Center, Suite 101, East Windsor, New Jersey, 08520

F.M. Ezz-Eldin and H.A. El-Batal, "Radiation Effects on Thermal Expansion of Some Ternary Alkali-Silicate Glasses," Journal of Non-Crystalline Solids, **152**, 1993, p. 195-200

Far West Technology, Inc., 330 D South Kellog, Goleta, California 93117

P.L. Higby, E.J. Friebele, C.M. Shaw, and M. Rajaram, "Radiation Effects on the Physical Properties of Low-Expansion-Coefficient Glasses and Ceramics," Journal of the American Ceramic Society, **71** (9), 1988, p. 796-802

L.W. Hobbs, "Network topology in aperiodic networks," Journal of Non-Crystalline Solids, **192 & 193**, 1995, p. 79-91

Hoya Corporation, 2-7-5 Naka-Ochiai, Shinjuku-ku, Tokyo 161-8525 Japan

J.H. Hubbell and S.M. Seltzer, "Tables of X-Ray Mass Energy-Absorption Coefficients," NIST Physics Laboratory online database, URL: http://www.physics.nist.gov/PhysRefData/XrayMassCoef/intro.html [cited 12 July 2000]

S. Klaumünzer, L. Changlin, S. Löffler, M. Rammensee, and G. Schumacher, "Plastic Flow of Vitreous Silica and Pyrex During Bombardment with Fast Heavy Ions," Nuclear Instruments and Methods in Physics Research, **B39** (189), p. 665-669

S. Klaumünzer, "Ion-Beam-Induced Plastic Deformation: A Universal Phenomenon in Glasses," Radiation Effects and Defects in Solids, 1989, vol. 110, p. 79-83

M.A. Knight, "Glass Densities by Settling Method," The Journal of the American Ceramic Society, **28** (11), Nov 1945, p. 297-302

Chr. Lehmann, *Interaction of Radiation with Solids and Elementary Defect Production*, North-Holland, 1977, p. 88, 90

C.S. Marians and L.W. Hobbs, Journal of Non-Crystalline Solids, **119**, 1990, p. 269

V. McLane, C.L. Dunford, P.F. Rose, *Neutron Cross Sections, Vol 2, Neutron Cross Section Curves*, National Nuclear Data Center, Brookhaven National Laboratory, Academic Press,Inc., 1981

T.B. Metcalfe, *Radiation Spectra of Radionuclides*, Noyes Data Corporation, Park Ridge, New Jersey, 1976

N.R. Moody, S.L. Robinson, J.P. Lucas, J. Handrock, and R.Q. Hwang, "Effects of Radiation and Hydrogen on the Fracture Resistance of Borosilicate Glasses," Journal of the American Ceramic Society, **78** (1), 1995, p. 114-120

N.E. Moyer and R.C. Buschert, "X-Ray Lattice Parameter Studies of Electron-Irradiated Silicon," Radiation Effects in Semiconductors, Plenum, NY, 1968, p. 444-451
S.F. Mughabghab, M. Divadeenam, N.E. Holden, *Neutron Cross Sections, Vol 1, Neutron Resonance Parameters and Thermal Cross Sections*, National Nuclear Data Center, Brookhaven National Laboratory, , Academic Press, Inc., 1981
P. Nitzsche, K. Lange, B. Schmidt, S. Grigull, and U. Kreissig, "Ion Drift Processes in Pyrex-Type Alkali-Borosilicate Glass during Anodic Bonding," Journal of the Electrochemical Society, **145** (5), May 1998, p. 1755-1762
J. Paymal, "Quelques Effets des Réactions (n, alpha) dans les Verres," Verres et Réfractaires, No 5, Sept-Oct 1961, p. 259-269
ibid, No 6, Nov-Dec, 1961, p. 341-351
ibid, No 1, Jan-Feb 1962, p.20-30
ibid, No 2, Mar-Apr 1962, p.100-113
W. Primak and R. Kampwirth, "The Radiation Compaction of Vitreous Silica," Journal of Applied Physics, **39** (12), 1968, p. 5651-58
W. Primak, "Fast-Neutron-Induced Changes in Quartz and Vitreous Silica," Physical Review, 110 (6), June 15, 1958, p. 1240-1254
S. Sato , H. Furuya, K. Asakura, and K. Ohta, "Radiation Effect of Simulated Waste Glass Irradiated with Ion, Electron, and γ-Ray," Nuclear Instruments and Methods in Physics Research, **B1** (1984), p. 534-537
Schott Corporation, 3 Odell Plaza, Yonkers, NY, 10701
J.E. Shelby, "Effect of radiation on the physical properties of borosilicate glasses," Journal of Applied Physics, **51** (5), May 1980, p. 2561-65
J.E. Shelby, "Radiation effects in hydrogen-impregnated vitreous silica," Journal of Applied Physics, **50** (5), May 1979, p.3702-3706
J. Kenneth Shultis and Richard E. Faw, *Radiation Shielding*, Prentice-Hall, 1996, p. 56
E. Snoeks and A. Polman, "Densification, anisotropic deformation, and plastic flow of SiO_2 during MeV heavy ion irradiation," Applied Physics Letters, **65** (19), November 1994, p. 2487-2489
C.A. Volkert and A. Polman, "Radiation-Enhanced Plastic Flow of Covalent Materials During Ion Irradiation," Materials Research Society Symposium Proceedings, **235**, 1992, p. 3-14
W.J. Weber, R.C. Ewing, C.A. Angell, G.W. Arnold, A.N. Cormack, J.M. Delaye, D.L. Griscom, L.W. Hobbs, A. Navrotsky, D.L. Price, A.M. Stoneham, M.C. Weinberg, "Radiation Effects in Glasses Used for Immobilization of High-Level Waste and Plutonium Disposition," Journal of Materials Research, **12** (8), August 1997, p. 1946-1975
W.H. Zachariasen, "The Atomic Arrangement in Glass," Journal of the American Chemical Society, **54**, 1932, p. 3841
R. Zallen, *The Physics of Amorphous Solids*, John Wiley & Sons, Inc., 1983, p. 6
W.A. Zdaniewski, T.E. Easler, and R.C. Bradt, "Gamma Radiation Effects of the Strength of a Borosilicate Glass," Journal of the American Ceramic Society, **66** (5), May 1983, p. 311-313
J.F. Ziegler, IBM-Research, 28-0, Yorktown, NY, 10598, e-mail: Ziegler@Watson.IBM.Com
J.F. Ziegler and J.M. Manoyan, "The Stopping of Ions in Compounds," Nuclear Instruments and Methods in Physics Research, **B35** (1988) p. 215-228

Nuclear Radiation-Induced Dimensional Changes in Borosilicate Glass Substrates Used for MEMS Oscillators

by

Clark L. Allred
Captain, United States Air Force

Master of Science Thesis
Materials Science and Engineering
Massachusetts Institute of Technology
2000
104 pages

ABSTRACT

A study was made of radiation-induced dimensional changes in Pyrex® and Hoya SD-2® glasses. These glasses are used as substrates for MEMS devices employing silicon oscillating beams, and changes in substrate dimension can compromise device performance. Silicon MEMS strain gauges mounted on glass substrates were exposed to gamma doses up to 385 Mrad. The device-substrate differential strain thus measured corresponds to an expansion in the glass following a linear trend with dose of about 5 (± 4) $\times 10^{-15}$ /rad and 4.5 (± 0.2) $\times 10^{-14}$ /rad for Pyrex and Hoya SD-2, respectively. Separate glass samples were irradiated with a neutron fluence composed primarily of thermal neutrons, and a floatation technique was employed to measure the resulting density changes in the glasses alone. Transport of Ions in Matter (TRIM) calculations were performed to relate fast (~1MeV) neutron atomic displacement damage to that from boron thermal neutron capture events, and measured density changes in the glass samples were thus proportionally attributed to thermal and fast neutron fluences. Maximum neutron fluences received by glass samples were estimated at 4×10^{16} n/cm^2 thermal and 6×10^{14} n/cm^2 fast. The glasses irradiated with thermal neutrons were found to exhibit linear compaction at a rate of -2.8×10^{-20} per n/cm^2 for Pyrex and -1.0×10^{-21} per n/cm^2 for Hoya SD-2. For fast neutron fluence, strain rate (per n/cm^2) was also linear: -6.1×10^{-21} for Pyrex and -7.9×10^{-22} for Hoya SD-2.

Bibliography

J.B. Bates et al., Journal of Chemical Physics, **61**, 1974, p. 4163

P.R. Bevington, *Data Reduction and Error Analysis in the Physical Sciences*, McGraw-Hill Book Company, New York, 1969, p.313

Y.-M. Chiang, D.P. Birnie III, and W.D. Kingery, *Physical Ceramics*, John Wiley & Sons, Inc., 1997, p. 89

S.L. Conners, "Effects of Gamma Radiation on the Structure and Properties of Borosilicate Glasses", M.S. Thesis, 1992, Alfred University, Alfred, New York

Corning Incorporated, Corning, NY, 14831

A. Cozma and B. Puers, "Characterization of the electrostatic bonding of silicon and Pyrex glass," Journal of Micromechanical Microengineering, **5** (1995), p. 98-102

J.H. Crawford, Jr., "Radiation Damage in Solids: A Survey," Ceramic Bulletin, **44** (12), 1965

H.A. El-Batal, "Effect of Thermal Neutrons on Thermal Expansion of some Ternary Borate Glasses," Nuclear Instruments and Methods in Physics Research, **B88**, 1994, p.411-417

Evans East, 104 Windsor Center, Suite 101, East Windsor, New Jersey, 08520

F.M. Ezz-Eldin and H.A. El-Batal, "Radiation Effects on Thermal Expansion of Some Ternary Alkali-Silicate Glasses," Journal of Non-Crystalline Solids, **152**, 1993, p. 195-200

Far West Technology, Inc., 330 D South Kellog, Goleta, California 93117

P.L. Higby, E.J. Friebele, C.M. Shaw, and M. Rajaram, "Radiation Effects on the Physical Properties of Low-Expansion-Coefficient Glasses and Ceramics," Journal of the American Ceramic Society, **71** (9), 1988, p. 796-802

L.W. Hobbs, "Network topology in aperiodic networks," Journal of Non-Crystalline Solids, **192 & 193**, 1995, p. 79-91

Hoya Corporation, 2-7-5 Naka-Ochiai, Shinjuku-ku, Tokyo 161-8525 Japan

J.H. Hubbell and S.M. Seltzer, "Tables of X-Ray Mass Energy-Absorption Coefficients," NIST Physics Laboratory online database, URL: http://www.physics.nist.gov/PhysRefData/XrayMassCoef/intro.html [cited 12 July 2000]

S. Klaumünzer, L. Changlin, S. Löffler, M. Rammensee, and G. Schumacher, "Plastic Flow of Vitreous Silica and Pyrex During Bombardment with Fast Heavy Ions," Nuclear Instruments and Methods in Physics Research, **B39** (189), p. 665-669

S. Klaumünzer, "Ion-Beam-Induced Plastic Deformation: A Universal Phenomenon in Glasses," Radiation Effects and Defects in Solids, 1989, vol. 110, p. 79-83

M.A. Knight, "Glass Densities by Settling Method," The Journal of the American Ceramic Society, **28** (11), Nov 1945, p. 297-302

Chr. Lehmann, *Interaction of Radiation with Solids and Elementary Defect Production*, North-Holland, 1977, p. 88, 90

C.S. Marians and L.W. Hobbs, Journal of Non-Crystalline Solids, **119**, 1990, p. 269

V. McLane, C.L. Dunford, P.F. Rose, *Neutron Cross Sections, Vol 2, Neutron Cross Section Curves*, National Nuclear Data Center, Brookhaven National Laboratory, Academic Press,Inc., 1981

T.B. Metcalfe, *Radiation Spectra of Radionuclides*, Noyes Data Corporation, Park Ridge, New Jersey, 1976

N.R. Moody, S.L. Robinson, J.P. Lucas, J. Handrock, and R.Q. Hwang, "Effects of Radiation and Hydrogen on the Fracture Resistance of Borosilicate Glasses," Journal of the American Ceramic Society, **78** (1), 1995, p. 114-120

N.E. Moyer and R.C. Buschert, "X-Ray Lattice Parameter Studies of Electron-Irradiated Silicon," Radiation Effects in Semiconductors, Plenum, NY, 1968, p. 444-451
S.F. Mughabghab, M. Divadeenam, N.E. Holden, *Neutron Cross Sections, Vol 1, Neutron Resonance Parameters and Thermal Cross Sections*, National Nuclear Data Center, Brookhaven National Laboratory, , Academic Press, Inc., 1981
P. Nitzsche, K. Lange, B. Schmidt, S. Grigull, and U. Kreissig, "Ion Drift Processes in Pyrex-Type Alkali-Borosilicate Glass during Anodic Bonding," Journal of the Electrochemical Society, **145** (5), May 1998, p. 1755-1762
J. Paymal, "Quelques Effets des Réactions (n, alpha) dans les Verres," Verres et Réfractaires, No 5, Sept-Oct 1961, p. 259-269
ibid, No 6, Nov-Dec, 1961, p. 341-351
ibid, No 1, Jan-Feb 1962, p.20-30
ibid, No 2, Mar-Apr 1962, p.100-113
W. Primak and R. Kampwirth, "The Radiation Compaction of Vitreous Silica," Journal of Applied Physics, **39** (12), 1968, p. 5651-58
W. Primak, "Fast-Neutron-Induced Changes in Quartz and Vitreous Silica," Physical Review, 110 (6), June 15, 1958, p. 1240-1254
S. Sato , H. Furuya, K. Asakura, and K. Ohta, "Radiation Effect of Simulated Waste Glass Irradiated with Ion, Electron, and γ-Ray," Nuclear Instruments and Methods in Physics Research, **B1** (1984), p. 534-537
Schott Corporation, 3 Odell Plaza, Yonkers, NY, 10701
J.E. Shelby, "Effect of radiation on the physical properties of borosilicate glasses," Journal of Applied Physics, **51** (5), May 1980, p. 2561-65
J.E. Shelby, "Radiation effects in hydrogen-impregnated vitreous silica," Journal of Applied Physics, **50** (5), May 1979, p.3702-3706
J. Kenneth Shultis and Richard E. Faw, *Radiation Shielding*, Prentice-Hall, 1996, p. 56
E. Snoeks and A. Polman, "Densification, anisotropic deformation, and plastic flow of SiO_2 during MeV heavy ion irradiation," Applied Physics Letters, **65** (19), November 1994, p. 2487-2489
C.A. Volkert and A. Polman, "Radiation-Enhanced Plastic Flow of Covalent Materials During Ion Irradiation," Materials Research Society Symposium Proceedings, **235**, 1992, p. 3-14
W.J. Weber, R.C. Ewing, C.A. Angell, G.W. Arnold, A.N. Cormack, J.M. Delaye, D.L. Griscom, L.W. Hobbs, A. Navrotsky, D.L. Price, A.M. Stoneham, M.C. Weinberg, "Radiation Effects in Glasses Used for Immobilization of High-Level Waste and Plutonium Disposition," Journal of Materials Research, **12** (8), August 1997, p. 1946-1975
W.H. Zachariasen, "The Atomic Arrangement in Glass," Journal of the American Chemical Society, **54**, 1932, p. 3841
R. Zallen, *The Physics of Amorphous Solids*, John Wiley & Sons, Inc., 1983, p. 6
W.A. Zdaniewski, T.E. Easler, and R.C. Bradt, "Gamma Radiation Effects of the Strength of a Borosilicate Glass," Journal of the American Ceramic Society, **66** (5), May 1983, p. 311-313
J.F. Ziegler, IBM-Research, 28-0, Yorktown, NY, 10598, e-mail: Ziegler@Watson.IBM.Com
J.F. Ziegler and J.M. Manoyan, "The Stopping of Ions in Compounds," Nuclear Instruments and Methods in Physics Research, **B35** (1988) p. 215-228

Nuclear Radiation-Induced Dimensional Changes in Borosilicate Glass Substrates Used for MEMS Oscillators

by

Clark L. Allred

Submitted to the Department of Materials Science and Engineering of the Massachusetts Institute of Technology on August 4, 2000 in partial fulfillment of the requirements for the Degree of Master of Science in Materials Science and Engineering

ABSTRACT

A study was made of radiation-induced dimensional changes in Pyrex® and Hoya SD-2® glasses. These glasses are used as substrates for MEMS devices employing silicon oscillating beams, and changes in substrate dimension can compromise device performance. Silicon MEMS strain gauges mounted on glass substrates were exposed to gamma doses up to 385 Mrad. The device-substrate differential strain thus measured corresponds to an expansion in the glass following a linear trend with dose of about 5 (± 4) $\times 10^{-15}$ /rad and 4.5 (± 0.2) $\times 10^{-14}$ /rad for Pyrex and Hoya SD-2, respectively. Separate glass samples were irradiated with a neutron fluence composed primarily of thermal neutrons, and a floatation technique was employed to measure the resulting density changes in the glasses alone. Transport of Ions in Matter (TRIM) calculations were performed to relate fast (~1MeV) neutron atomic displacement damage to that from boron thermal neutron capture events, and measured density changes in the glass samples were thus proportionally attributed to thermal and fast neutron fluences. Maximum neutron fluences received by glass samples were estimated at 4×10^{16} n/cm^2 thermal and 6×10^{14} n/cm^2 fast. The glasses irradiated with thermal neutrons were found to exhibit linear compaction at a rate of -2.8×10^{-20} per n/cm^2 for Pyrex and -1.0×10^{-21} per n/cm^2 for Hoya SD-2. For fast neutron fluence, strain rate (per n/cm^2) was also linear: -6.1×10^{-21} for Pyrex and -7.9×10^{-22} for Hoya SD-2. The gamma irradiation strain gauge results cannot be explained by the radiation-induced compaction previously reported for Pyrex, and are thought to result from either changes in glass radiation response caused by the anodic bonding process used to make the MEMS strain gauges or from radiation-assisted creep of the strain gauge anchors. The neutron irradiation results for Pyrex show good agreement with those of previous studies.

Technical Supervisor: Dr. Jeffrey Borenstein
Title: Principal Member of the Technical Staff

Thesis Advisor: Professor Linn W. Hobbs
Title: Professor of Materials Science

ACKNOWLEDGEMENTS

August 4, 2000

Thanks go to the people in the United States Air Force who decided to give me an opportunity for schooling. Upon my return to a "real" Air Force job, I hope my job performance will prove them right in supporting higher education for Air Force people. Thanks also go to the education office folks (John Sweeney, George Schmidt, Loretta Mitrano, and Michael Villani) for running the Draper Fellow program, without which I wouldn't be here at all.

This thesis is, of course, the result of efforts by many people not included on the title page. Jeff Borenstein and Linn Hobbs deserve credit for guiding me during the whole process. It was they who came up with the idea of using the pointer beam strain gauges in the radiation experiments. Prof. Hobbs furnished me with his analysis of the existing literature, and suggested the TRIM calculations. Dr. Borenstein arranged for the fabrication of the pointer beams and signed purchase requests in a very liberal fashion. I particularly appreciate Jeff's decision to hire me as a Draper Fellow!

Thanks are due to many others. Edward McCormack and his machine shop crew fabricated parts for my experiments. Ken Kaiser consulted (and furnished equipment) for temperature control issues. Dick Caruso quickly processed purchase requests. Mert Prince, Connie Cardoso, and Brenda Hugh helped me fabricate samples, often at the last minute. George Mitchell and Kevin Hoxie helped with making my pointer beam hot plate. Greg Kirkos consulted on mechanics issue. John Kaupinnen and Ralph Shaver helped get me set up in a lab for the sink/float work. Lance Niles provided me device schematics. The irradiations, dosimetry, and fluence estimates were done by Gordon Kohse at the MIT reactor, with Mary Montesalvo and David McKee supporting the irradiations at UMass Lowell. I appreciate the criticism (mostly constructive) and suggestions of the "radiation meeting" regulars and guests: Kaplesh Kumar, Ralph Hopkins, Nicole Gerrish, Andrew Meulenberg, and William Kelleher.

My wife, Sophie, has accepted constraints on her career choices that result from my participation in the Draper Fellow program and service in the Air Force. She has also supported me both emotionally and logistically during the more demanding phases of classes, qualifying exams, and research. I owe a very great deal to her advice, tolerance, and optimism, as well as to the example of discipline and courage she set for me while she earned her own graduate degree.

This thesis was prepared at The Charles Stark Draper Laboratory, Inc., under IR&D project number 1002.

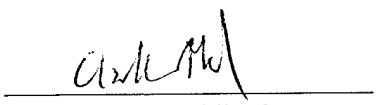

Clark L. Allred

THE VIEWS EXPRESSED IN THIS ARTICLE ARE THOSE OF THE AUTHOR AND DO NOT REFLECT THE OFFICIAL POLICY OR POSITION OF THE UNITED STATES, DEPARTMENT OF DEFENSE, OR THE U.S. GOVERNMENT

ASSIGNMENT

Draper Laboratory Report Number T-1383

In consideration for the research opportunity and permission to prepare my thesis by and at The Charles Stark Draper Laboratory, Inc., I hereby assign my copyright of the thesis to The Charles Stark Draper Laboratory, Inc., Cambridge, Massachusetts.

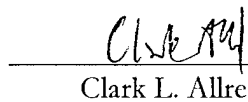

Clark L. Allred August 4, 2000

CONTENTS

TABLE OF CONTENTS (continued)

LIST OF FIGURES

LIST OF TABLES

1 INTRODUCTION AND OVERVIEW

1.1 Scope of thesis

The goal of the research reported in this thesis is to understand dimensional changes that a borosilicate glass substrate can undergo when exposed to radiation. In order for glass substrate-mounted MEMS devices (such as silicon oscillating beams) to behave predictably when used in a radiation environment, one must understand the effect of that environment on material properties such as density, coefficient of thermal expansion, and elasticity for the materials involved in the system. This study treats only density (and hence, length) changes which can set up differential strains between an oscillator and its substrate, affecting the stress-dependent frequency of beam oscillation.

Forms of radiation that are considered here include 1 MeV neutrons (referred to below simply as "fast" neutrons), thermal neutrons, and 1 MeV gamma rays. Real radiation environments (*e.g.*, outer space, nuclear reactors) will, of course, have a broader energy spectrum for neutrons and gamma rays. Typical nuclear reactor environments include neutron energy spectra with centroid energies not far from 1 MeV. For ^{235}U, the average energy of emitted neutrons is about 1.68 MeV.[1.1] Shielding between fissioning nuclei and the target can modify this average energy. For precise radiation damage calculations, geometry and nature of surrounding materials, angle of incidence, and incident energy spectrum for the radiation must be known. It is nevertheless useful to model a simpler situation (monoenergetic neutrons and gamma rays) to obtain order-of-magnitude predictions of radiation-induced dimensional changes. These predictions can then be scaled by taking into account the amount of energy (relative to 1 MeV) deposited in a material by radiation particles.

Two glasses chosen principally for their close thermal expansion coefficient match with silicon, Pyrex®[1.2] and Hoya SD-2®[1.3], were studied. The compaction rates of Hoya SD-2 and Pyrex under fast neutron bombardment were established for the first time. The compaction rate of Hoya SD-2 with thermal neutron fluence was measured for the first time, and the larger compaction rate of Pyrex with thermal neutron fluence was confirmed. Evidence for increased radiation-resistance in anodically bonded Pyrex and/or radiation-induced creep at the anodic bond interface was found with the novel application of a MEMS pointer beam strain gauge in a gamma irradiation experiment. It was shown that the differential strain induced by gamma radiation in MEMS devices anodically bonded to glass wafers is much less in magnitude than would be expected by considering the strains that would have been caused by similarly irradiating the raw glass and silicon.

The approach taken here to the problem can be summarized in four steps: 1) a survey of the literature, 2) Monte-Carlo simulations of thermal and fast neutron collisions cascades, 3) gamma ray irradiations of both glasses using MEMS strain gauges to measure expansion/compaction, and 4) neutron irradiation of both glasses followed by a floatation technique ("sink/float") used to measure density changes.

1.2 Literature survey

Compaction of Pyrex with gamma irradiation has been studied by Shelby[1.4], Conners[1.5], Sato[1.6], and Zdaniewski.[1.7] Of these studies, Shelby's covers the greatest dose range. Since Conners' and Sato's finding support Shelby's findings, Shelby's work is used here as a reference for our findings. Shelby's data reveal an initially linear trend of compaction with dose of -1.4×10^{-13} strain per rad at doses up to $\sim 2 \times 10^{9}$ rad. The effect begins to saturate at higher doses.

The effects of thermal neutron irradiation in Pyrex were studied by Paymal.[1.8-1.11] He employed a floatation technique called "sink/float" (the same technique used later by Shelby) to measure small irradiation-induced density differences in several glass types. He observed a compaction rate with dose that at lower thermal neutron fluences ($< 1 \times 10^{17}$ n/cm^2) was approximately linear, with a slope of -2×10^{-20} strain per n/cm^2.

No studies involving fast neutron-induced strain are known for either glass. Primak,[1.12] however, did report the initial compaction rate of vitreous silica with fast neutron exposure to be -5.6×10^{-22} strain per n/cm^2. Shelby's[1.4] results for gamma irradiation of vitreous silica show that SiO_2 compacts an order of magnitude less quickly with dose than does Pyrex.

1.3 Monte-Carlo simulations

One mechanism for the causing dimensional changes in glass is the collision of a fast neutron with atoms in the glass network structure. The atoms so struck can be forced from their network sites with substantial kinetic energy, in turn leading to other atomic displacements and subsequent network rearrangements. This sequence of atomic displacements is referred to as a collision cascade, and the atom directly displaced by an incident fast neutron is called the primary knock-on atom (PKA).

Collision cascades can also be caused by nuclear reactions that yield energetic particles. The reaction of interest in this thesis is the absorption of a thermal neutron by ^{10}B, an isotope 20% naturally abundant in boron and present in both Pyrex and Hoya SD-2. Upon absorbing a thermal neutron, the ^{10}B nucleus splits into a lithium nucleus with a kinetic energy of ~0.9 MeV, and an alpha particle with kinetic energy of ~1.6 MeV. Each of these products can then each initiate a collision cascade.

Both thermal and fast neutron collision cascades involve similar PKA energies, and the majority of displaced atoms will be displaced by ions created from secondary collisions. Therefore, it seems reasonable to assume that the network rearrangement processes involved in both types of collision cascades will be similar, and that the dimensional change in a glass can be related directly to the number of atoms displaced in these collision cascades. To relate fast neutron-induced compaction to thermal neutron-induced compaction, we need an idea of how many displacements occur in each type of cascade.

Monte-Carlo simulations using TRIM (version 2000.38), a computer program widely used in the ion-implantation industry, were carried out for both thermal and fast neutron collision cascades in both Pyrex and Hoya SD-2. Inputs to TRIM included glass composition and the energy distribution of PKAs. Table 1.1 summarizes the results for glass wafers 780 μm thick.

	Pyrex	Hoya SD-2
Displacements per incident fast neutron	22	24
Displacements per incident thermal neutron	100	31

Table 1.1 TRIM calculation results

1.4 Gamma irradiation of MEMS pointer beam strain gauges

A MEMS pointer beam strain gauge, developed at Charles Stark Draper Laboratory (CSDL) to monitor differential strain in the silicon pointer beam and the glass substrate to which it is anodically bonded, was employed in a gamma irradiation experiment. The gauges (referred to hereafter as "pointer beams") consist of a beam suspended by and perpendicular to two beams which are slightly offset where they join the main beam. These two beams are

in turn suspended from silicon columns that are anchored to the glass. The two support beams are offset so that, when the anchor points are moved further apart or closer together, the main beam is caused to rotate slightly. Teeth at the end of the main beams serve as reference marks for beam movement.

The gamma radiation was expected to cause dimensional changes in the glass, but not in the silicon.[1.13] Any pointer beam displacement, it was assumed, should correspond directly to strain in the glass substrate. The slopes of linear fits to the data obtained are shown in Table 1.2. The uncertainty indicated in the slope is due to two alternative gamma source geometries of which we were unaware at the time of the experiment. Reduced χ^2 values for the fits were close to 0.7 for Pyrex and 0.5 Hoya SD-2, irrespective of source geometry. This indicates that while the slope on the fitted lines is small, it is of statistical significance.

	Strain/rad
Pyrex	$5.24\ (\pm\ 3.78) \times 10^{-15}$
Hoya SD-2	$4.50\ (\pm\ 0.16) \times 10^{-14}$

Table 1.2 Pointer beam gamma irradiation results

Shelby's results for Pyrex provide a point of reference for these results. The pointer beams results indicate a strain/rad slope 26 times smaller than Shelby reports. We propose two possible explanations for this discrepancy: 1) the anodic bonding process has significantly altered the radiation sensitivity of the Pyrex, and/or 2) radiation-induced creep occurred at the anodic bond interface, allowing the pointer beam anchor points to slip as the glass wafer expanded. These results are of great significance to the operation of MEMS

devices, since they indicate a smaller net radiation response for anodically bonded MEMS devices than was predicted based upon the responses of the individual materials.

1.5 Neutron irradiation of glass samples

Five samples of each glass were irradiated with neutrons in MIT's reactor and then used in a sink/float experiment to determine irradiation-induced density changes. Exposure times ranged from 30 s to 6000 s in a neutron flux comprised of 1×10^{11} n/cm^2/s fast neutrons and 6.7×10^{12} n/cm^2/s thermal neutrons. Linear fits were made to the data with reduced χ^2 values of 1.01 for Pyrex and 1.58 for Hoya SD-2. Compaction was apportioned between thermal and fast neutron collision cascades using the displacement numbers calculated using TRIM, with the results indicating that less than 1% of the compaction was due to fast neutrons. Using the TRIM displacement numbers, however, one may make a prediction of the response of the glasses to both thermal and fast neutrons. The strain/fluence relationships thus obtained are listed in Table 1.3, along with values relating strain to displacements per atom (dpa).

	Strain/n/cm^2 thermal	Strain/n/cm^2 fast (1 MeV)	Strain/dpa
Pyrex	-2.77×10^{-20}	-6.07×10^{-21}	-1.49
Hoya SD-2	-1.01×10^{-21}	-7.89×10^{-22}	-0.19

Table 1.3 Neutron irradiation-induced strains

The Hoya SD-2 is seen to undergo almost an order of magnitude less compaction than the Pyrex at a given fast neutron fluence. The response of Hoya SD-2 to thermal

neutrons is even smaller in proportion to that of the Pyrex; this can be partly attributed to the smaller boron concentration in Hoya SD-2.

The values for fast neutron-induced compaction in Pyrex and Hoya SD-2 are based upon the assumption of equivalent damage mechanisms for thermal and fast neutron collision cascades. We can test this assumption by comparing our results with those of the studies cited in section 1.2 and check for consistency. The strain/fluence relationship for Pyrex is in good agreement with Paymal's result. There are no data available for direct comparison with the fast neutron results, but comparison of the fast neutron-induced strain in Pyrex with Primak's results for vitreous silica demonstrates that the Pyrex compacts by about an order of magnitude more than does vitreous silica at a given dose. Shelby showed that this same relative response in radiation compaction holds for gamma irradiation, providing (albeit indirect) support for validity of the assumption that thermal and fast neutron damage can be compared through the relative number of displacements in their collision cascades.

[THIS PAGE INTENTIONALLY LEFT BLANK]

2 BACKGROUND

2.1 A physical perspective on radiation damage in glass

2.1.1 Structure of glass

Glass is a metastable solid that can be prepared from the melt by rapid cooling. "Rapid" is a relative term: in this case, it means rapid enough that the material in question does not have enough time to undergo the kinetic processes involved in crystallization. For a simple crystal structure, such as a close-packed pure metal, this is very rapid indeed. A metallic glass can be prepared by quenching at a rate of about 10^6 °C/s.[2.1] In the case of an oxide such as silica, the atomic organization required to maintain local charge neutrality makes crystallization a slower process, and vitreous silica can be prepared from the melt simply by cooling to room temperature at a cooling rate of about ~10^{-4} °C/s.

A model for the structure of covalently bonded glasses was proposed by Zachariasen[2.2]. Now known as the continuous-random-network model, it describes an oxide glass as being a randomly arranged network of polyhedra that are the basic oxide units. Polyhedra are shown in Figure 2.1 for SiO_2 and B_2O_3, two key components of borosilicate glass.

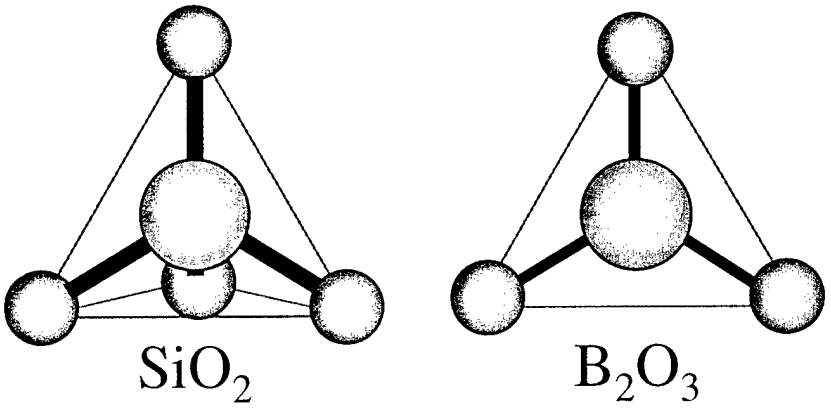

Figure 2.1 Silica tetrahedron and borate triangle used in random continuous network

These polyhedra can be joined at the corners (by means of a bridging oxygen) to form a network. In silica, the O-Si-O bond angles are rigidly fixed due to the four-fold coordination of the silicon atoms, but the oxygen atoms are only bonded to two silicon atoms. A greater flexibility in the A-O-A bond angles results. The basic polyhedra can therefore link into a network composed of rings containing varying numbers of member polyhedra. A two-dimensional representation of such a network is shown in Figure 2.2.

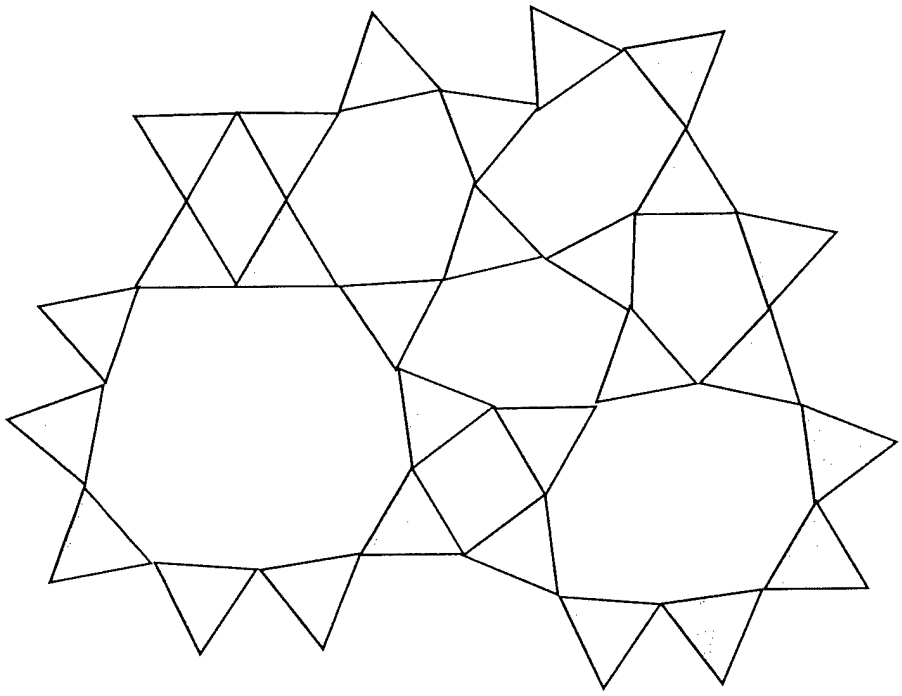

Figure 2.2 Continuous random network

The addition of alkali atoms such as sodium to a borosilicate glass alters its chemical structure and physical properties. Alkali atoms act as network *modifiers* in silica, reducing connectivity in the network[2,3] by providing local charge neutrality for non-bridging oxygen

(an oxygen on a silica tetrahedron that is left dangling). When Al^{3+} and B^{3+} are present, the addition of alkali atoms can have the opposite effect of increasing connectivity in the network by providing charge neutrality for four-coordinated Al and B atoms (B^{3+} and Na^{1+} effectively substituting for a Si^{4+}). Physical properties that change with the addition of alkali atoms include increased fracture toughness[2.4] and lowered thermal expansivity[2.5]. With increasing alkali content (as the B/Na or Al/Na ratio falls below one), connectivity is no longer increased and Na^{1+} returns to its role as a network modifier. One can therefore expect the radiation response of a material to depend not only on Al and B concentration, but also on the ratio of these concentrations to that of alkali atoms.

2.1.2 Radiation-induced alteration of glass structure

Radiation has several mechanisms for affecting a material's structure. Incident gamma rays can interact with electrons in the material by Compton scattering. Electrons so scattered can then ballistically collide, elastically and inelastically, with atoms in the material. Both gamma rays and scattered electrons can ionize atoms, as well as give rise to a phenomenon called radiolysis, by which atomic displacement and bond rearrangement results from electronic exitations[2.6]. Fast neutrons can ballistically collide with atoms, thus displacing them and causing related electronic defects. Thermal neutrons can provoke nuclear reactions (see discussion in Chapter 3) which produce energetic ions which can both electronically and ballistically impart energy to a material. A summary of radiation interactions in materials is shown in Figure 2.3[2.7]. One can imagine these effects in the context of the random continuous network model. Ruptured bonds, whether caused by radiolysis or collisional removal of atoms from a ring, lead to atomic rearrangements and ring size changes. These ring-size changes, it is thought, lead to density changes.

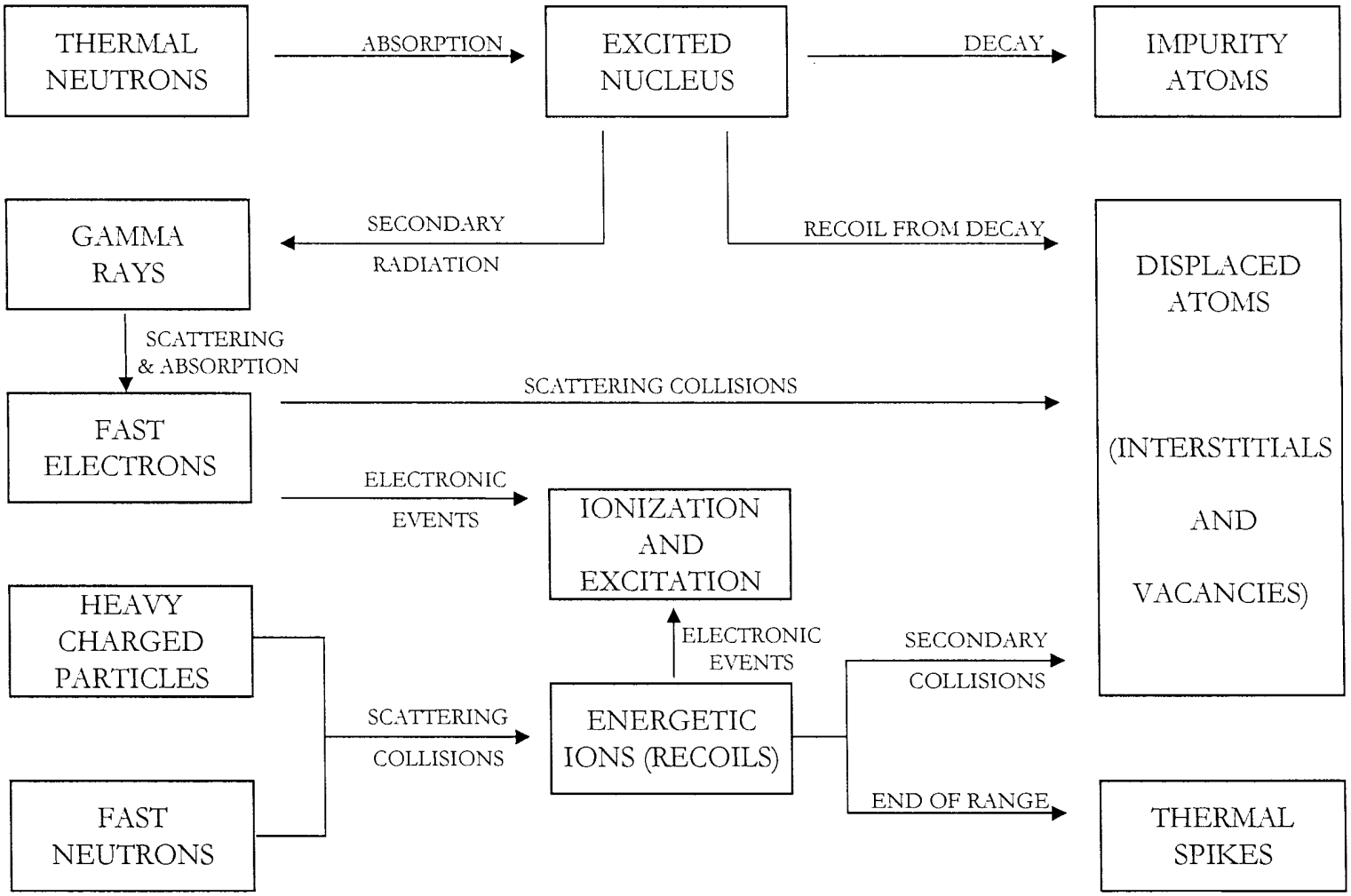

Figure 2.3 Radiation damage processes in solids

Characterizations in the literature of the relationship between ring size (a parameter that radiation may change in a material) and material density vary. A review of radiation effects in glasses[2.6] cites topological modeling studies[2.8] in claiming that "larger rings are responsible for the higher density of the denser silica polymorphs because they can fold back on themselves, and the densification of vitreous silica by irradiation could arise from opening up of 6-membered rings to larger rings in regional boundaries." On the other hand, Ezz-Eldin[2.9] speculates that "damage by irradiating species can cause compaction of SiO_2 [silicate glasses] by breaking bonds between tetrahedra, allowing the formation of different ring configurations such that the average ring size is smaller, thus leading to denser structure." He then sites evidence[2.10] that "smaller rings do form." A more recent study[2.11] states that "whereas it might be supposed that the presence of large rings implies lower density, in fact the opposite is true... As the polymorphs become denser,... the ring size increases and the distribution of ring size widens." The author goes on to cite the example of crystalline forms of SiO_2, and indeed finds that average ring size trades monotonically with density.

Not all silicate glasses compact under irradiation. Paymal[2.12-2.15] reports that while Pyrex compacts with thermal neutron exposure, a borosilicate glass with PbO additions clearly expands. The ring model says nothing about whether or not a glass will expand or compact upon radiation -- it only relates ring size to density. Shelby[2.16] wrote that "it becomes quite obvious that the densification mechanism will require considerable study before the details of the process become fully understood... it is quite possible that the results reported here result from competing processes which involve both positive and negative dilatations." Paymal[2.12-2.15] proposed just such a theory for his neutron damage observations in which the energy deposited by fast lithium and helium ions in a glass is mostly concentrated in a small end-of-trajectory region, causing a thermal spike. The high-

temperature melt is rapidly cooled by the glass matrix, "freezing in" an expanded region. The glass immediately around this expanded region is forced to compact. The relative volume of these expanded/compacted regions determines the macroscopic density change. While being a nice conceptual model, this theory still does not address the fundamental issue of directly relating composition to radiation response.

There is evidence that boron concentration as well as sodium concentration (relative to that of boron) affect radiation response. Shelby[2.16] writes that "it is... quite possible that the effects reported here are strongly related to the two-phase nature of most borosilicate glasses... the glass consists of a continuous phase with a composition very near that of vitreous silica... the second phase... contains most of the alkali and boron atoms." This alkali borate phase is suspected of being more susceptible to radiation compaction than vitreous silica, with the overall material's compaction depending on the relative volume of this second phase, as well as the coordination of the boron within that phase. As discussed above, this boron coordination will depend on the alkali content of the phase.

2.2 Gamma radiation damage

Shelby[2.16], Conners[2.17], Sato[2.18], and Zdaniewsky[2.19] report measurements of gamma radiation-induced density changes in Pyrex. All four employed a variant of the sink/float method described in Chapter 5. Their results are summarized in Figures 2.4 and 2.5.

Good agreement is found between results of Shelby, Conners, and Sato. The mean difference of 29 % in strain between the results of Shelby and Conners at high doses may be due to differences in glass compositions and/or processing history that may have existed between glass samples. Zdaniewsky's results are for doses of 10^2, 10^4, 10^6, and 10^8 rad. The compaction he measured occurs much more quickly with dose than in the other studies.

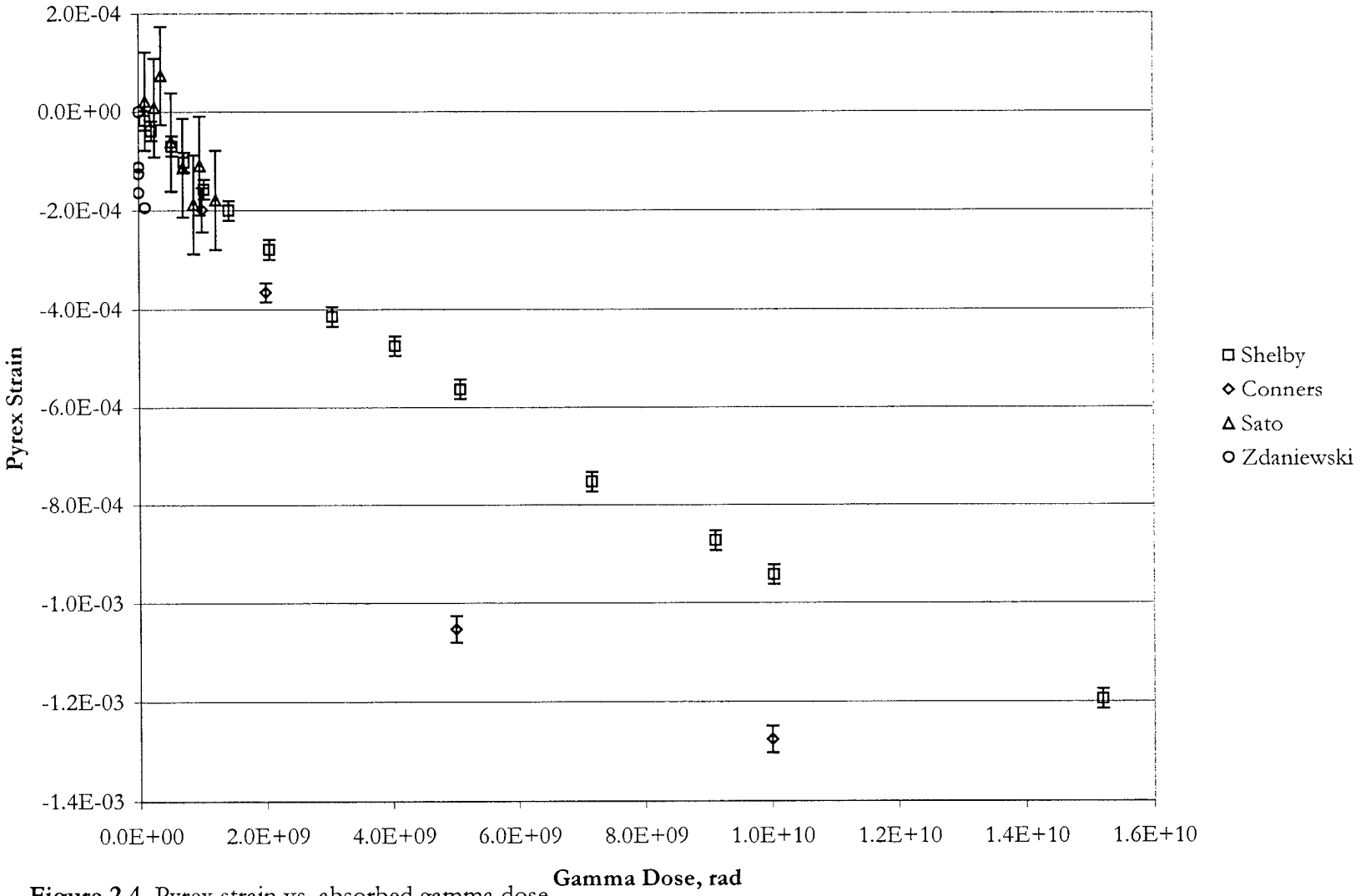

Figure 2.4 Pyrex strain vs. absorbed gamma dose

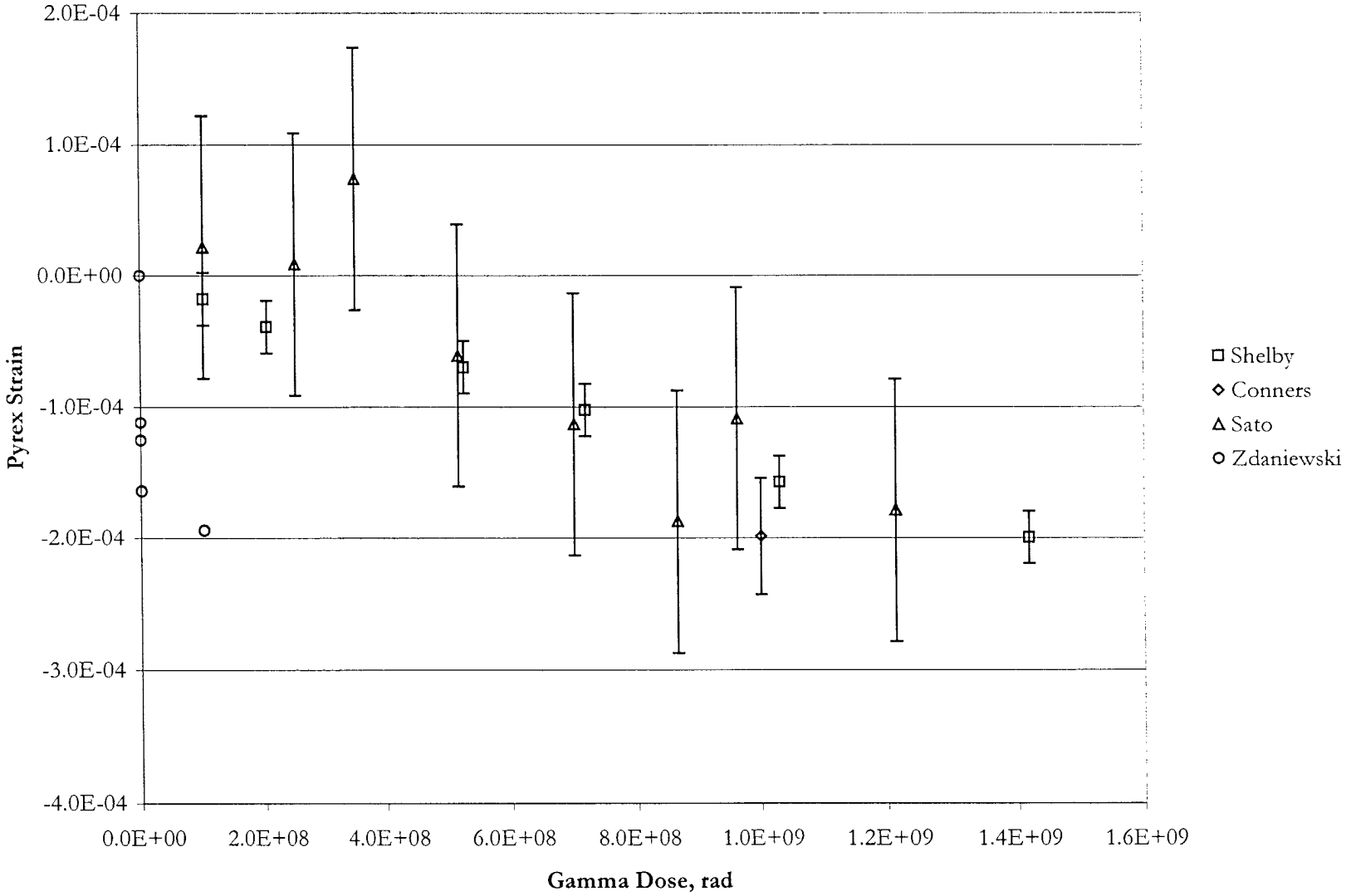

Figure 2.5 Pyrex strain vs. absorbed gamma dose, low dose regime

Unfortunately, while citing Shelby's study, he does not comment on the possible reasons for the discrepancy in densification trend.

Shelby's study compared the compaction of several borosilicate glasses to that of vitreous silica. He concluded that with increased boron content, increased compaction occurred. A comparison of strain in Pyrex to that in SiO_2 is shown in Figure 2.6. While having the same slope on this log-log plot, the curve for Pyrex shows an order of magnitude more strain at a given gamma dose. It should be noted that the slope of compaction vs. gamma dose (on a log-log plot) for silica varies by as much as a factor of three in studies by Shelby[2.16], Higby[2.20], and Primak[2.21]. Higby attributes this variation to minor differences in impurities or in the degree of phase separation. It is not surprising, given these differences in silica results, to see the relatively minor variations in the behavior of different samples of Pyrex shown in Figure 2.4.

2.3 Neutron radiation damage

Paymal[2.12-2.15] carried out an extensive study on the effects of thermal neutron damage (the mechanisms for which are discussed in Chapter 3) on the properties of borosilicate glass. His model of competing and interdependent regions of compaction and swelling, mentioned above, was fitted to his data for compaction in Pyrex. The resulting relationship is:

$$\Delta\rho = 420 - 510e^{-3.28\times10^{-18}\,D} + 90e^{-0.55\times10^{-18}\,D} \qquad (2.1)$$

In Equation 2.1, $\Delta\rho$ is the change in density in units of 10^{-4} g/cm^3 and D is the thermal neutron fluence in n/cm^2. A conversion of this relationship for strain in Pyrex is shown in Figure 2.7.

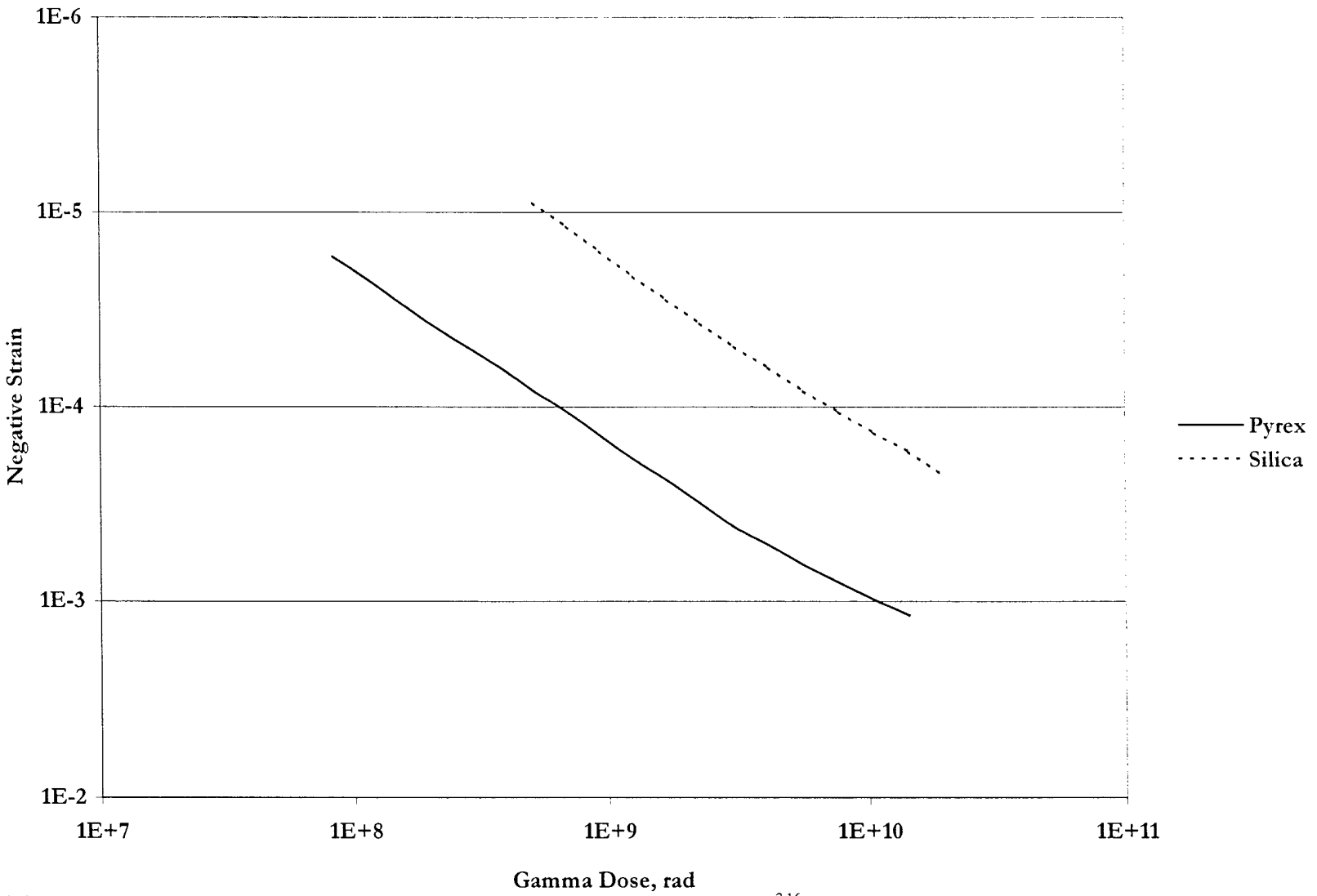

Figure 2.6 Strain in Pyrex and silica vs. absorbed gamma dose (from Shelby[2.16])

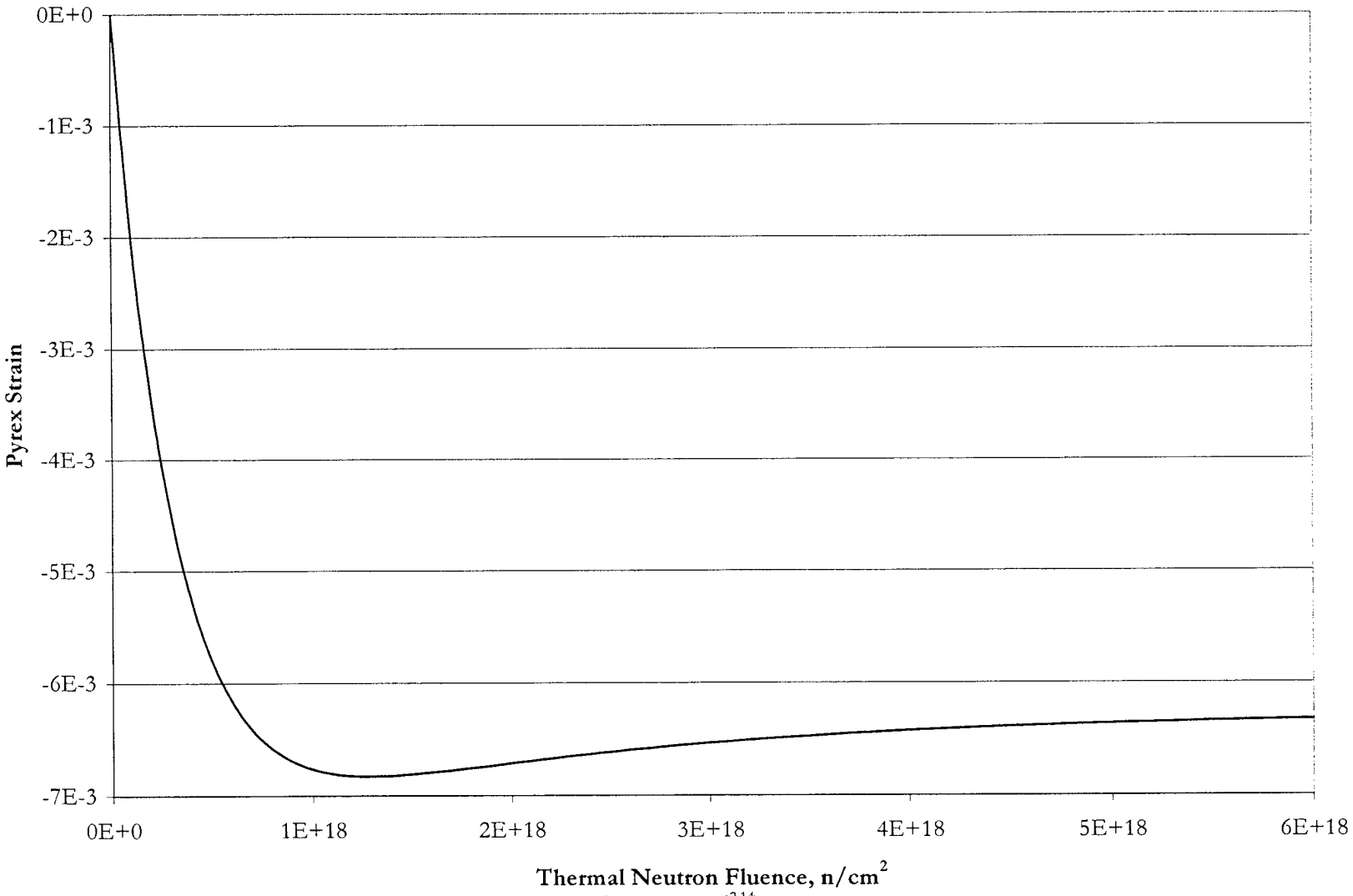

Figure 2.7 Thermal neutron-induced strain in Pyrex (from Paymal[2.14])

Paymal attributes the saturation of strain evident in Figure 2.7 to overlap of the end-of-trajectory thermal spike regions. A similar saturation is displayed by fast neutron damage in vitreous silica in results from Primak[2.22]. These results are shown in Figure 2.8. The shape of this curve agrees with that of the Paymal thermal neutron curve for Pyrex, but does not reveal the relative sensitivity of the two materials to atomic displacements. While vitreous silica will be unaffected by thermal neutrons (it contains no boron), it is nevertheless possible to compare the thermal neutron damage in Pyrex to the fast neutron damage in vitreous silica by means of Monte Carlo simulations (discussed in detail in Chapter 3). These simulations predict 22 atomic displacements in Pyrex per incident fast neutron and 100 displacements for each incident thermal neutron. Results will be slightly different for vitreous silica, but with similar densities for Pyrex and silica the difference will be minimal. If we consider the low-dose linear region in Figure 2.7 and 2.8 at the strain of -1×10^{-3}, and multiply the corresponding fluences by the above displacement numbers for incident fast and thermal neutrons, we obtain that to achieve this strain $\sim 4 \times 10^{18}$ atomic displacements are required in Pyrex, while $\sim 4 \times 10^{19}$ atomic displacements are required in vitreous silica. This order-of-magnitude difference in radiation response is the same as observed for gamma radiation in Figure 2.6.

2.4 Glass compositions

Table 2.1 shows compositions for the glasses under consideration here. The Evans East[2.23] company was employed to perform X-ray photoelectron spectroscopy (XPS) analysis on Pyrex®[2.24], Borofloat®[2.25] (a Pyrex equivalent), and Hoya SD-2®[2.26] glass wafer samples. The Pyrex and Borofloat samples were found to be compositionally similar to within the signal-to-noise limitations of the measurement, and so have been averaged together. The

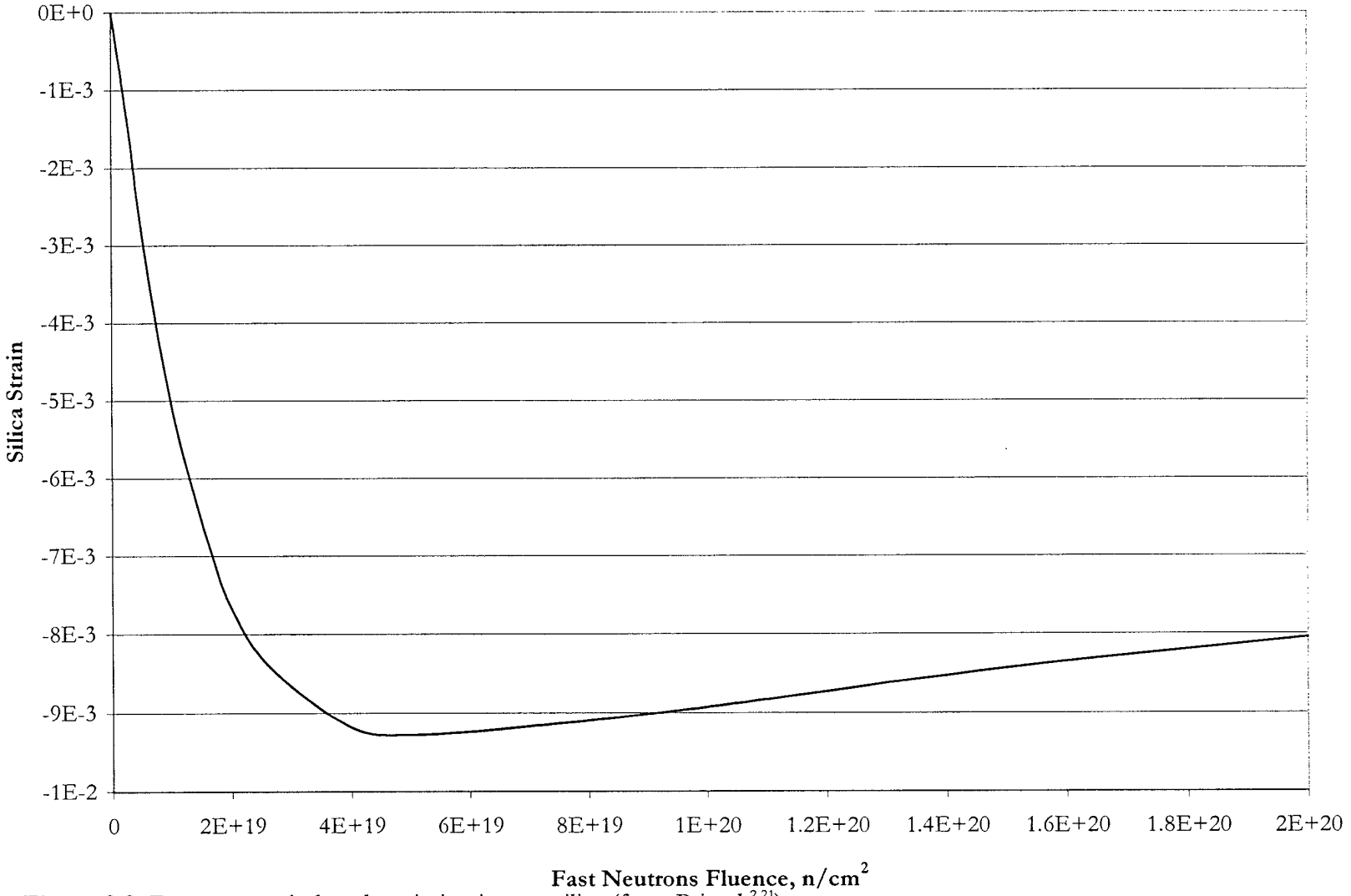

Figure 2.8 Fast neutron-induced strain in vitreous silica (from Primak[2.21])

	O	Si	B	Al	Na	K	Ca	C	Mg	Zn
Pyrex (this study)	63.6	26.3	6.4	1.1	1.2	0.3	--	1.2	--	--
Pyrex, Shelby[2.15]	64.1	26.9	4.8	0.8	2.8	0.4	0.1	--	0.1	--
Pyrex, Paymal[2.12]	64.3	27.6	4.6	0.5	2.2	0.7	--	--	--	--
Hoya SD-2	61.0	21.1	1.1	12.2	0.5	--	--	0.6	3.0	0.8

Table 2.1 XPS results for composition (atomic %) of Pyrex and Hoya SD-2 glasses

Hoya SD-2 data are also the average of two measurements. The manufacturer-provided data for Pyrex and Hoya SD-2 list densities of 2.23 g/cm^3 and 2.60 g/cm^3, respectively.

It can be seen that while Pyrex is clearly a borosilicate glass, Hoya SD-2 is primarily an aluminosilicate glass, modified by boron and magnesium. Atom number densities (based on composition and mass density) are found to be approximately 6.90×10^{22} /cm^3 for Pyrex and 7.65×10^{22} /cm^3 for Hoya SD-2.

3 MONTE-CARLO SIMULATIONS

3.1 Introduction to TRIM

Energetic particles incident on a material can lose energy through collisions with atomic nuclei and by interactions with electrons. Collisions with nuclei can result in atoms being displaced from their initial positions and, then as energetic ions, colliding with other nuclei and causing electronic excitations in the material. This sequence of primary, secondary, and higher-order collisions is called a "collision cascade". Figure 3.1 shows a schematic for a collision cascade resulting from a 1 MeV neutron striking an oxygen atom in Pyrex. The primary knock-on oxygen atom strikes another oxygen, dislodging it from its site, then both atoms continue on through the material, diplacing more atoms of various species.

The **Tr**ansport of **I**ons in **M**atter, or TRIM, is a computer code available free of charge from James F. Ziegler at IBM Research as part of the SRIM (Stopping Range of Ions in Matter) software package[3.1]. SRIM runs on a PC with a DOS operating system. Widely used in the field of ion implantation, TRIM performs Monte-Carlo simulations of collision cascades for any ion passing through elemental materials as well as compounds. Data provided by TRIM includes the average number of atomic displacements in a cascade, the percentage of energy lost by both incident ions and recoil atoms to ionization and atomic displacement, and the range of incident ions in a material. One can even generate a file containing the locations of all collisions within a cascade, along with the corresponding recoil energies.

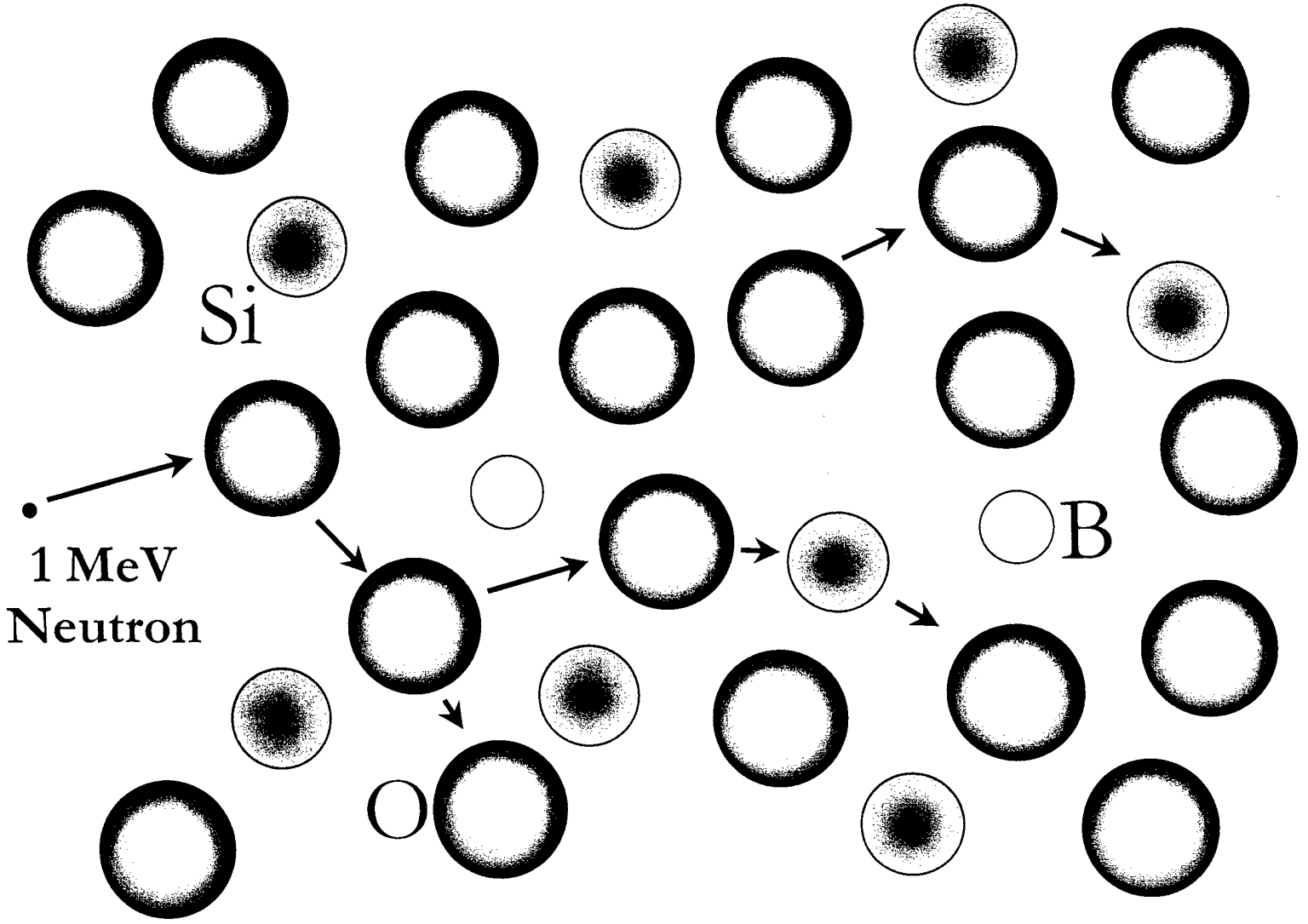

Figure 3.1 Schematic of 1 MeV neutron collision cascade in Pyrex

TRIM (version 2000.38) simulations were carried out for the interaction of fast and thermal neutrons in Pyrex and Hoya SD-2 glasses. The purpose of doing this was two-fold: 1) data were found in the literature[3.2-3.5] for thermal neutron damage in Pyrex, and an equivalence was needed between fast and thermal neutron collision cascades in order to estimate fast neutron damage, and 2) planned experiments on glass would involve exposure to both thermal and fast neutrons, and a way was needed to apportion the observed damage between these two causes.

The key piece of data that TRIM can furnish to help estimate this fast neutron/thermal neutron equivalence is the number of displacements per collision cascade. In the TRIM lexicon, "vacancies" are equivalent to the "displacements" referred to here. In calculating vacancies, TRIM takes into account that an energetic ion that transfers enough energy to a stationary ion to dislodge it from its site may not have enough energy itself after the collision to escape the site. In this case, the incoming ion replaces the ion initially at the site, and no vacancy results. "Displacements" calculated here are this net vacancy result from TRIM, with replacement collisions already taken into account.

3.2 Glass models

The stopping power of a material is the amount of energy lost to that material by an effluent charged particle per distance travelled[3.6]. Quoting Ziegler,[3.7] "...the stopping [power] of a compound may be estimated by the linear combination of the stopping powers of the individual elements. This [Bragg's] rule is reasonably accurate, and measured stopping of ions in compounds usually deviates less than 20% from that predicted by Bragg's rule." Furthermore, "the accuracy of Bragg's rule is limited because the energy loss to the electrons in any material depends on the detailed orbital and excitation structure of the matter, and any

differences between elemental materials and compounds will cause Bragg's rule to become inaccurate."

TRIM accommodates the simulation of ion transport in compounds like glass using a "cores and bonds" (CAB) model.[3.6] The "cores" are closed-shell atoms, and the "bonds" are the bonding valence electrons which, depending upon the exact nature of a bond, will contribute differing amounts to the overall stopping power of the material. The TRIM file COMPOUND.DAT contains compositions for many common nuclear materials, and detailed bond information on a subset of these.

Element	Pyrex atom %	Hoya SD-2 atom %
O	65.0	60.95
Si	25.0	21.1
B	7.0	1.05
Al	1.0	12.2
Na	2.0	0.5
C	--	0.6
Zn	--	0.75
Mg	--	2.95

Table 3.1 Glass compositions used in TRIM calculations

Table 3.1 shows the glass compositions used for the TRIM simulations. The Pyrex composition differs slightly from that actually measured by XPS (see Chapter 2). There are two reasons for this: 1) at the time the Pyrex TRIM calculations were performed, the XPS data were not available and 2) a model for Pyrex was already included in the TRIM database. It was assumed at the time of the calculations that the full CAB model was used, but further inspection of the TRIM COMPOUND.DAT file revealed that no bonding information is

present. It is therefore presumed that Bragg's rule alone is being used in the TRIM calculations for both Pyrex (using the default Pyrex model) and Hoya (with manually entered compositions).

3.3 Fast neutron damage simulations

3.3.1 Introduction to fast neutron scattering

TRIM calculations were carried out for 1 MeV neutrons incident on both Pyrex and Hoya SD-2 glass. As TRIM will not accept a neutron as an incident particle, the nuclei recoiling from a fast neutron collision must serve this purpose. The only such particle considered here was the first atom struck by a fast neutron, or the primary knock-on atom (PKA). For energies up to 1 MeV, the cross section for kinetic energy transferred to the nucleus (T) by a neutron of energy E_1 can be approximated by [3.8]:

(3.1) $$\sigma(T;E_1) = \text{const}/T_m \quad ,$$

where

(3.2) $$0 \leq T \leq T_m = [4m_1m_2/(m_1 + m_2)^2]\, E_1 = [4A/(1+A)^2]\, E_1$$

In the above equations, m_1 is the neutron mass, m_2 is the target atom mass, A is the target atomic mass number, and T_m is the maximum transferred kinetic energy possible. Equation (3.2) follows from classical mechanics using conservation of energy and momentum for an incident neutron striking a nucleus initially at rest. Equation (3.1) says that all possible values for transferred kinetic energy are equally likely. This approximation breaks down at neutron energies substantially higher than 1 MeV.

The cross section for scattering of a fast neutron depends upon its energy as well as the scattering nucleus. Neutron scattering cross sections are available in the literature for the naturally occurring isotopic averages of elements in our glasses,[3.9] as well as for individual isotopes. The symbols used in [3.9] are the following:

σ_{tot} : total cross section

σ_{el} : elastic scattering cross section

σ_{inl} : inelastic scattering cross section

σ_{abs} : absorption cross section

σ_{non} : nonelastic cross section,

where:[3.6]

$$\sigma_{tot} = \sigma_{el} + \sigma_{inl} + \sigma_{abs}$$

$$\sigma_{non} = \sigma_{inl} + \sigma_{abs}$$

For 1 MeV incident neutrons, most of the elements in Pyrex and Hoya SD-2 have scattering cross-sections that are purely elastic. Exceptions are sodium and zinc, which have nonelastic cross sections that are 13% and 4%, respectively of their elastic cross sections. These small nonelastic contributions to scattering are made even smaller for the overall glass by the minor presences of sodium and zinc in our glasses. Therefore, the simplifying assumption of elastic scattering was made for all primary knock-ons.

The product σN, where σ is the microscopic cross section discussed above and N is the number density of atoms, is called the macroscopic cross section, Σ. [3.6] The mean free path, λ, of a neutron is given by $1/\Sigma$. The probability of a neutron not scattering before travelling a distance x in a material is given by:[3.6]

(3.3) $$P_{not}(x) = e^{-\Sigma x}$$

The probability of a neutron scattering before travelling a distance x is therefore:

$$P_{scat}(x) = 1 - e^{-\Sigma x} \tag{3.4}$$

3.3.2 TRIM calculation set-up

TRIM can read an input file of individual recoiling nuclei and calculate a collision cascade for each. Since our glasses contain several different elements, one must calculate the relative number of primary knock-on atoms for each constituent atom type. One must also account for different energies between PKA's, as given by Eq. 3.1.

The number density of each element in both glasses was calculated based on the density of the glass and the atomic fraction of the element. Multiplying this number density by the microscopic cross section for elastic neutron scattering from [3.6] gives the macroscopic cross section. This then can be used in Eq. 3.4 to give the fraction of incident neutrons that will be scattered by this element. The glass wafer thickness (the distance "x" in Eq. 3.4) used for these calculations was 780 μm, that of a typical MEMS substrate.

The most probable scatterer in Pyrex and Hoya SD-2 is oxygen, scattering 2.8% and 2.9%, respectively, of incident 1 MeV neutrons. Silicon is the next largest contributor, scattering around 0.5% of incident neutrons in both glasses, with other elements scattering relatively smaller numbers of neutrons. Multiple scattering of neutrons is therefore ignored when preparing a list of primary knock-on atoms for the TRIM calculation. Each scattering event as predicted by Eq. 3.4 is considered to be one involving a 1 MeV neutron, and the total probability for scattering in a glass is assumed to be the sum of the individual scattering probabilities of each element. Furthermore, the neutron flux and energy is assumed to be uniform throughout the glass wafer; *i.e.*, no consideration is given to the fact that the amount

of energy deposited by an incident neutron flux will be slightly greater near the entrance side of the wafer than near the exit side due to attenuation of neutron kinetic energy. The numbers of each type of PKA used in TRIM calculations are shown in Table 3.2.

Element	Pyrex Number of PKAs	Hoya SD-2 Number of PKAs	Energy Range (keV)
O	1100	1100	(0 - 221)
Si	262	212	(0 - 133)
B	23	6	(0 - 310)
Al	3	65	(0 - 138)
Na	14	3	(0 - 160)
C	--	3	(0 - 284)
Zn	--	6	(0 - 59)
Mg	--	18	(0 - 152)
K	3	--	(0 - 97)

Table 3.2 Primary Knock-on Atoms input into TRIM

We note that the composition of the input PKAs varies somewhat from the TRIM default Pyrex composition (*e.g.*, the presence of potassium). The composition used to generate the values in Table 3.2 comes from Paymal[3.3]. Again, the TRIM runs for Pyrex predate the XPS measurements, and it was desirable to leave the native TRIM Pyrex model intact for the target material. The schematic shown earlier in Figure 3.1 for a 1 MeV neutron collision cascade is representative of Pyrex, with oxygen, silicon, and boron present in correct proportions and their relative sizes indicating their cross section for scattering the fast neutron (*i.e.*, the relative probability of being the primary knock-on atom).

The motivation for running proportional numbers of PKAs was to reduce computation time. One could have simply run thousands of each type of PKA, then averaged the results together proportionately to the neutron scattering probability of each element, as described above. Instead of doing this, it was judged that ~1400 total PKAs

gave acceptable statistical certainty in the averaged result for displacements per PKA, and this total number was shared among the elements according to their importance. The 1100 oxygen PKAs took about 6 hours to calculate on a Pentium 120 MHz computer.

The last column in Table 3.2 shows the range for possible energy transfer from the incident 1 MeV neutron to the PKA (see Eq. 3.2). To simulate the spectrum of possible starting energies of primary knock-on atoms (Eq. 3.1), equally spaced energies for PKAs were included in the TRIM input file. For example, 100 of the 1100 oxygen PKAs started with 0 keV, 100 others started with 22.1 keV (being one tenth of T_m = 221 keV), and so on up to the last 100 atoms which started with 221 keV. The PKA energies for the other elements were similarly represented by 0, $T_m/10$, ..., T_m. For elements having n fewer than eleven PKAs, the energy range was simply broken into n intervals. TRIM calculations carried out later revealed that assigning all PKAs an energy of $T_{ave} = T_m/2$ yields very similar results to the above procedure, *i.e.*, the number of displacements in a collision cascade varies fairly linearly with initial PKA energy in these energy ranges. Figure 3.2 shows the locations in the X-Y plane of displacements calculated by TRIM for two oxygen recoil collision cascades. One is for the case of maximum energy transfer of 221 keV, the other for one-tenth of that.

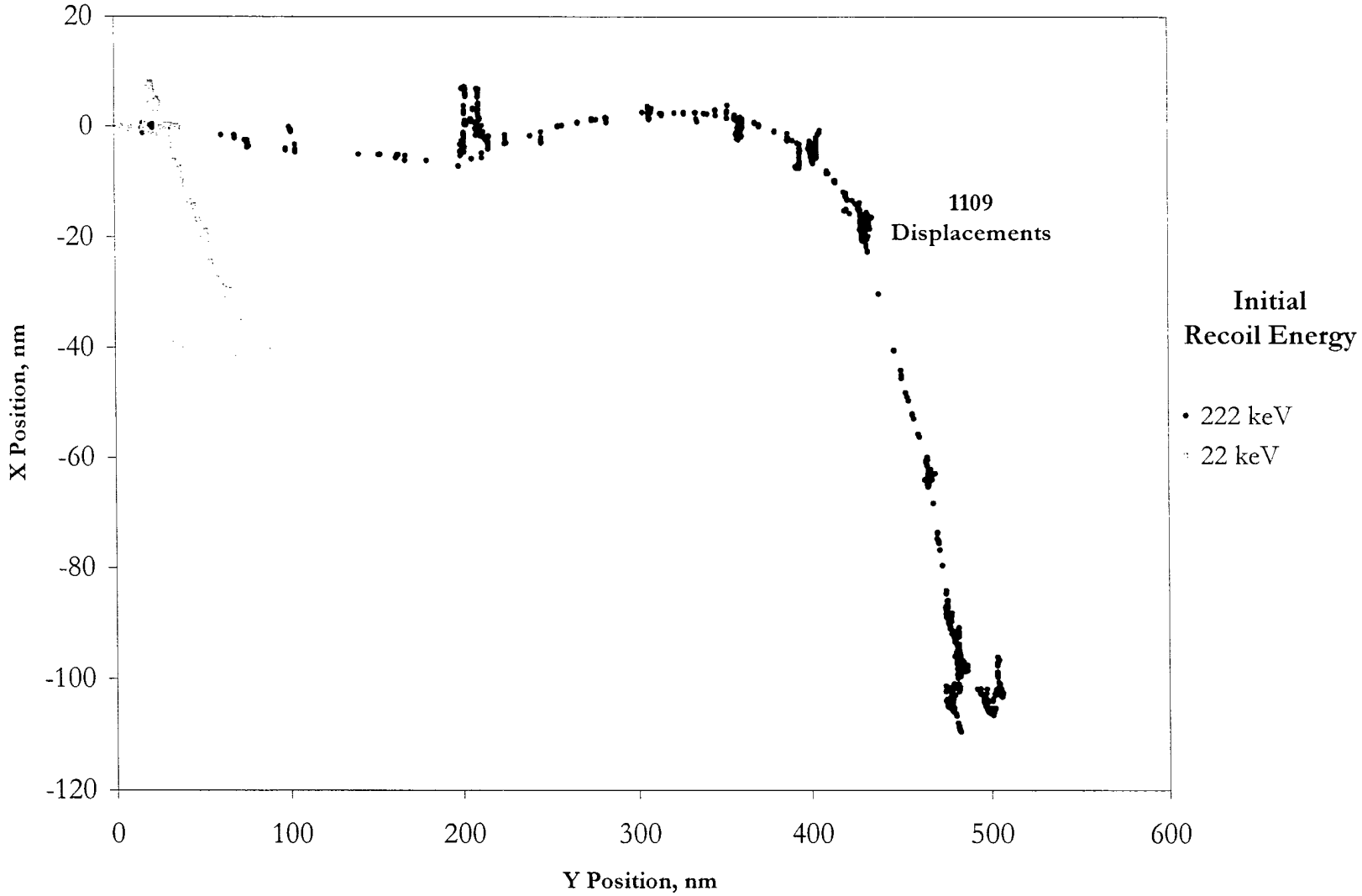

Figure 3.2 TRIM-calculated vacancies in oxygen recoil cascade in Pyrex

The results of the fast neutron TRIM calculations are summarized in Table 3.3.

	Pyrex	Hoya SD-2
Displacements per fast neutron collision	614	644
Probability of fast neutron collision	0.036	0.038
Displacements per incident fast neutron	22	24

Table 3.3 Fast neutron (1 MeV) TRIM results

3.4 Thermal neutron damage simulations

3.4.1 Introduction to boron thermal neutron capture

Incident thermal neutrons do not pose any threat of collisionally displacing atoms in the two glasses considered. Their 0.025 eV average energy is well below the 15-30 eV displacement threshold for atoms in the glass network. We are instead concerned with the recoiling alpha particle (helium ion) and the recoiling lithium ion that result from the capture of a thermal neutron by a ^{10}B nucleus. The reaction is:[3.2]

(3.5) $$^{10}_{5}B + ^{1}_{0}n \rightarrow ^{4}_{2}He + ^{7}_{3}Li + 2.5\,MeV$$

The 2.5 MeV is apportioned between the He and Li ions according to their masses:

$E_{He} = (2.5\ MeV)\ M_{Li} / (M_{He} + M_{Li}) = 1.59\ MeV$

$E_{Li} = (2.5\ MeV)\ M_{He} / (M_{He} + M_{Li}) = 0.91\ MeV$

TRIM calculations are therefore simpler to set up for the thermal neutron case than for fast neutrons, as one has simply to calculate displacement of monoenergetic helium and lithium ions, then add the two results. Figure 3.3 shows a schematic for a thermal neutron capture by a boron atom in Pyrex. A boron atom, upon absorbing the incident thermal neutron, is replaced by energetic lithium and helium particles.

3.4.2 Thermal neutron TRIM set-up and results

The cases of incident helium and lithium particles were calculated separately with TRIM. The sum of the average vacancies per collision cascade gives the effect of a boron neutron absorption. Because manually created files can allow TRIM to simulate ions originating within a material (as would be the case for neutron absorption), both helium and lithium originations were considered for this case. The results were the same for incident ions and for ions starting from inside the glass (*i.e.*, the surface binding energy information included in the TRIM calculation had negligible effects on the results). Overnight runs were carried out, accumulating ~17,000 lithium ions and ~38,000 helium ions (the statistics are stable long before this many ions are treated).

As with the fast neutron case, one must determine how many of the incident thermal neutrons will be absorbed in the glass. The cross section for thermal neutron absorption for ^{10}B is 3837 barns (1 barn = 1×10^{-24} cm^2), and that of naturally occurring boron is 767 barns.[3.11] Using this cross section, the number density of boron in Pyrex (3.2×10^{21} boron/cm^3) and Hoya SD-2 (8.0×10^{20} boron/cm^3), and a glass thickness of 780 μm in Eq. 3.4 yields probabilities for thermal neutron of absorption of 17.3% and 4.7% in Pyrex and Hoya SD-2, respectively.

The results of the TRIM calculations are summarized in Table 3.4.

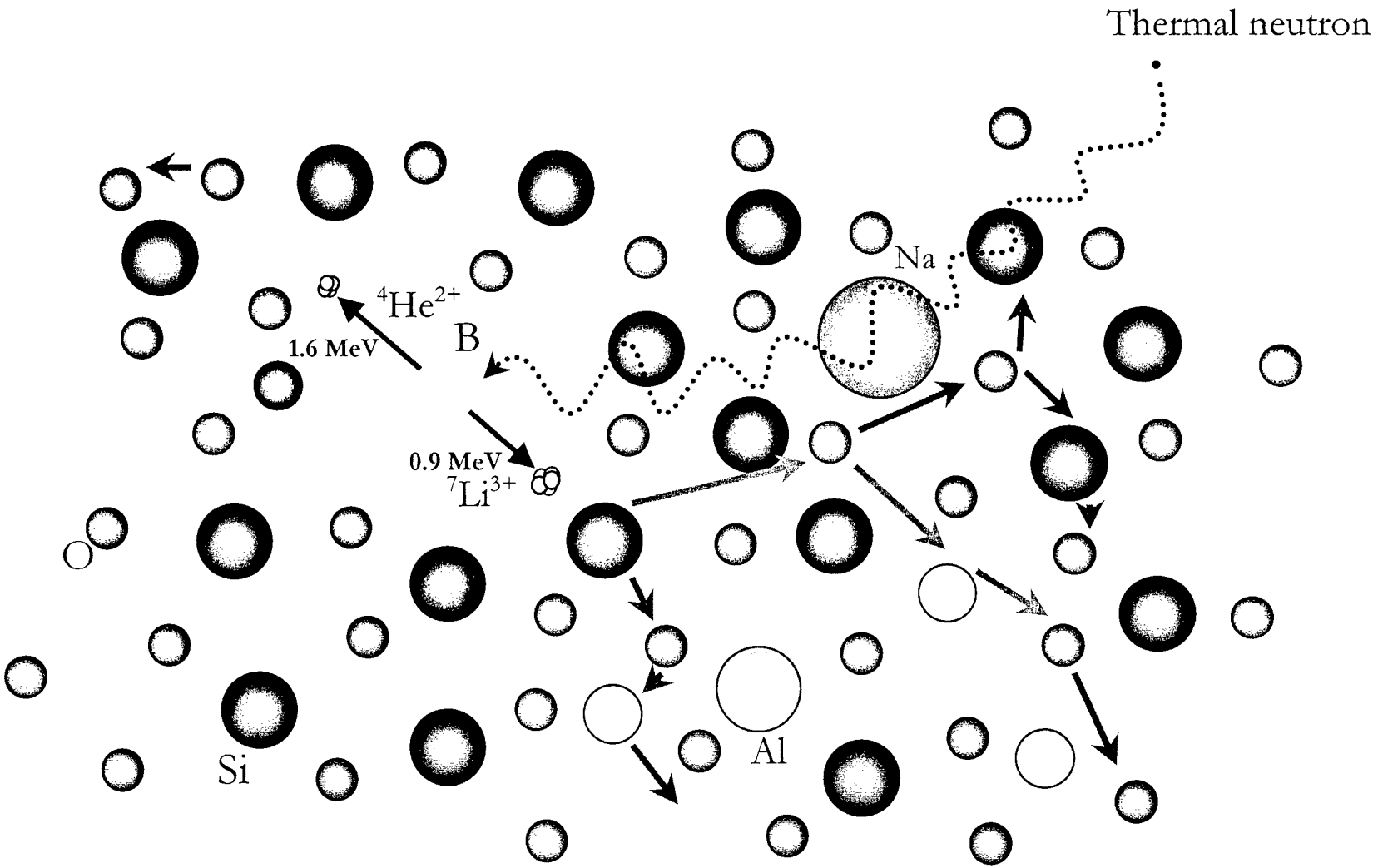

Figure 3.3 Schematic thermal neutron capture and resulting collision cascade

	Pyrex	Hoya SD-2
Displacements per thermal neutron absorption	578	664
Probability of thermal neutron absorption	0.173	0.047
Displacements per incident thermal neutron	100	31

Table 3.4 Thermal neutron TRIM results

To calculate displacements per atom for the values in Table 3.3 and Table 3.4, one may use the atom number densities (based on composition and mass density) of 6.90×10^{22} /cm^3 for Pyrex and 7.65×10^{22} /cm^3 for Hoya SD-2.

4 GAMMA IRRADIATION OF POINTER BEAMS

4.1 Pointer beam device

A MEMS pointer beam strain gauge has been developed at Charles Stark Draper Laboratory (CSDL). Its primary use has been as a monitoring tool for wafer bonding and fabrication processes, as it gives an indication of differential strains present between a glass substrate and the silicon wafer bonded to it.

A diagram of the pointer beam device is shown in figure 4.1.

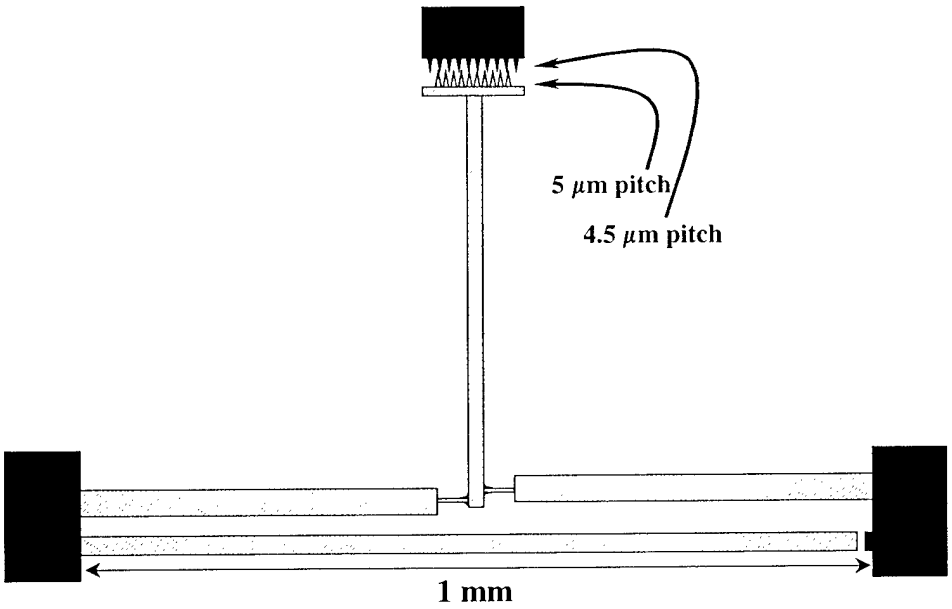

Figure 4.1 Pointer beam strain gauge

The areas shaded in black represent portions of the device that are anodically bonded to the glass substrate. The hashed regions represent silicon parts suspended above the surface of the substrate. The entire suspended portion is thus supported by the two silicon blocks at the bottom of Figure 4.1.

The key to the strain gauge lies in the slight offset between the two horizontal supports for the vertical beam. Thus, if the silicon is in compression, the top of the vertical beam will swing to the left. If the silicon is in tension, it will swing to the right. The row of teeth spaced at 5 μm attached to the vertical beam, when referenced to the row of teeth spaced at 4.5 μm on the bonded silicon block at the top of Figure 4.1 serve as a vernier caliper, allowing one to measure the degree of compression or tension. The beam at the bottom of Figure 4.1 that runs parallel to the offset beams plays no role in the strain measurement: its detached end (on the right) serves to measure strain gradients in the silicon as it curls out of plane.

A finite element analysis performed by CSDL staff showed that the displacement of the pointer beam teeth with respect to the anchored reference teeth is given by:

$$d = (0.035\mu m)\varepsilon, \tag{4.1}$$

where d is the tip displacement in microns and ε is the strain in parts per million (ppm). Since the vernier reads to 1/10 of a tooth width, or 0.5 μm, this yields a strain resolution of about 14 ppm.

The offset of the horizontal beams in Figure 4.1 is critical to this d/ε relationship. To examine the effect of possible fabrication flaws in this offset, we consider a simple geometric construction in which the horizontal beams are attached to the main vertical beam by freely moving hinges. The resulting relationship is:

$$d = (SL_O/\delta)\,\varepsilon, \tag{4.2}$$

where d and ε are as above, S is the length of the vertical beam from tip to midway between the horizontal beam attachment points (the "hinges"), L_O is the initial distance between the anodically bonded anchors (the distance labeled "1mm" in Figure 4.1), and δ is the offset

distance between hinges. Taking S to be 535 μm, L_O to be 1 mm, and δ as its nominal 10 μm, we get:

(4.3) $$d = (0.054\ \mu m)\ \varepsilon$$

This geometric model therefore predicts 50% greater sensitivity to strain than does the finite element model. It has not taken flexure bending into account, but is still useful as a model for examining the sensitivity of d/ε to the offset δ.

The pointer beam devices used in the gamma irradiations were fabricated at CSDL with a 0.1 μm tolerance for in-plane distances. Examining equation 4.2, we find that a 0.1 μm change in δ results in a 1% change in d/ε. A 1% variation among pointer beam strain sensitivities would not significantly affect the results we obtained.

Three wafers were made: one Pyrex wafer and two Hoya SD-2 wafers. The devices were arrayed on glass wafers, among other MEMS diagnostic devices, as shown in Figure 4.2. The black squares indicate the locations of test device arrays. At each of these locations, one pointer beam is present, giving a total of 57 pointer beams per wafer. The glass used was about 780 μm thick, and the silicon was 10 μm thick.

4.2 Experimental procedure

4.2.1 Pre-irradiation measurements

To read the strain gauge, one needs a microscope. A reflected-light microscope with a magnification of 1000X was used to make measurements. The as-fabricated beam positions for each numbered device were measured and recorded. The average starting deflection of the pointer beams is shown in Table 4.1 (positive deflection indicates the silicon is in tension).

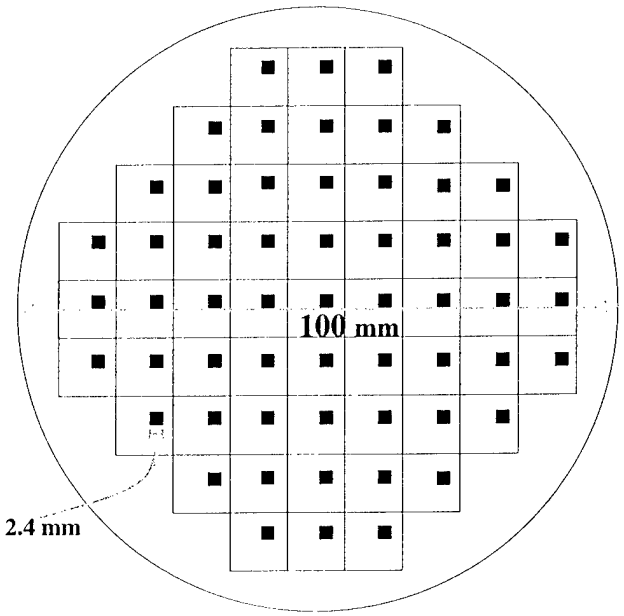

Figure 4.2 Pointer beam array on glass wafer

Wafer	Pointer Beam Average Pre-Irradiation Deflection (teeth)
Pyrex	+0.34
Hoya B	+0.14
Hoya C	+0.09

Table 4.1 Pointer beam pre-irradiation positions

Tooth shape and orientation showed considerable variation from one device to the next. As a result, some degree of interpretation was involved in making a deflection reading. In some cases, it was clearly possible to make fractional-tooth readings. When time allowed, multiple measurements of the same pointer beam were made, and the results averaged. One pointer beam on the Pyrex wafer was found to be at 0.85 teeth. This pointer beam was discounted as defective, and not used.

4.2.2 University of Massachusetts at Lowell facility

A cobalt-60 gamma source at the University of Massachusetts at Lowell was used to irradiate the pointer beam samples. The source consisted of a 61 cm × 61 cm plaque of ^{60}Co strips. The strips were of varying activities. To irradiate the "gamma cave" (the room in which the samples sat), the ^{60}Co plaque would be moved into a holder on an aluminum window that separated the source from the samples. The gamma cave was a very humid environment because the concrete wall with the aluminum window also served, on its other side, as the wall of a large water tank in which the ^{60}Co source was kept. The air inside was sufficiently humid that water condensed on the aluminum window and sample holder.

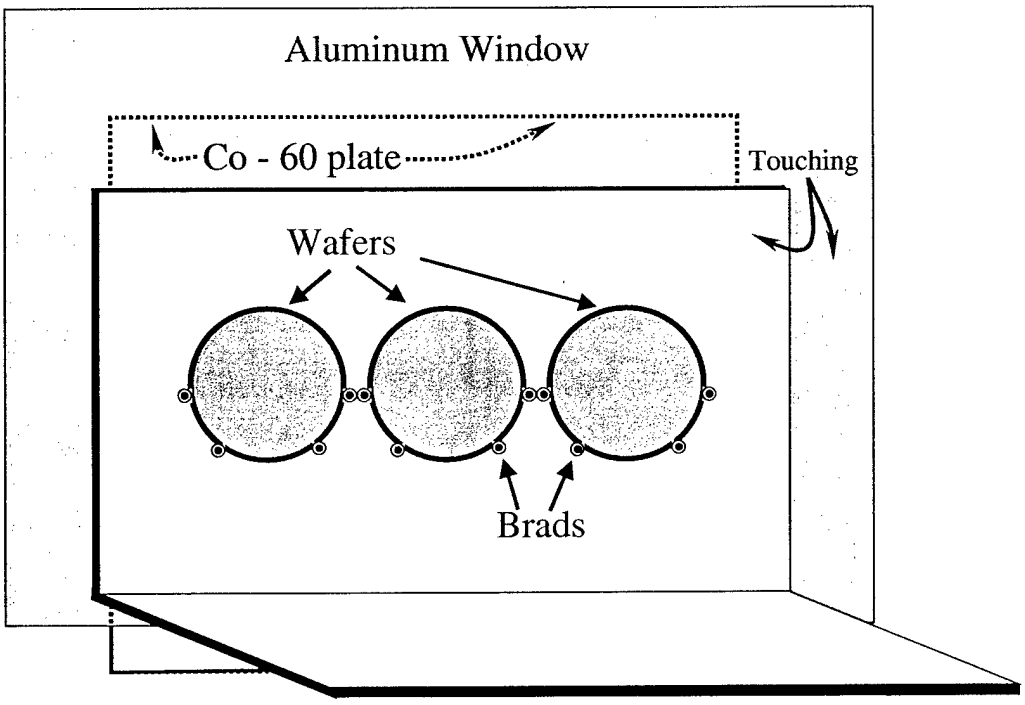

Figure 4.3 Pointer beam holder

4.2.3 Pointer beam wafer holder

An aluminum holder for the samples was fashioned and put into position against the aluminum window as shown in Figure 4.3. An aluminum sheet 1.6 mm thick was bent into an L-shape, then brads were fixed onto it so that the wafers could be slid from the top of the holder down to where they were supported by the brads. Edges on the brads prevented the wafers from tipping off the holder. The MEMS devices faced away from the holder. The wafers, designated Pyrex, Hoya B, and Hoya C, were set into the left, middle, and right holder positions, respectively.

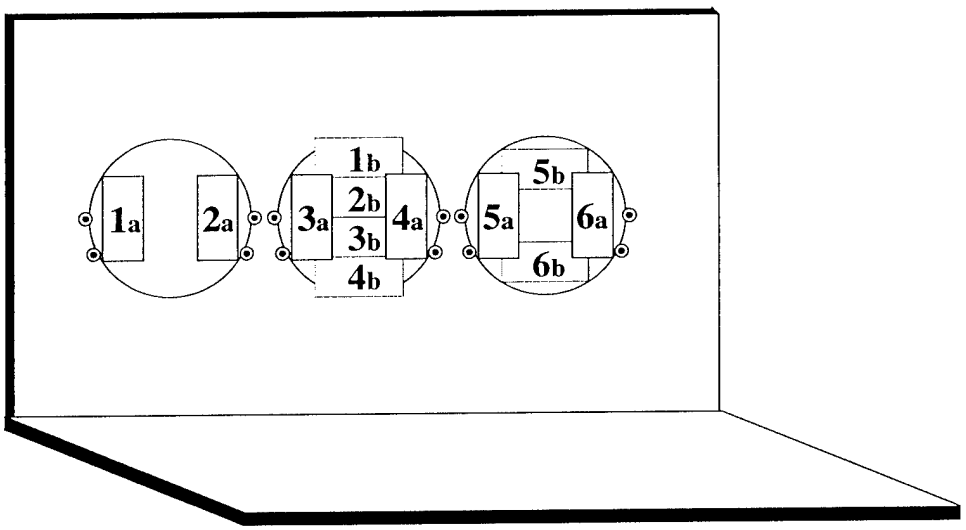

Figure 4.4 Placement of dosimeters

4.2.4 Dosimetry

Prior to the irradiation, dosimetry measurements were made by Lowell personnel using FWT-70-40M Optichromic Dosimeters.[4.1] Six dosimeter packages were placed on the sample holder, as shown in Figure 4.4 by the dark rectangles labeled as series "a". Each

dosimeter package held two dosimeters, the readings of which were averaged to give one reading per package. The results are shown in Figure 4.5 with the package centers' horizontal positions measured with respect to the center of the middle wafer. The data appear to follow a roughly gaussian trend, and a fitted gaussian curve is shown in Figure 4.5.

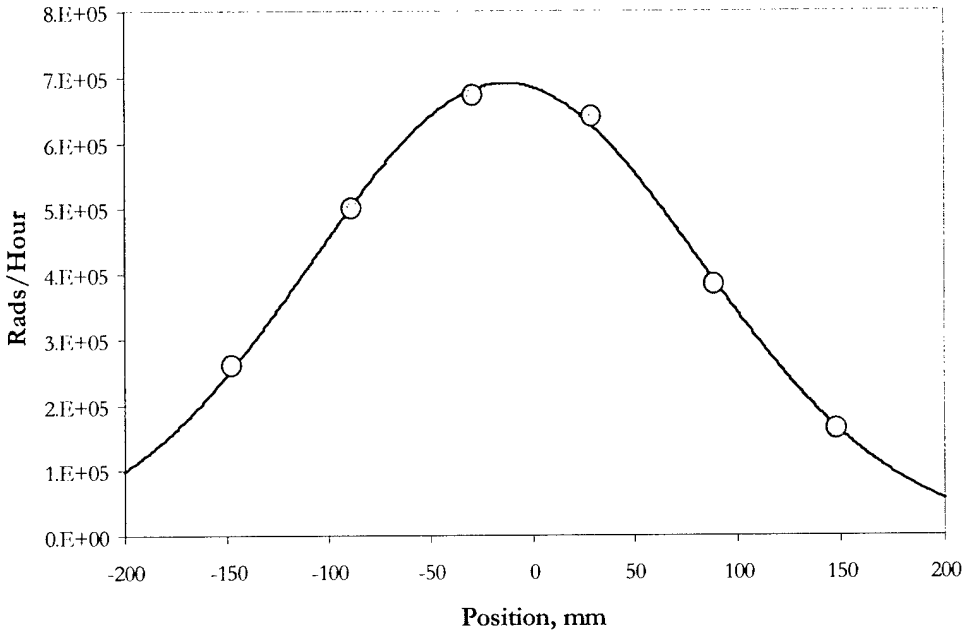

Figure 4.5 Dose rate at the sample holder

A second dosimetry measurement was made at a later date in which four dosimeters were distributed vertically across the center wafer position and two more dosimeters were placed at the top and bottom of the right wafer position. This arrangement is shown in Figure 4.4 by lighter colored rectangles labeled series "b". The measured dose rates were found to be constant to within 5% on the center wafer, and within 10% on the right wafer.

The results of both dosimetry measurements are summarized in Table 4.2.

Dosimeter	Dose rate, krads	Dosimeter	Dose rate, krads
1a	260	1b	720
2a	500	2b	708
3a	672	3b	744
4a	640	4b	744
5a	384	5b	612
6a	164	6b	564

Table 4.2 Dosimeter readings

Given the placement of the wafers near the vertical center of the aluminum window (near the flat peak of the assumed gaussian vertical variation), doses were determined for individual pointer beams based solely on their horizontal positions and the fitted dose rate curve in Figure 4.5. The average dose rate measured at the right wafer position differed by about 50% in the two measurement series, though the center wafer position measurements remain within 7% of each other. Since the wafer positions are not symmetric about the gaussian in Figure 4.5, it is suspected that in the second dosimetry measurement the Co-60 source plaque was placed in its holder with an opposite orientation with respect to the first set of measurements. The ^{60}Co source was removed and replaced several times over the course of the irradiations without verification of the orientation of the source, so a large uncertainty in the radiation dose received for the left and right wafers must be assumed. The effect of this different source placement is considered in the discussion below.

The doses quoted from the dosimeter measurements are water-equivalent doses (the dose that would have been absorbed by water at the dosimeter positions). To find the doses absorbed by Pyrex and Hoya SD-2 glasses for the same gamma flux, a conversion factor was

calculated. A Co-60 gamma emission spectrum of two lines of equal intensity, 1.17 MeV and 1.33 MeV, was assumed.[4.3] Degradation of the emission spectrum upon propagation through the aluminum window and sample holder was accounted for using mass attenuation coefficients from NIST's website,[4.2] then the absorbed dose was calculated using mass energy-absorption coefficients, μ_{en}/ρ, also from NIST.[4.2] Values for absorbed dose were next calculated for water and the glasses, then compared. Pyrex and Hoya SD-2 absorbed doses were both found to be 0.89 times those measured by the dosimeters for water. It turns out that the thin aluminum windows present have a negligible effect for present purposes on the ^{60}Co emission spectrum, and the conversion factor can simply be taken as the ratio of the μ_{en}/ρ values for the materials involved.

4.2.5 Irradiations and measurements

The irradiation of the wafers was often interrupted by the removal of the ^{60}Co source in order to perform other simultaneous experiments in the gamma cave. The wafers were taken to CSDL for measurement during these interruptions. The pointer beams on all three wafers were all measured after 317, 471, and 630 hours of irradiation. The Hoya C wafer had its pointer beams additionally measured after 184 hours of irradiation.

4.3 Results

The results of the pointer beam measurements are summarized in Figure 4.6 and Figure 4.7.

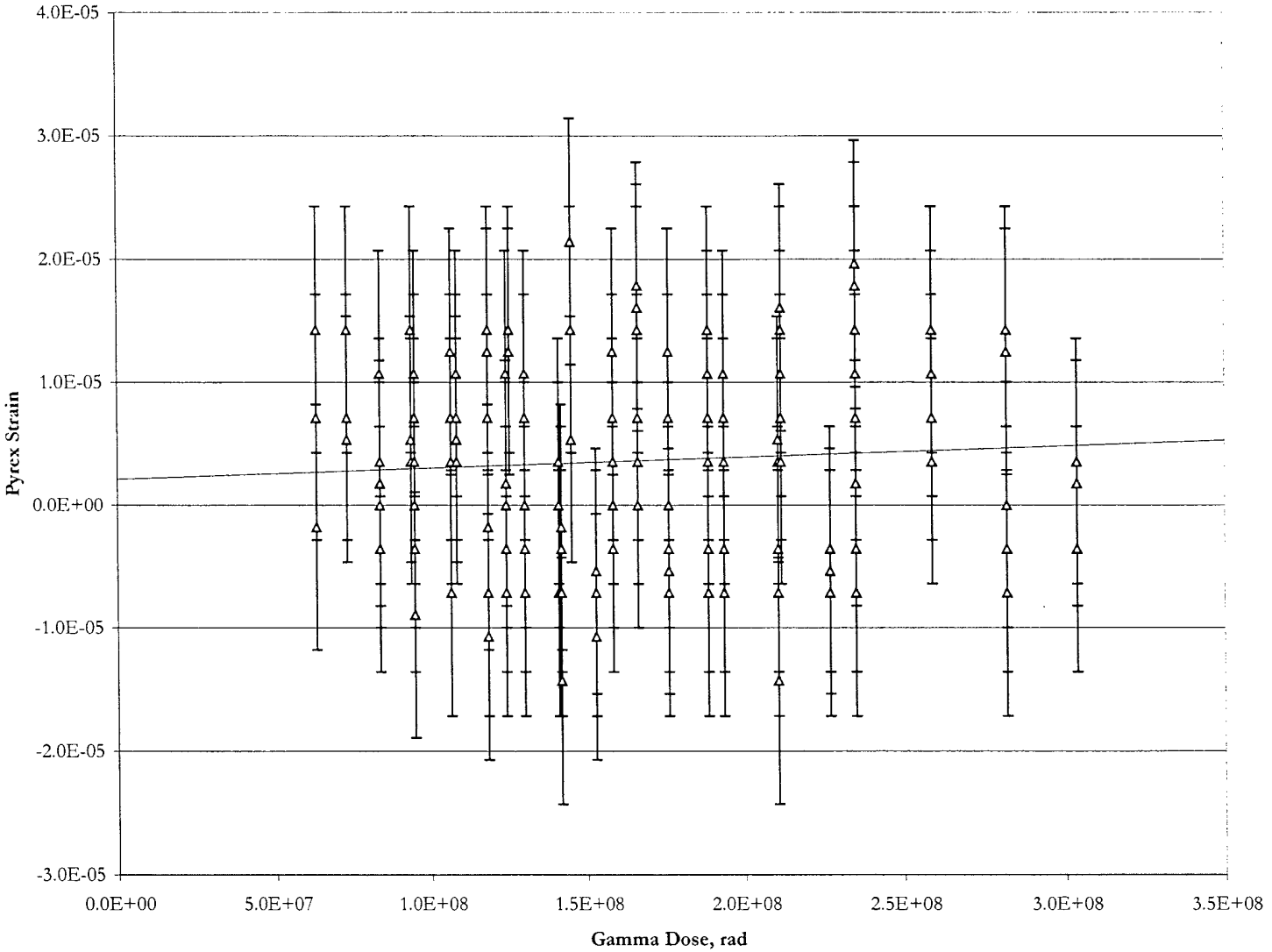

Figure 4.6 Gamma-induced strain in a Pyrex glass wafer

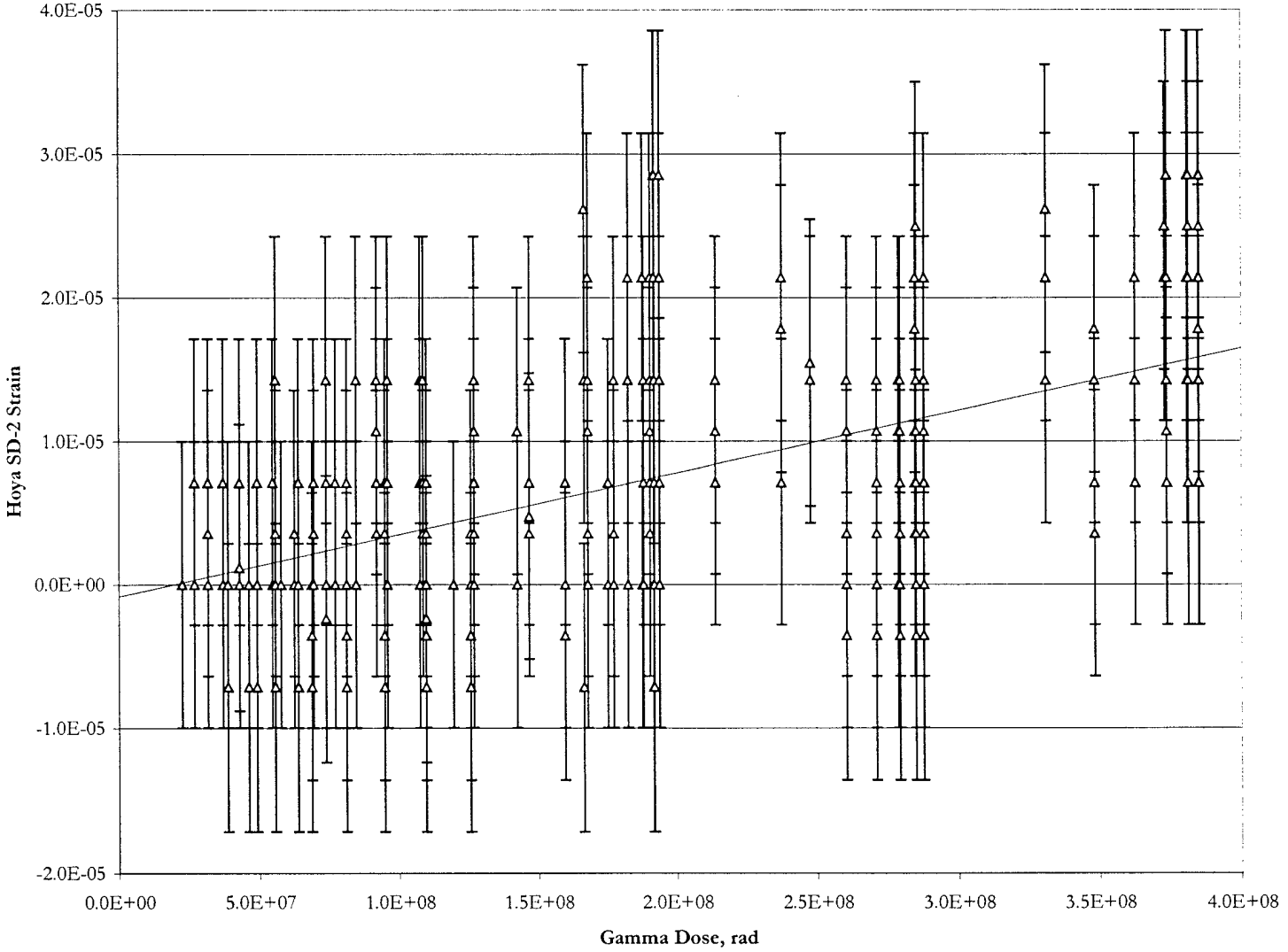

Figure 4.7 Gamma-induced strain in Hoya SD-2 glass wafers

A line has been fitted to the data using a least-squares technique. Error bars are shown with $\pm$ 1 $\times 10^{5}$ strain, which is slightly better than the 14 ppm resolution of the vernier on the pointer beams. Table 4.3 shows a summary of the fits to the data.

	Strain/rad	Intercept (strain)	Reduced χ^2
Pyrex	9.02×10^{-15}	2.13×10^{-6}	0.65
Hoya SD-2	4.34×10^{-14}	-8.51×10^{-7}	0.48

Table 4.3 Pointer beam gamma irradiation results

The different dosimetry profile that would result if the ^{60}Co source were inserted into its holder in an orientation inverted about the vertical axis in Figures 4.3 and 4.5 has been considered. Dose values were reassigned to individual pointer beams based on the curve that results from inverting the gaussian curve shown in Figure 4.5 about the ordinate axis. A line was then fitted to both the Pyrex and the Hoya SD-2 data. The resulting slope for the Hoya SD-2 data was 4.65×10^{-14} strain per rad, and 1.46×10^{-14} strain per rad for the Pyrex data. This is a 7% difference for Hoya SD-2 and a factor of 6 difference for Pyrex from the values in Table 4.3. These values represent the extreme case that the source sat for the entire irradiation duration in the opposite orientation than previously thought. Table 4.4 summarizes these fits, and Figures 4.8 and 4.9 show the pointer beam data replotted for this alternate dosimetry.

	Strain/rad	Intercept (strain)	Reduced χ^2
Pyrex	1.46×10^{-15}	3.39×10^{-6}	0.66
Hoya SD-2	4.65×10^{-14}	-2.35×10^{-6}	0.49

Table 4.4 Pointer beam gamma irradiation results (alternate ^{60}Co orientation)

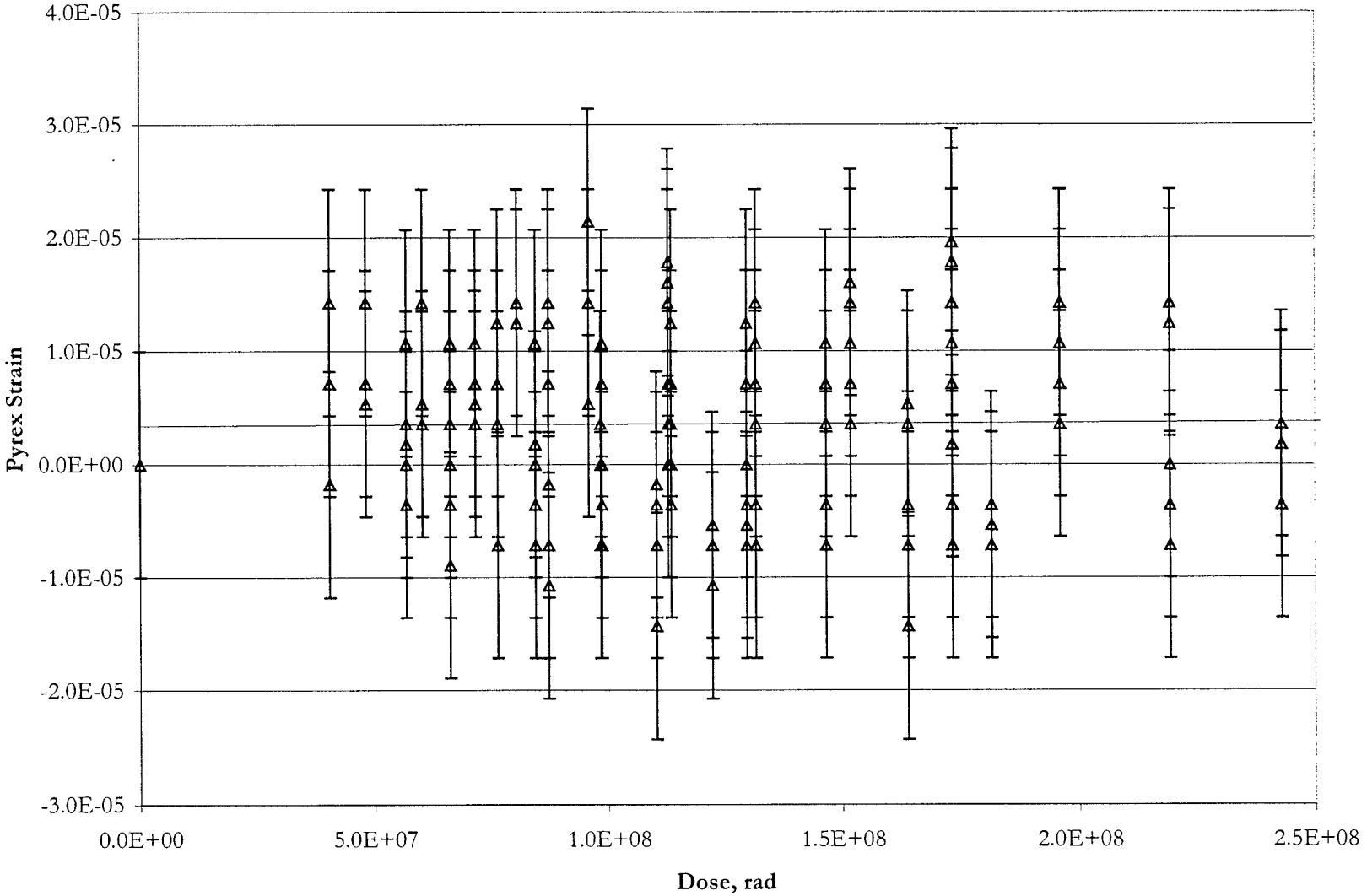

Figure 4.8 Gamma-induced strain in Pyrex glass wafer, alternate ^{60}Co orientation

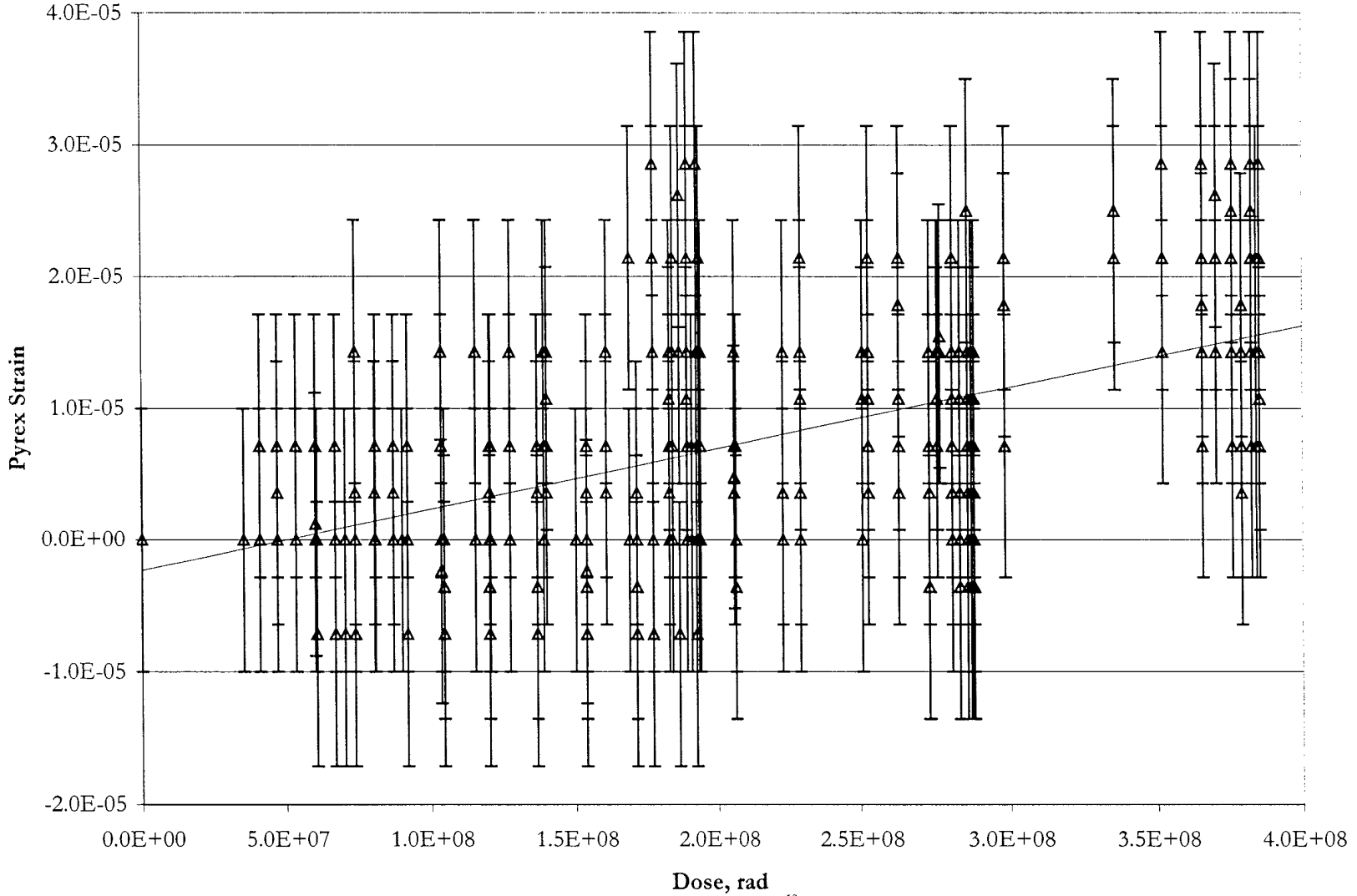

Figure 4.9 Gamma-induced strain in Hoya SD-2 glass wafer, alternate ^{60}Co orientation

Table 4.5 compares the fitted slopes (strain per rad) for the two extreme cases of constant source orientation and presents the more likely averaged values.

	Strain/rad Source orientation #1	Strain/rad Source orientation #2	Strain/rad Average
Pyrex	9.02×10^{-15}	1.46×10^{-15}	$5.24\ (\pm\ 3.78) \times 10^{-15}$
Hoya SD-2	4.34×10^{-14}	4.65×10^{-14}	$4.50\ (\pm\ 0.16) \times 10^{-14}$

Table 4.5 Pointer beam gamma irradiation averaged results

4.4 Discussion

While a trend of rising positive strain with increasing dose is clearly seen in only the Hoya SD-2 data, it is statistically shown to be present in both glasses. The reduced chi-squared[4.4] values for the fits indicate with high certainty that an upward trend is present.

These results apparently contradict measurements in Pyrex by Shelby[4.5]. At 100 Mrad, Shelby shows strain of approximately -20 ppm, whereas the present data show a strain in the Pyrex of about +3 ppm. As Shelby's results have been confirmed by later experiments,[4.6, 4.7] there must be some other element acting in the pointer beam experiment to give results so clearly different.

Several explanations for the Pyrex results have been proposed. Firstly, radiation might be compacting the silicon pointer beams along with the glass substrate. In pure silicon, the radiolysis mechanism involving Si-O bonds is absent, and the silicon is therefore not susceptible to the radiolytic damage caused by γ rays in glass. Compton scattered atomic electrons with kinetic energy equal to the incoming γ ray can be produced, however.[4.8] Bombardment of silicon with 1 MeV electrons shows that expansion in silicon occurs.[4.9] Not only should this expansion *increase* the differential strain with respect to a compacting glass substrate, but its magnitude is negligibly small when to compared to the expected Pyrex

compaction.

Secondly, one must consider that the glass being irradiated has been through bonding and microfabrication processes during the construction of the pointer beams. The bonding process, called anodic bonding, is particularly suspect as a cause for changes in material properties. During anodic bonding, the glass is heated to 350-400 °C while in contact with a silicon wafer. Electrodes on either side of the two wafers are set at a potential difference of 500-1000 V. The large electric field that results causes sodium ions to drift away from the bonding interface as a layer of SiO_2 forms at the interface of the two wafers.[4.10, 4.11] The Vicker's hardness of Pyrex has been observed to increase two-fold after anodic bonding.[4.10] It is possible that the chemical and microstructural changes induced in Pyrex by the anodic bonding dramatically change the response of the glass to gamma irradiation.

Thirdly, the pointer beams may not be performing as designed. To verify the functioning of the pointer beams, a thermal calibration apparatus has been designed and built. An aluminum plate with a thermistor, a temperature controller, and heaters attached to it will heat the glass wafer from underneath while a silicon circumferential ring with a glass wafer resting on it act as an oven for the pointer beams. Heating the pointer beams and the wafer to which they are bonded causes a differential strain to develop between the pointer beams and the glass substrate due to differing coefficients of thermal expansion. By measuring beam deflection and temperature, one can calibrate the beam deflection-to-strain relationship. Unfortunately, this experiment is still awaiting a microscope powerful enough to image the vernier on the pointer beams, but with an objective lens able to withstand the heat of the experiment.

Lastly, effects such as radiation-induced creep, interface debonding, and non-

densifying deformation may be possible. Experiments involving heavy ion bombardment of silicon, silica, and Pyrex have shown that non-densifying radiation-induced viscous flow can occur[4.12]. At high enough doses, the dimensional expansion of silica and Pyrex (even in the absence of stress) perpendicular to the irradiating ions can reverse the shrinkage due to saturating compaction that is evident at lower doses.[4.13, 4.14] The expected compaction of the glass substrate is providing a stress that may assist the radiation-induced viscous flow in a thin SiO_2 layer at the anodic bond, thus allowing the pointer beam anchors to slip, removing the strain in the silicon pointer beams. This would not explain the slight tension present in the beams after irradiation, and the further study must be done to determine if the gamma irradiation is of sufficient energy and dose to cause viscous flow under stress.

[THIS PAGE INTENTIONALLY LEFT BLANK]

5 NEUTRON IRRADIATION OF GLASS

5.1 Overview

While the TRIM calculations discussed in chapter 3 serve to estimate displacements in fast and thermal neutron collision cascades, they do not indicate how many of these displacements are permanent, nor how the number of displacements affects the expansion or compaction of a material. In order to determine the effect of fast and thermal neutrons on the density of Pyrex and Hoya SD-2 glass, glass samples were exposed to neutron fluences and the resulting change in their density was measured using a technique called sink/float.

5.2 Experimental procedure

5.2.1 Sample preparation

Pyrex and Hoya SD-2 wafers approximately 0.78 mm thick were diced using a diamond saw. Squares approximately 3 mm × 3 mm were cut for use in the sink/float apparatus. Sink/float compares the density of one material sample to that of another. Accordingly, samples were needed both to be irradiated and to be left unirradiated for comparison purposes. For each planned exposure level, samples were prepared in pairs, with one to be irradiated and one not. To minimize the probability of the glass pieces within a sample pair having an initial density difference, care was taken to take sample pairs from the same wafer, and even to take adjacent pieces of glass as pairs. Figure 5.1 shows an example of how the pairs were selected from a Pyrex wafer.

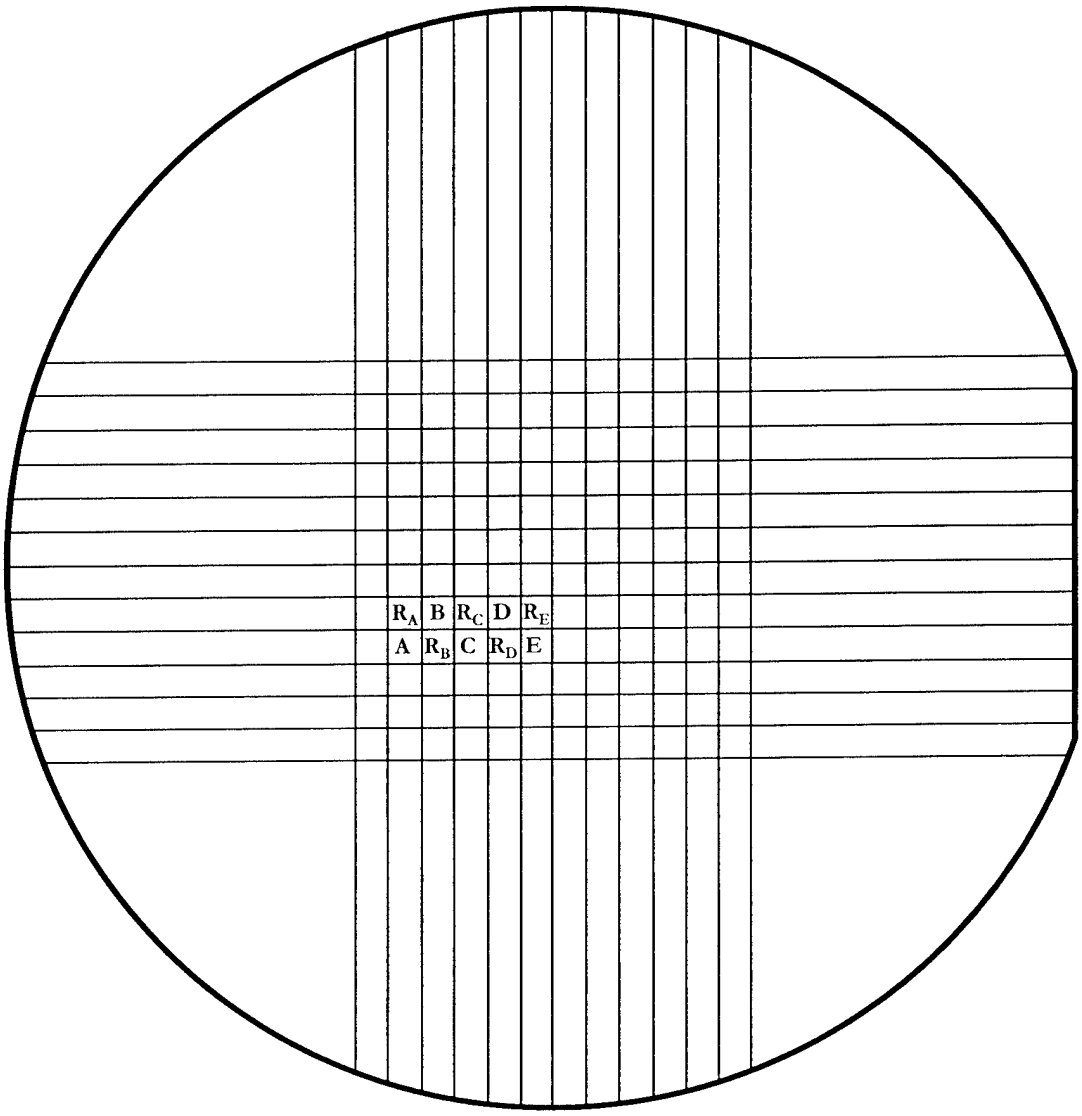

Figure 5.1 Cut Pyrex wafer and sample assignments (R: reference)

In anticipation of the need for distinguishing between the irradiated samples and their reference samples, the reference samples had a corner cut off. While some discoloration due to irradiation was expected, whether or not this would suffice for distinguishing the two samples during a sink/float measurement was not known. Figure 5.2 shows the dimensions of an irradiated sample and its companion reference sample.

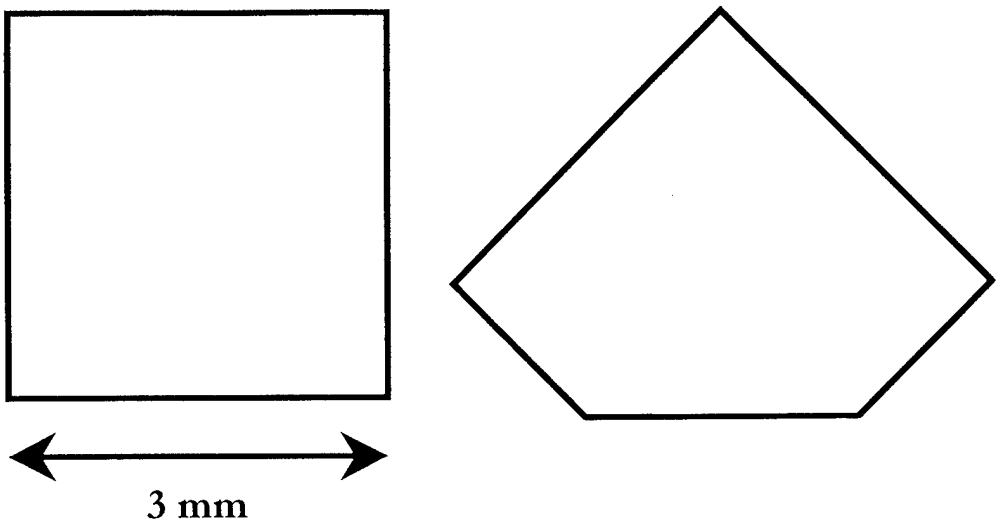

Figure 5.2 Glass sample pair

5.2.2 Neutron irradiations

Samples were irradiated by MIT nuclear reactor personnel in a pneumatic tube, designated as 1PH1, inserted into the core of the MIT reactor. Estimates furnished by MIT personnel of the fast and thermal neutron fluxes for samples within 1PH1 are 1×10^{11} $n/cm^2/s$ fast and 6.7×10^{12} $n/cm^2/s$ thermal. Samples were held within plastic tubes ("rabbits") that are 2.5 cm in diameter and about 6.1 cm long. The temperature during irradiation was not monitored, but did not exceed the softening point (~ 90 °C) of the polystyrene supports that held the samples within the rabbits, as evidenced by the lack of deformation in any of the supports upon withdrawal of the rabbits from 1PH1.

An irradiation schedule was decided for the glass samples based on work by Paymal[5.1] and the TRIM calculations discussed in chapter 3. Based upon the experiment design (discussed below), it was determined that a strain in compaction of 1×10^{-3} was the greatest that would be practical to measure. Paymal's data for Pyrex compaction was for

thermal neutrons only, and predictions made based on the low-fluence linear portion of his strain-to-fluence curve show that a 6000 second exposure would result in approximately this 1×10^{-3} strain value. Due to the comparatively low fast neutron flux and the similarity of thermal and fast neutron displacement rates (100 displacements per incident thermal neutron, 22 for a fast neutron), the effects of fast neutrons were expected to be very small.

No radiation effects data were available for Hoya SD-2 glass, so it was decided that it would be exposed to the same fluences as the Pyrex. While its lower boron content should result in fewer displacements due to thermal neutron absorption, no predictions could be made as to how much strain would result. The radiation schedule for the glass samples is shown in Table 5.1.

Pyrex	Hoya SD-2	Irradiation Time, s	Thermal Neutron Fluence, n/cm^2	Fast Neutron Fluence, n/cm^2
A	A	30	2.0×10^{14}	3.0×10^{12}
B	B	60	4.0×10^{14}	6.0×10^{12}
C	C	600	4.0×10^{15}	6.0×10^{13}
D	D	1800	1.2×10^{16}	1.8×10^{14}
E	E	6000	4.0×10^{16}	6.0×10^{14}

Table 5.1 Glass sample irradiation schedule

5.2.3 Sink/float measurements

5.2.3.1 Background on the sink/float technique

The ideas behind the sink/float technique for measurement of density differences in our glass samples are primarily drawn from Knight[5.5], Shelby[5.6], and Conners.[5.7] The method has also been used by Sato[5.8] and Zdaniewsky[5.9], Paymal[5.1-5.4], and again by Shelby[5.10]. Shelby and Conners (who was a graduate student working with Shelby) report the greatest precision for the technique, with Shelby[5.10] reporting 50 ppm precision for $\Delta\rho/\rho$, Conners showing

~90 ppm precision, and Sato claiming 300 ppm precision. Converting to strain ($\Delta l/l$), these precisions would be ~ 17 ppm, 30 ppm, and 100 ppm, respectively.

To perform a sink/float measurement, a pair of glass samples (one irradiated, one not, as described above) are placed in a test tube containing a heavy liquid in which they just float. The liquid is then heated by means of a water bath. If the starting density of the liquid is sufficiently close to that of the glass, a few degrees of heating will cause the liquid density to grow smaller than that of the glass (the thermal expansion of the glass is much smaller than that of the liquid). The glass samples will now sink, and at different temperatures if their densities are different. By knowing the thermal expansion coefficient for the liquid, one can relate the difference in sinking temperatures to a density difference.

An approximate formula that relates a difference in sinking temperature to a density difference can be derived as:

$$\frac{\Delta\rho}{\rho} = \frac{3\Delta T(\alpha_G - \alpha_L)}{1 - 3\Delta T\alpha_G} \tag{5.1}$$

In Equation 5.1, ΔT is the difference in sinking temperature between the irradiated and unirradiated glass samples, α_G is the linear coefficient of thermal expansion of the glass, α_L is the linear coefficient of thermal expansion of the liquid (a third of the volumetric coefficient of thermal expansion), and ρ is the glass density. Since the thermal expansion of the glass is $\sim 10^{-6}$ and that of the liquid is $\sim 10^{-4}$, a good approximation can be made simply by:

$$\frac{\Delta\rho}{\rho} = 3\Delta T\alpha_L \tag{5.2}$$

Assuming an uncertainty of 0.01 °C in each temperature reading and neglecting the uncertainty in the coefficient of thermal expansion for the liquid, one obtains a predicted uncertainty in a strain calculation of about 6 ppm. This is valid for small strains. As the

strain rises, however, the uncertainty in the coefficient of thermal expansion of the liquid becomes important, giving a total of about 17 ppm for a 1×10^{-3} strain in Pyrex for an assumed 1 % uncertainty in the liquid's coefficient of thermal expansion.

5.2.3.2 Apparatus design

A schematic of the sink/float device is shown in Figure 5.3. Shown are six heavy liquid-filled 38 mm o.d. × 200 mm Pyrex test tubes (round-bottomed, in actuality) suspended by O-rings from holes in a plexiglass lid that are cut in a regular circular pattern. The tubes are stoppered with Neoprene® rubber, a material resistant to degradation through contact with vapor from the organic liquids in the test tube. The lid rests on a cylindrical 25 cm o.d. × 25 cm Pyrex jar. A 2.5 cm o.d. × 25 cm (only bottom 12.5 cm heated) 500 watt immersion heater is suspended from a hole in the center of the lid. The heater is attached to a Variac® transformer. The jar is filled with water to above the fluid level in the test tubes, and a 7.6 cm stir bar is at the bottom of the jar, for use with a heavy-duty stir plate. A horizontal line is drawn about 5 cm up from the test tube bottoms.

A platinum resistance temperature detector probe was inserted through a rubber stopper and immersed as shown in the liquid of one of the test tubes. The probe was attached to a precision thermometer with 0.01 °C readout and 0.05 °C accuracy at the temperatures of interest.

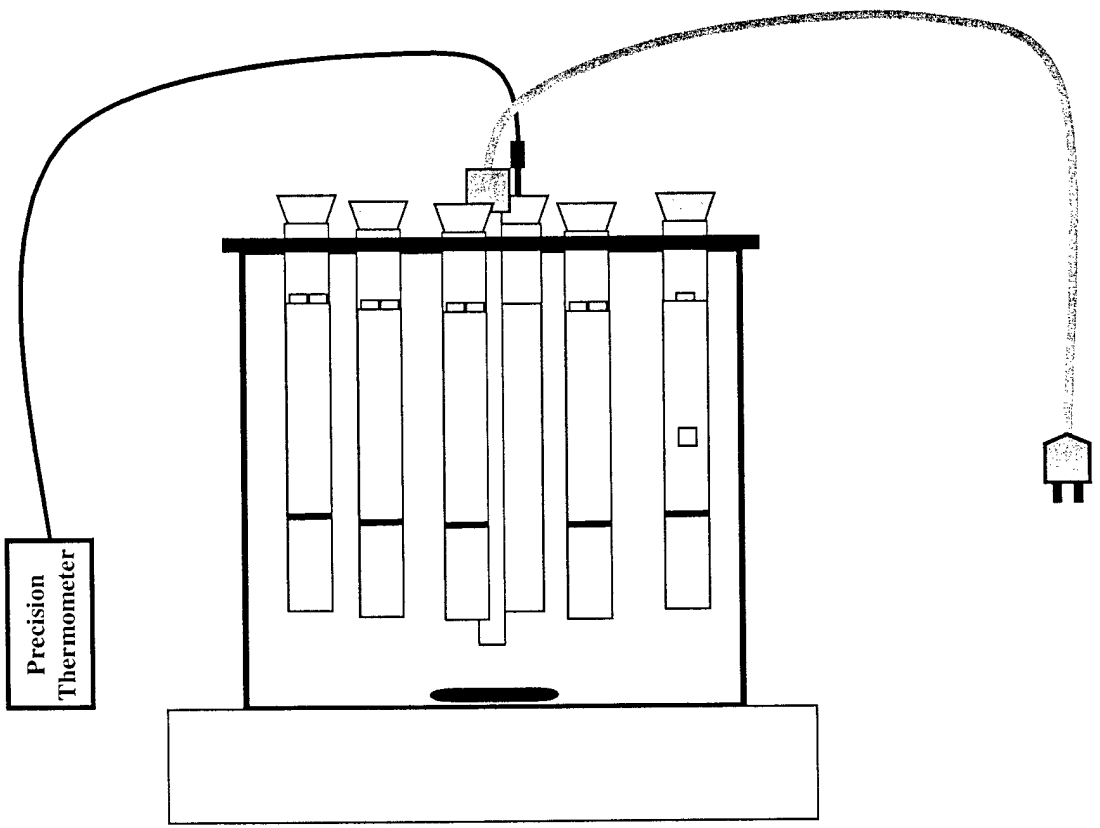

Figure 5.3 Sink/Float apparatus schematic

5.2.3.3 Set-up of sink/float

The glass samples were still radioactive when the experiment began. Only Pyrex sample E (see Table 5.1) was above background level, but all of the Hoya SD-2 samples were measurably active, most notably with ^{122}Sb. It is not certain whether the antimony is intrinsic to the glass or if it somehow came to be present during handling.

All samples came back tinted a brown color, evidence of trapped electronic defects. The color of the Pyrex samples varied continuously and conspicuously from light to medium brown as the sample exposure rose. In the case of the Hoya SD-2, the coloration seemed to be quite equal among the three samples (C, D, E) receiving the highest doses, which points to a possible saturation of the electronic defects. These observations are just cursory impressions, however, and no quantification of this effect was made using optical absorption spectrometry or other techniques.

Samples were cleaned by rinsing them with acetone. During the cleaning of the Hoya SD-2 samples, problems with air currents in the vent hood led to a complete mix-up of samples. The relative activities, however, helped to sort them out. Their activities had been individually measured upon their arrival at CSDL, and monotonically rose with exposure time.

The heavy liquids used were tetrabromoethane (also known as acetylene tetrabromide) and bromonaphthalene. The first was suspected of being quite hazardous, so all work was performed in a vent hood while wearing goggles, a respirator with organic vapor filter cartridges, and Viton® gloves.

The tetrabromoethane has a density of 2.96 g/cm^3, and the bromonaphthalene has a density of 1.48 g/cm^3. Mixtures of these liquids were made in a 1L beaker. Initial liquid proportions were based on the manufacturers' densities cited here for the liquids and the

glasses (ρ_{Pyrex} = 2.23 g/cm^3, $\rho_{Hoya\ SD\text{-}2}$ = 2.60 g/cm^3). All of the sample pairs were individually dropped in the mixture to verify that they all floated, and the liquid was adjusted by adding milliliter quantities of the lighter or denser liquid. The densest sample was identified and then just made to float.

5.2.3.4 Sink/float execution

5.2.3.4.1 Pyrex

Measurement runs were first performed on Pyrex. The apparatus had equilibrated overnight at about 22 °C. After getting a feel for the temperature response to heating, the transformer output was set to 54 volts, with a resulting observed current of 0.4 amperes, or 22 watts. This gave a 0.11 ± 0.02 °C per minute liquid heating rate. The liquid temperature rose steadily and predictably -- a given 0.01 °C increment is traversed in about 6 seconds. The system showed a response time of about 10 minutes to a change in heater power. A high stir setting was used, with the presence of the tubes preventing a vortex from forming (with the tubes removed at this setting, the vortex extends to the very bottom of the jar).

A sample was declared as "sunk" when it crossed the line drawn on the test tubes. Samples tended to stick to the surface of the liquid (and, less often, to each other), and only very vigorous shaking freed them up. Samples took several minutes to sink once they had left the surface, sometimes hovering at a fixed depth before resuming the fall.

Sinking of samples usually occurred in the center of the tube, and convective currents within the test tubes appeared to be present. After sinking and hitting the bottom of the test tube, Pyrex sample E (the densest, most irradiated) would move to the side of the tube and rise again about 2/3 of the way to the top. It would repeat this cycle three times, with each subsequent rise height being smaller than the one before, then stick at the bottom.

In all cases, the recorded sinking temperature recorded was that of a sample's first crossing of the reference line.

Viewing of the samples was clear and easy. This was greatly helped by the magnifying effect of the water-filled cylindrical jar and the heavy liquid-filled test tubes. The irradiation-induced darkening of samples C, D, and E would have been sufficient to easily distinguish between irradiated and unirradiated glass samples, but for samples A and B, the cut corner on the unirradiated sample was necessary. A typical falling position was edge-on, so the cut corner probably made minimal difference in the drag characteristics of the sample.

"First fall" (of sample E) occurred between 28.15 °C and 28.65 °C. It took about one hour to heat to this point. Sinking temperatures for the unirradiated glass occurred in the 31.89-32.39 °C range. The temperatures are those read in one test tube -- the others probably do not share this temperature, but it is the difference in sinking temperatures that it is desired to know. Sinking temperatures varied for a given sample in a given tube to within about a 0.1 °C standard deviation.

On subsequent runs, the water bath was emptied by siphoning then refilled with tap water (colder than room temperature). Rapid heating was applied to about 24 °C, then the 22 watts setting was resumed. Given the observed ~ 10 minutes needed to achieve steady-state temperature rise, this left plenty of time before "first fall".

Runs were made in which the starting temperature was high and all samples were firmly at the bottom of the test tubes at the start. By stirring without heating, the liquid temperature cooled. The cooling rate obtained this way was impractically low, so cool water was added. This process was not well controlled, and resulted in results that do not at all agree with the heating runs.

Runs were made in which the tube shaking was varied as to degree -- there was some concern that the jiggling of test tubes was a contributor to currents within the heavy liquids. A run made with no shaking clearly delayed the sinking of samples due to the liquid surface-tension attraction. Five of the Pyrex runs were done with an "only as necessary" test tube shaking policy; *i.e.*, tubes were jiggled about every minute until the samples started to sink. Once both samples in a tube were detached from the liquid surface, no further shaking took place. A run was done with constant shaking of the test tubes throughout the run, and the results are in agreement with five other runs.

5.2.3.4.1 Hoya SD-2

The Hoya SD-2 measurements proceeded as above, with two differences to note. First, the attraction of the surface for the samples seemed somewhat less than for the Pyrex case. Second, the liquid density required significantly more adjustment than that of the Pyrex -- based on the published liquid densities and the final proportions in the mixture, the Hoya SD-2 glass appears to have a density of 2.62 g/cm^3. About 62 ml extra tetrabromoethane was needed to get all the samples to float, then 5 ml extra bromonaphthalene was added ("extra" referring to a planned density of 2.60 g/cm^3 and 780 ml total fluid). As a result of more careful mixing, the liquid mixture was much closer to the "first fall" point than for the Pyrex. In the first run, starting from 22.14 °C, first fall occurred at 22.53 °C. There was concern that this sinking temperature so close to the starting point wasn't allowing steady state to be reached, so chilled water was added to the water bath on subsequent runs. Start temperatures for the heavy liquid were then close to 20 °C. The results from the first run resemble those of subsequent runs, so have been kept.

All runs were performed with the above-described "only as necessary" tube shaking approach.

5.3 Results and discussion

The results for six measurements each of Pyrex and Hoya SD-2 are shown in Figure 5.4 and Figure 5.5, respectively. The error bars shown represent the standard deviation of the six measurements divided by the square root of six, then averaged across all five samples. This is the uncertainty for the mean value of the six measurements.[5.11] It is important to distinguish between this scatter, which is indicative of the repeatability and precision of the sink/float method, and the *accuracy* of the conversion of a measured ΔT to a strain. An inaccuracy in the thermal expansivity of the heavy liquids used will add to the inaccuracy of the strain values, but will not contribute to scatter. Scatter in the points is due solely to uncertainty in temperature readings, convective currents, and delays in sinking due to liquid surface attraction. In the ideal situation (no current-induced inaccuracies, no surface-sticking), and with our 0.01 °C temperature control, we expect 6 ppm scatter in the data. Table 5.2 summarizes the observed scatter.

	Pyrex	**Hoya SD-2**
Average σ	55 ppm	16 ppm
Average $\frac{\sigma}{\sqrt{6}}$	22 ppm	6 ppm

Table 5.2 Average scatter σ of six measurements and resultant uncertainty of the mean

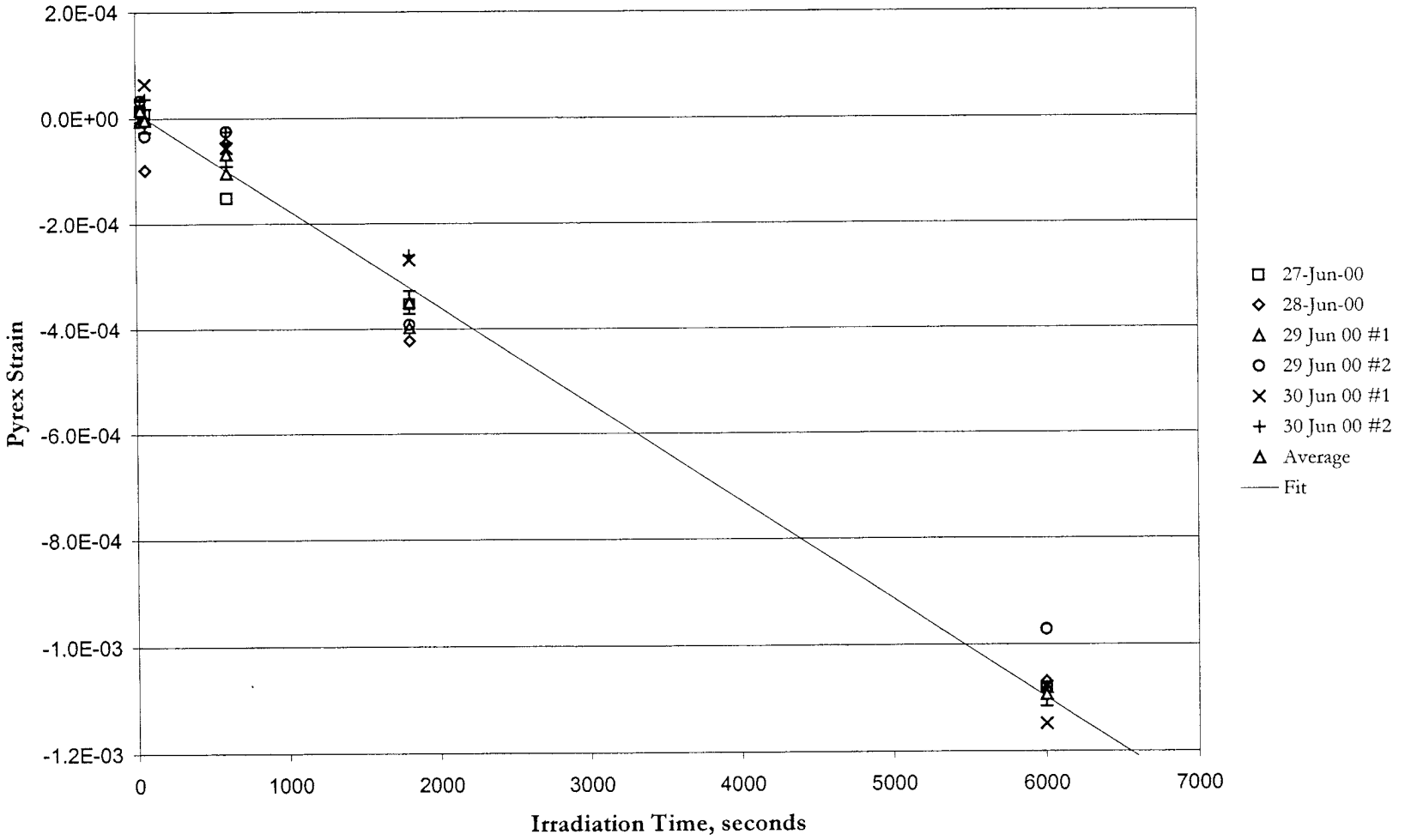

Figure 5.4 Neutron irradiation-induced strain in Pyrex as measured by sink/float

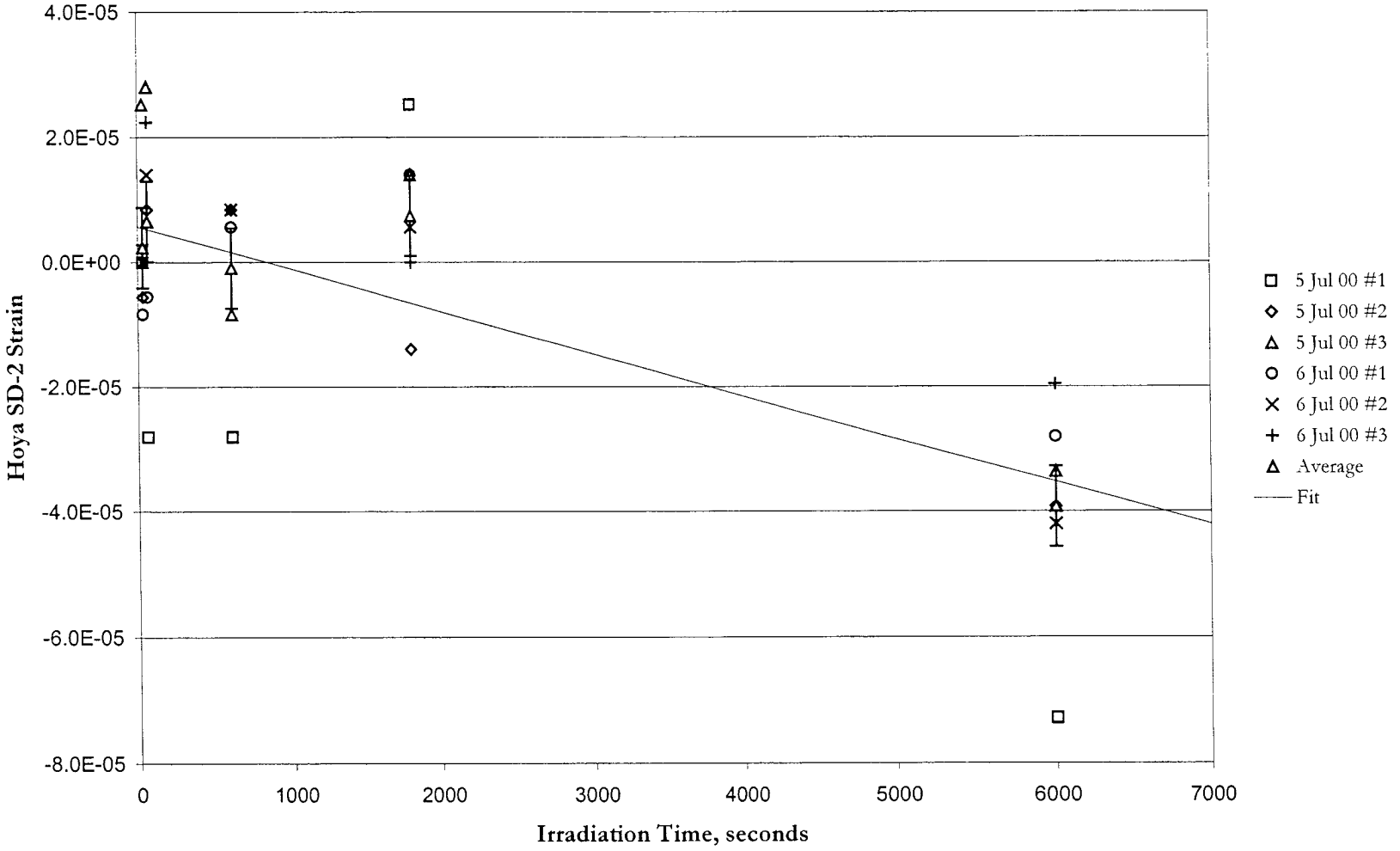

Figure 5.5 Neutron irradiation-induced strain in Hoya SD-2 as measured by sink/float

The Pyrex scatter has an order of magnitude greater scatter than the ideal case, yet is similar to the results attained by Shelby and Conners. The Hoya SD-2 data is more tightly grouped. This may be related to the above observation that these samples seemed to stick less to the liquid's surface. The average of six points attains the precision of the ideal sensitivity of a single measurement.

Additional uncertainty (but not scatter) is introduced by the uncertainty of the thermal expansivity of the liquid. The data analysis here has been done using a value measured by Conners[5.7]. Conners used sink/float to detect gamma-induced density changes in glasses with densities from 2.13 g/cm^3 to 2.52 g/cm^3. Her liquid mixtures were all composed of the same two chemicals used here, tetrabromoethane and bromonaphthalene. She observed that the volumetric thermal expansion for all of her liquids averaged to 840 ppm/°C, with a standard deviation of 8 ppm/°C, and this was the value she then applied to all of her data analysis. A 1% uncertainty in the value for the thermal expansivity of the liquid introduces a 1% uncertainty into the level of strain being measured.

The linear fit shown gives a reduced χ^2 for four degrees of freedom of 1.01 for the Pyrex and 1.58 for the Hoya SD-2, indicating reasonable fits to the data.[5.11] The fit was made to the averaged points using the values in the second row of Table 5.2 as uncertainties, and included the zero point, to which an uncertainty equal with that of the other fitted points was assigned. Figures 5.6 and 5.7 show an enlarged view of the low-irradiation time data, and Figure 5.8 shows a comparison between the Pyrex and the Hoya SD-2 results. Table 5.3 presents a summary of the linear fits.

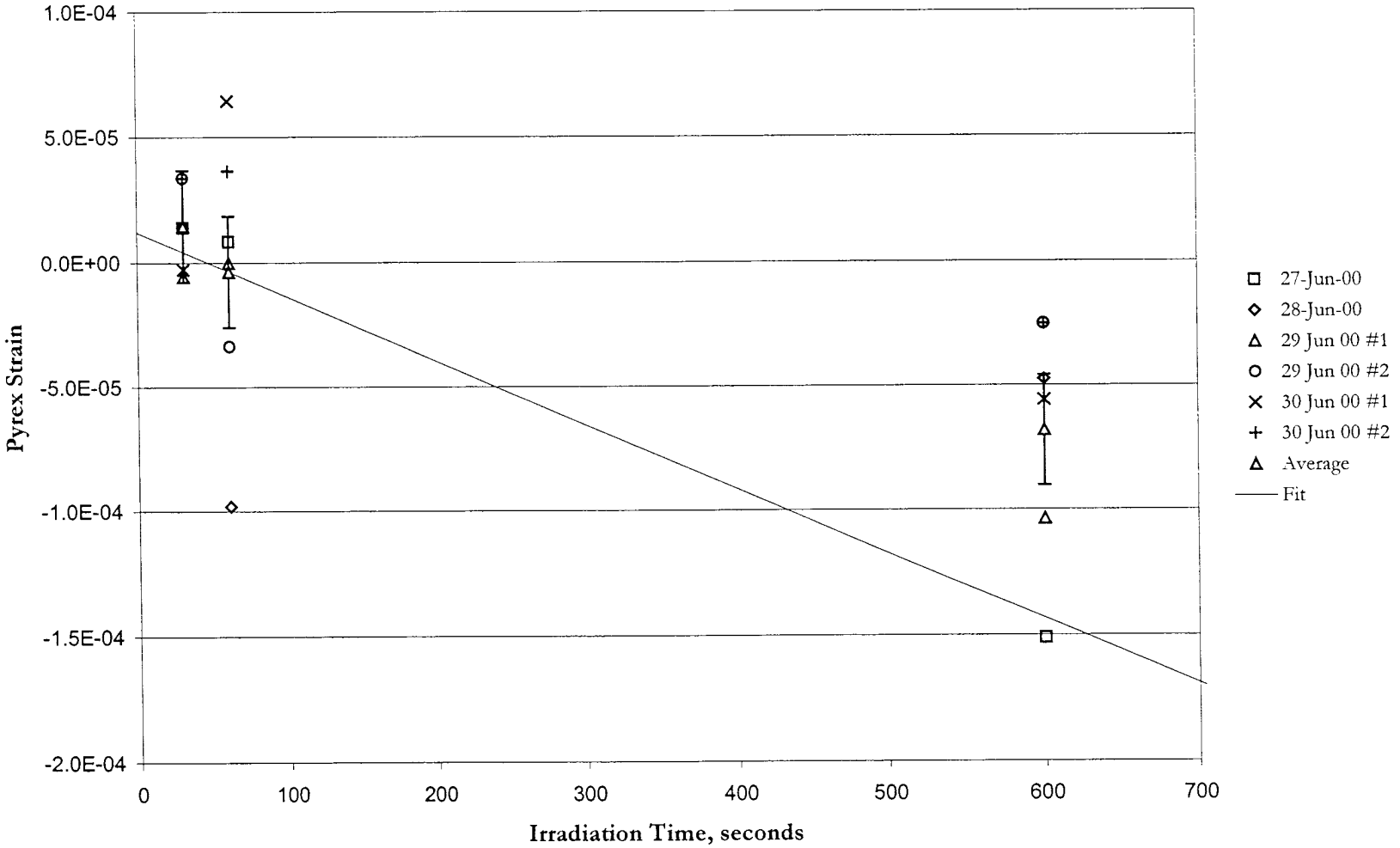

Figure 5.6 Neutron irradiation-induced strain in Pyrex as measured by sink/float technique

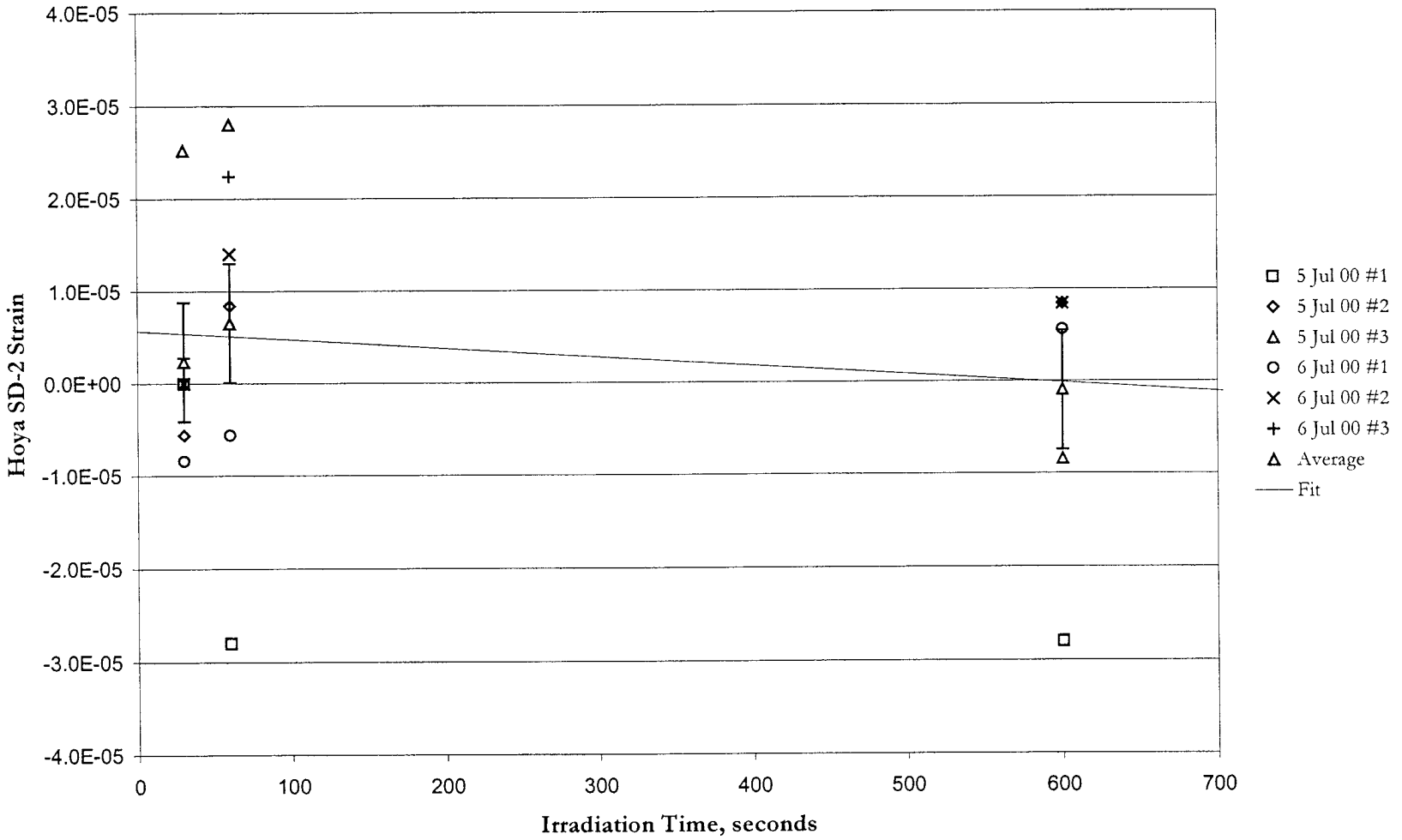

Figure 5.7 Neutron irradiation-induced strain in Hoya SD-2 as measured by sink/float technique

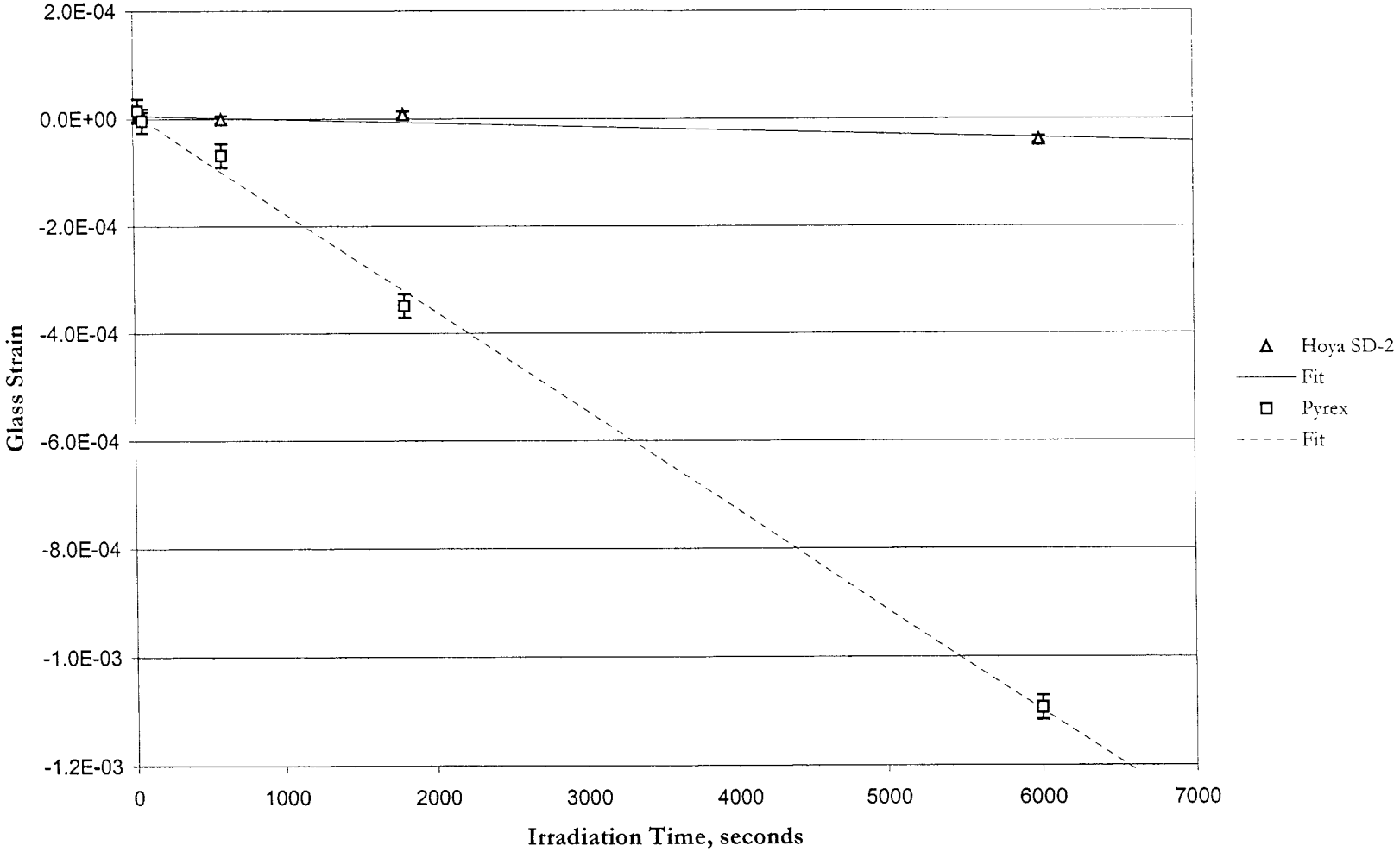

Figure 5.8 Neutron irradiation-induced strain in Pyrex and Hoya SD-2 as measured by sink/float

	Slope, strain/s	Intercept	Reduced χ^2
Pyrex	-1.85×10^{-7}	1.19×10^{-5}	1.01
Hoya SD-2	-6.82×10^{-9}	5.68×10^{-6}	1.58

Table 5.3 Linear fitting results for sink/float data

Using the slopes from the fits shown in Table 5.3 and combining this with the fast and thermal neutron collision cascade information from Chapter 3 and the glass compositions and densities presented in Chapter 2, we obtain the values shown in Table 5.4 for thermal neutron- and fast neutron-induced strain. Neutron incidence into a thickness of 0.78 mm is assumed.

	strain/dpa	strain/n/cm^2 thermal	strain/n/cm^2 fast (1 MeV)
Pyrex	-1.49	-2.77×10^{-20}	-6.07×10^{-21}
Hoya SD-2	-0.19	-1.01×10^{-21}	-7.89×10^{-22}

Table 5.4 Strain in glass related to neutron fluence and displacements per atom

[THIS PAGE INTENTIONALLY LEFT BLANK]

6 DISCUSSION

The results for thermal neutron damage Pyrex agree closely with those obtained by Paymal[6.1-6.4], though there is some question as to whether the results are directly comparable, as Paymal does not explicitly state what his sample dimensions are. He does give several of clues, but they seem to be contradictory. He mentions[6.2] a Pyrex sample size of 5 mm × 5 mm × 5 mm in connection with post-irradiation thermal annealing studies, also using the sink/float method, but does not connect this with the fluence vs. density change measurements. As to the latter, he claims[6.3] without justification that one can estimate the number of thermal neutrons absorbed by the Pyrex according to the relationship: n=3D, where n is the number of boron-absorbed neutrons per cm^3, and D is the number of incident thermal neutrons per cm^2. My calculation based on the boron density in Pyrex and its cross-section for thermal neutron capture yields a relationship of n=2.43D in the limit of a very thin sample. For a 5 mm thick sample, I calculate that the relationship should be n=1.41D. In the case of our 3 mm x 3mm x 0.78 mm samples, an average over the three dimensions gives a relationship of n=1.89D. We might therefore expect to have 1.3 more displacements per volume than Paymal, and about that much more strain. All of the analyses in Chapter 5 assume neutrons incident in the thin (0.78 mm) direction, and therefore a uniform displacement concentration for the glass. For a thick material unidirectionally irradiated, the ~4 mm mean free path of thermal neutrons in Pyrex (~16 mm in Hoya SD-2) can lead to a strain gradient in the material.

Figure 6.1 shows a comparison of the sink/float data from the present study to Paymal's data. As fast neutrons were present in the current data, their effect was accounted

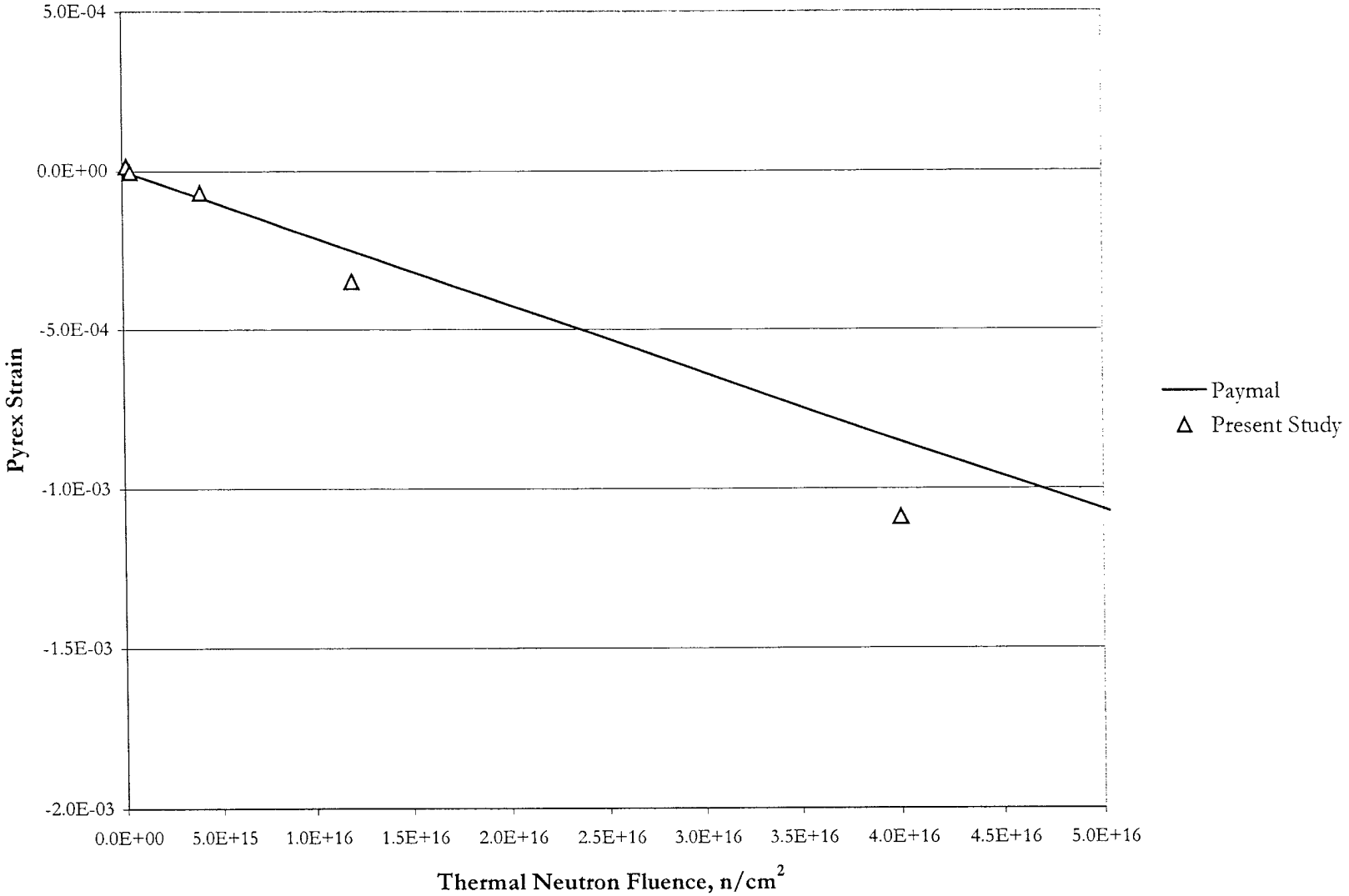

Figure 6.1 Comparison of thermal neutron-induced strain results

for and removed by means of ratioing the total strain by the TRIM numbers for fast and thermal neutron displacements from Chapter 3. The calculated contribution of fast neutrons is only 0.3% of the total strain. The differences between the current results and Paymal's are no greater than those between the results of Shelby and Conners discussed in Chapter 2, and may be related to compositional differences or thickness effects.

With such good agreement for our neutron damage results in Pyrex with those of previous studies, it can be confidently said that Hoya SD-2 glass has greater resistance to compaction due to atomic displacement damage as caused by fast and thermal neutrons than Pyrex. The numbers shown in Table 5.4 clearly demonstrate this, with Hoya SD-2 compacting almost an order of magnitude less for a given 1 MeV neutron fluence.

It is clear that the gamma radiation effect on pre-anodic bonding Hoya SD-2 has not been established by our results in Chapter 4. At the same time, we may have evidence of interfacial, creep, and/or viscous flow phenomena in the MEMS devices used in the gamma experiments. We may also have evidence for the anodic bonding process fundamentally changing the radiation response of Pyrex and Hoya SD-2.

A comparison of the Pyrex pointer beam results with previous sink/float gamma irradiation studies (see Figure 2.4) is shown in Figure 6.2. One might conclude that the pointer beam results, while not showing the expected clear trend of compaction, do not really disagree with these other studies. Sato's data show expansion at these doses, and Shelby's error bars almost overlap those of the pointer beams. Shelby's data, however, follow a very clean curve towards compaction that is confirmed by his measurements at higher doses. At higher doses, Sato's data merge with Shelby's, and with the relative uncertainty shown only one of his measurements differs much from Shelby's. In addition, a

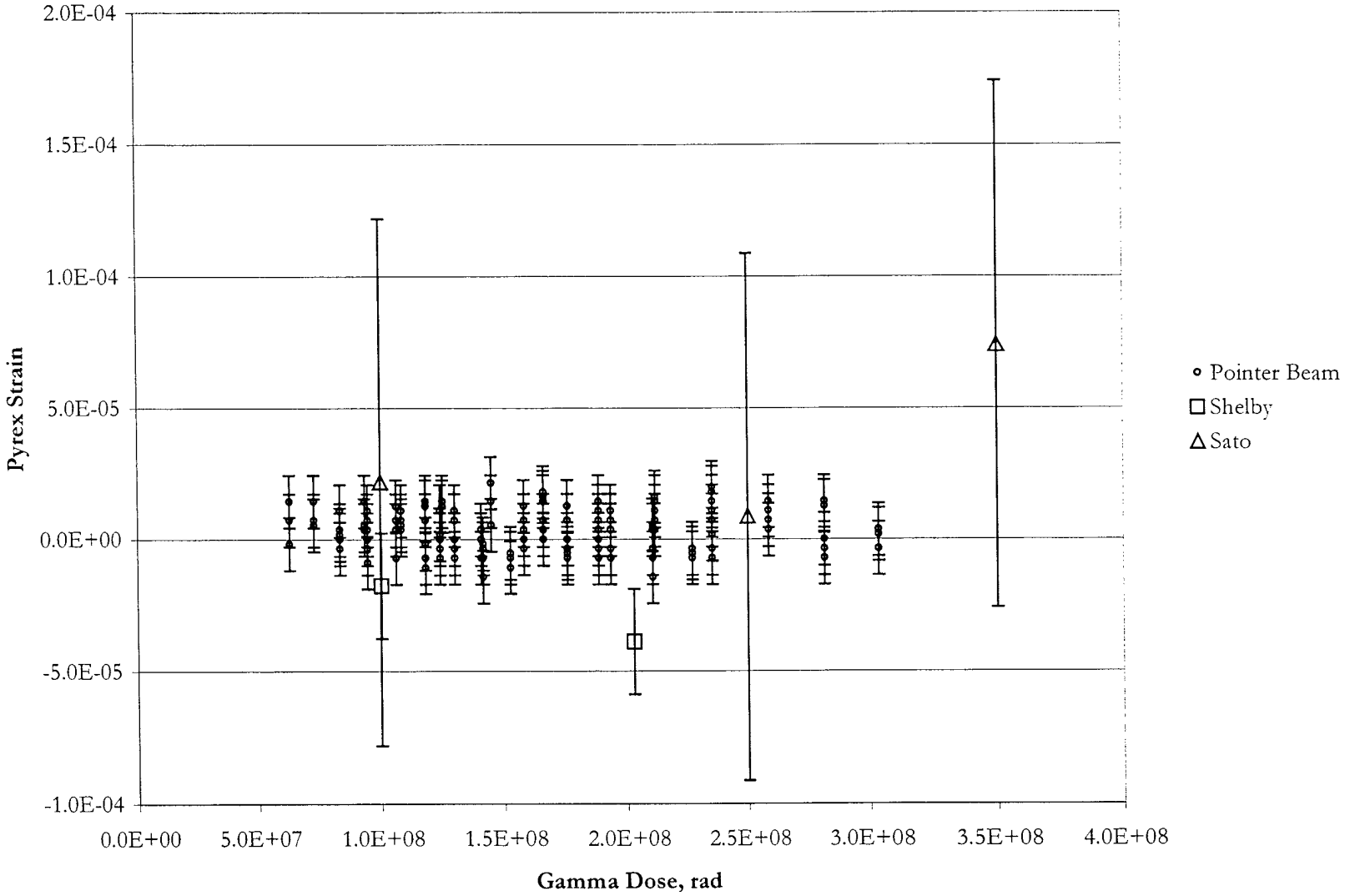

Figure 6.2 Comparison of pointer beam data to previous sink/float work

statistical analysis shows with high degree of certainty of the presence of an upward trend in the pointer beam data, as discussed in Chapter 3.

A valid objection may be raised as to the validity of the TRIM calculations discussed in Chapter 3 for our glasses on the grounds that atomic bonding information was left out of the glass model. Only *relative* magnitudes of displacements were used, however, as the data were used only to convert thermal neutron damage to fast neutron damage within a single glass type. There is some support to be found for the validity of such comparisons to be found in the following observations: 1) the fast neutrons certainly did not do significantly *more* damage in comparison to thermal neutrons than predicted by TRIM, given the close agreement of our neutron compaction results in Pyrex and those of Paymal and 2) the conversion made in section 2.3 of Pyrex thermal neutron strain to fast neutron strain using TRIM results yielded strain values of Pyrex vs. vitreous silica that might have been guessed from the gamma irradiation results shown in Figure 2.6. It is important to also note that no conclusions have been drawn directly from TRIM calculations; *viz*, no predictions have been made of strain based solely on a dpa number, but have been made for fast neutrons based on thermal neutron data that have been multiplied by fast/thermal neutron dpa numbers from TRIM.

It is important to realize that the radiation doses absorbed by samples in the present study are well below the saturation values shown for thermal neutrons in Figure 2.7, for fast neutrons in Figure 2.8, and for gamma irradiation in Figure 2.4 (saturation of strain is not shown here, but a roll-over of the data starts to happen at about 5×10^9 rad). The fundamental relationship of strain-to-dose is certainly not linear. For the relatively small exposures in our experiments, however, a line seems as appropriate as anything else for extrapolating to intermediate or smaller doses of radiation.

7. CONCLUSION

7.1 Summary of principal findings

Density measurements for neutron-irradiated Pyrex and Hoya SD-2 glass samples were carried out. In the analysis of the data, the fast neutron-induced compaction was separated from the primarily thermal neutron-induced damage by ratioing the measured compaction by the average number of displacements in a fast neutron collision cascade relative to the number of displacements for a thermal neutron absorption event. Monte-Carlo calculations of the number of displacements in each type of collision cascade were carried out using TRIM. Table 7.1 summarizes the findings for the relationships between strain and neutron fluence, as well as those between strain and displacements per atom (dpa) for both glasses. Figures 7.1 and 7.2 represent in graphical form the values in Table 7.1.

	Strain/(n/cm^2) thermal	Strain/(n/cm^2) fast (1 MeV)	Strain/dpa
Pyrex	-2.77×10^{-20}	-6.07×10^{-21}	-1.49
Hoya SD-2	-1.01×10^{-21}	-7.89×10^{-22}	-0.19

Table 7.1 Neutron irradiation-induced strains

Silicon pointer beam strain gauges bonded to glass wafers were irradiated with gamma rays. The differential strain between the irradiated Pyrex wafer and pointer beams was found to be much smaller than was predicted based upon previous gamma irradiation studies of Pyrex. It is thought that this surprising result has its origin in radiation-induced creep at the silicon-glass bond layer, and/or in changes in the glass radiation response induced by the anodic bonding process used in the manufacture of the pointer beams.

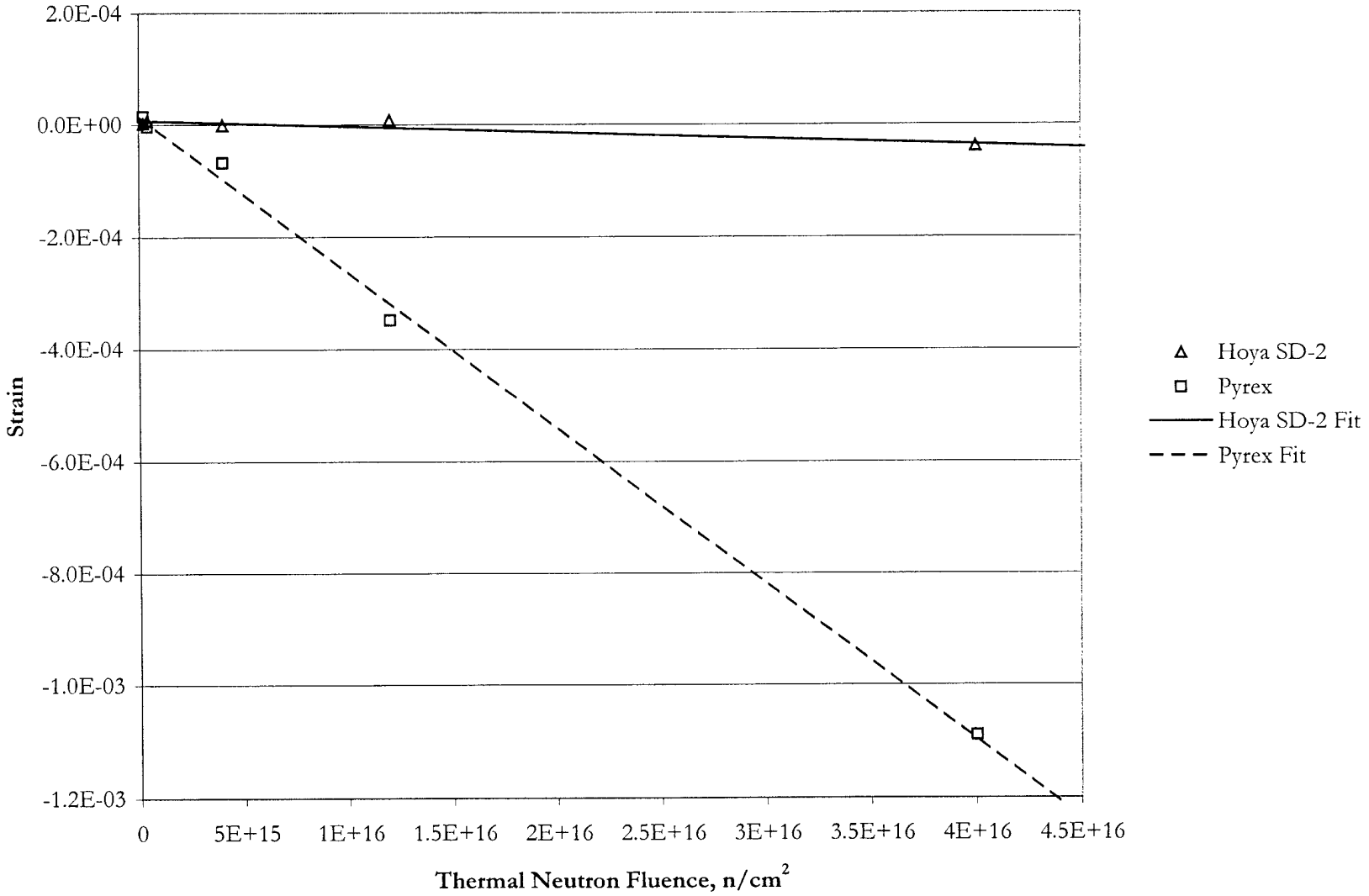

Figure 7.1 Thermal neutron-induced strain

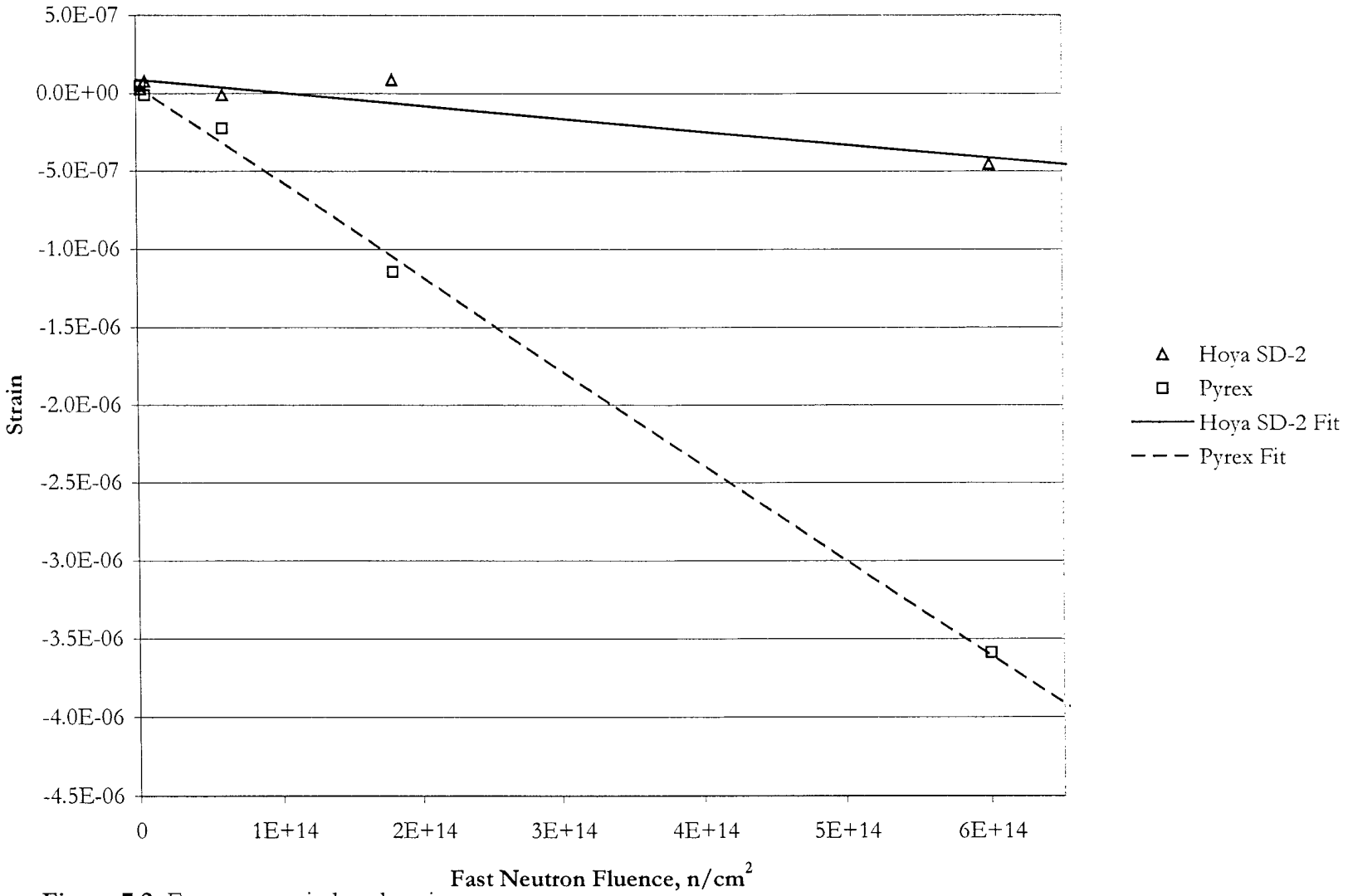

Figure 7.2 Fast neutron-induced strain

The relationships between induced differential strain and gamma dose for both glasses are listed in Table 7.2.

	Strain/rad
Pyrex	$5.24\ (\pm\ 3.78) \times 10^{-15}$
Hoya SD-2	$4.50\ (\pm\ 0.16) \times 10^{-14}$

Table 7.2 Pointer beam gamma irradiation results

7.2 Importance of findings to MEMS

At the beginning of this study, our goal was to identify the radiation-induced dimensional changes in Pyrex and Hoya SD-2. Given a relationship of strain to dose (such as those listed in Tables 1.2 and 1.3), the hope was that one could determine the induced strain in a glass substrate, as well as the resulting stress in the silicon devices bonded to it. With a well defined radiation environment (and a knowledge of the silicon response to radiation), the suitability of Pyrex and Hoya SD-2 as substrates for a particular application could be determined.

Our experiments and calculations produced values relating strain to thermal and fast neutron fluence for both glasses. The relationship between strain and gamma dose has been investigated previously for Pyrex. Our gamma irradiation experiment, aimed at producing a similar relationship for Hoya SD-2, indicates, however, that the radiation effect on anodically bonded MEMS devices is not simply the sum of the parts (the "parts" being the separate radiation-induced dimensional changes on the glass and on the silicon). Interfacial effects or changes made in the glass chemical structure by the anodic bonding process evidently play a role in the overall MEMS radiation response. The relationships between dose and dimensional change established here are not only useful for predicting strains in the separate materials, but provide data necessary to a better understanding of anodically-bonded MEMS devices.

7.3 Suggestions for future work

The pointer beam gamma results highlight the importance of studying the anodically bonded silicon-glass system in order to define the roles of individual system pieces in the overall radiation response. Irradiation-induced creep and viscous flow of the bulk materials and of the anodic bond interface layer should be studied. One possible method might be a variant of the wafer curvature method used in an ion irradiation study of vitreous silica.[7.1] Another approach is fast and thermal neutron irradiation of pointer beam devices. By comparing the sink/float results with pointer beam results, one could compare the effects of radiation in as-supplied glass to its effects in the bonded MEMS device and substrate. Similarly, glass samples should be exposed to gamma radiation and then measured with the sink/float technique.

Sink/float experiments should be performed on irradiated (with gamma rays and neutrons) glass that has been through the anodic bonding process. It is possible to anodically bond a glass wafer to a silicon wafer and then free them from each other. In this fashion, it would be possible to measure the irradiation effects on bulk glass after bonding, and isolate these effects from those at the bond interface.

In addition to those already carried out on thermal neutron irradiated glasses, experiments involving fast neutron exposures should be carried out on both glasses using sink/float measurements and pointer beams. The predictions presented here for fast neutron-induced glass compaction rely on TRIM calculations coupled with experimental data for thermal neutron irradiations. The results thus obtained should be confirmed by direct experiment.

Finally, the thermal calibration of the pointer beams mentioned in Chapter 4 should be performed to confirm the proper function of the pointer beams.

APPENDIX A

Pointer Beam Strain Measurements

Pyrex

Dose, rad	Strain	Dose, rad	Strain	Dose, rad	Strain	Dose, rad	Strain
6.30E+07	-1.79E-06	1.18E+08	7.14E-06	1.53E+08	-5.36E-06	2.11E+08	-1.43E-05
6.30E+07	1.43E-05	1.18E+08	-7.14E-06	1.53E+08	-1.07E-05	2.11E+08	3.57E-06
6.30E+07	7.14E-06	1.18E+08	7.14E-06	1.58E+08	-3.57E-06	2.11E+08	-7.14E-06
7.29E+07	5.36E-06	1.18E+08	1.43E-05	1.58E+08	-3.57E-06	2.11E+08	-3.57E-06
7.29E+07	1.43E-05	1.18E+08	1.25E-05	1.58E+08	0.00E+00	2.12E+08	1.07E-05
7.29E+07	1.43E-05	1.18E+08	-1.07E-05	1.58E+08	0.00E+00	2.12E+08	1.43E-05
7.29E+07	7.14E-06	1.18E+08	-7.14E-06	1.58E+08	0.00E+00	2.12E+08	7.14E-06
7.29E+07	1.43E-05	1.24E+08	-3.57E-06	1.58E+08	1.25E-05	2.12E+08	1.07E-05
8.36E+07	-3.57E-06	1.24E+08	1.79E-06	1.58E+08	7.14E-06	2.12E+08	7.14E-06
8.36E+07	1.79E-06	1.24E+08	-3.57E-06	1.58E+08	3.57E-06	2.12E+08	1.61E-05
8.36E+07	-3.57E-06	1.24E+08	1.07E-05	1.58E+08	-3.57E-06	2.12E+08	7.14E-06
8.36E+07	1.07E-05	1.24E+08	-7.14E-06	1.66E+08	3.57E-06	2.12E+08	1.43E-05
8.36E+07	0.00E+00	1.24E+08	1.07E-05	1.66E+08	1.61E-05	2.12E+08	3.57E-06
8.36E+07	3.57E-06	1.24E+08	0.00E+00	1.66E+08	7.14E-06	2.27E+08	-3.57E-06
8.36E+07	0.00E+00	1.25E+08	1.25E-05	1.66E+08	1.79E-05	2.27E+08	-5.36E-06
9.36E+07	5.36E-06	1.25E+08	1.43E-05	1.66E+08	0.00E+00	2.27E+08	-7.14E-06
9.36E+07	3.57E-06	1.25E+08	1.43E-05	1.66E+08	1.43E-05	2.35E+08	1.07E-05
9.36E+07	1.43E-05	1.30E+08	-7.14E-06	1.66E+08	7.14E-06	2.35E+08	1.79E-06
9.48E+07	-8.93E-06	1.30E+08	1.07E-05	1.76E+08	-3.57E-06	2.35E+08	7.14E-06
9.48E+07	-3.57E-06	1.30E+08	7.14E-06	1.76E+08	-5.36E-06	2.35E+08	-3.57E-06
9.48E+07	-3.57E-06	1.30E+08	-7.14E-06	1.76E+08	0.00E+00	2.35E+08	1.43E-05
9.48E+07	1.07E-05	1.30E+08	0.00E+00	1.76E+08	-7.14E-06	2.35E+08	1.79E-05
9.48E+07	3.57E-06	1.30E+08	-7.14E-06	1.76E+08	7.14E-06	2.35E+08	1.96E-05
9.48E+07	0.00E+00	1.30E+08	-3.57E-06	1.76E+08	7.14E-06	2.35E+08	-7.14E-06
9.48E+07	7.14E-06	1.41E+08	-7.14E-06	1.76E+08	1.25E-05	2.35E+08	1.43E-05
9.48E+07	3.57E-06	1.41E+08	0.00E+00	1.76E+08	-7.14E-06	2.59E+08	1.07E-05
9.48E+07	0.00E+00	1.41E+08	3.57E-06	1.76E+08	-3.57E-06	2.59E+08	1.43E-05
1.06E+08	3.57E-06	1.41E+08	3.57E-06	1.88E+08	7.14E-06	2.59E+08	1.43E-05
1.06E+08	-7.14E-06	1.41E+08	0.00E+00	1.88E+08	3.57E-06	2.59E+08	7.14E-06
1.06E+08	7.14E-06	1.41E+08	3.57E-06	1.88E+08	1.07E-05	2.59E+08	3.57E-06
1.06E+08	7.14E-06	1.41E+08	3.57E-06	1.88E+08	1.43E-05	2.59E+08	1.43E-05
1.06E+08	7.14E-06	1.41E+08	3.57E-06	1.88E+08	-7.14E-06	2.59E+08	7.14E-06
1.06E+08	1.25E-05	1.42E+08	-1.79E-06	1.88E+08	1.43E-05	2.82E+08	1.25E-05
1.06E+08	7.14E-06	1.42E+08	-1.43E-05	1.88E+08	1.43E-05	2.82E+08	-7.14E-06
1.06E+08	3.57E-06	1.42E+08	-3.57E-06	1.88E+08	-3.57E-06	2.82E+08	1.43E-05
1.06E+08	-7.14E-06	1.42E+08	-7.14E-06	1.93E+08	-7.14E-06	2.82E+08	-3.57E-06
1.08E+08	5.36E-06	1.42E+08	-1.43E-05	1.93E+08	1.07E-05	2.82E+08	0.00E+00
1.08E+08	7.14E-06	1.45E+08	5.36E-06	1.93E+08	7.14E-06	3.04E+08	3.57E-06
1.08E+08	1.07E-05	1.45E+08	2.14E-05	1.93E+08	-7.14E-06	3.04E+08	1.79E-06
1.08E+08	1.07E-05	1.45E+08	1.43E-05	1.93E+08	-3.57E-06	3.04E+08	-3.57E-06
1.08E+08	3.57E-06	1.45E+08	1.43E-05	1.93E+08	3.57E-06		
1.18E+08	-1.07E-05	1.45E+08	1.43E-05	1.93E+08	-3.57E-06		
1.18E+08	-1.79E-06	1.53E+08	-7.14E-06	2.11E+08	5.36E-06		

Hoya SD-2

Dose, rad	Strain	Dose, rad	Strain	Dose, rad	Strain	Dose, rad	Strain
2.25E+07	0.00E+00	4.90E+07	7.14E-06	6.92E+07	0.00E+00	9.57E+07	7.14E-06
2.25E+07	0.00E+00	4.90E+07	-7.14E-06	7.38E+07	-2.38E-06	9.57E+07	7.14E-06
2.25E+07	0.00E+00	4.90E+07	7.14E-06	7.38E+07	1.43E-05	9.57E+07	1.43E-05
2.68E+07	0.00E+00	4.90E+07	0.00E+00	7.38E+07	0.00E+00	1.07E+08	0.00E+00
2.68E+07	0.00E+00	4.90E+07	0.00E+00	7.38E+07	0.00E+00	1.07E+08	0.00E+00
2.68E+07	7.14E-06	4.90E+07	0.00E+00	7.38E+07	7.14E-06	1.07E+08	7.14E-06
2.68E+07	0.00E+00	5.46E+07	0.00E+00	7.38E+07	0.00E+00	1.07E+08	7.14E-06
2.68E+07	7.14E-06	5.46E+07	0.00E+00	7.38E+07	7.14E-06	1.07E+08	1.43E-05
3.17E+07	3.57E-06	5.46E+07	0.00E+00	7.70E+07	7.14E-06	1.08E+08	1.43E-05
3.17E+07	7.14E-06	5.46E+07	7.14E-06	7.70E+07	7.14E-06	1.08E+08	1.43E-05
3.17E+07	3.57E-06	5.46E+07	0.00E+00	7.70E+07	0.00E+00	1.08E+08	1.43E-05
3.17E+07	7.14E-06	5.46E+07	0.00E+00	8.11E+07	0.00E+00	1.08E+08	7.14E-06
3.17E+07	3.57E-06	5.56E+07	3.57E-06	8.11E+07	0.00E+00	1.08E+08	3.57E-06
3.17E+07	0.00E+00	5.56E+07	0.00E+00	8.11E+07	3.57E-06	1.08E+08	1.43E-05
3.70E+07	7.14E-06	5.56E+07	0.00E+00	8.11E+07	7.14E-06	1.10E+08	-2.38E-06
3.70E+07	7.14E-06	5.56E+07	-7.14E-06	8.11E+07	-3.57E-06	1.10E+08	7.14E-06
3.70E+07	0.00E+00	5.56E+07	0.00E+00	8.11E+07	-7.14E-06	1.10E+08	-7.14E-06
3.70E+07	0.00E+00	5.56E+07	0.00E+00	8.45E+07	0.00E+00	1.10E+08	-3.57E-06
3.70E+07	0.00E+00	5.56E+07	1.43E-05	8.45E+07	0.00E+00	1.10E+08	3.57E-06
3.70E+07	0.00E+00	5.75E+07	0.00E+00	8.45E+07	0.00E+00	1.10E+08	0.00E+00
3.70E+07	7.14E-06	5.75E+07	0.00E+00	8.45E+07	1.43E-05	1.10E+08	0.00E+00
3.70E+07	0.00E+00	5.75E+07	0.00E+00	8.45E+07	0.00E+00	1.19E+08	0.00E+00
3.70E+07	0.00E+00	6.23E+07	0.00E+00	8.45E+07	1.43E-05	1.19E+08	0.00E+00
3.87E+07	-7.14E-06	6.23E+07	3.57E-06	8.45E+07	0.00E+00	1.19E+08	0.00E+00
3.87E+07	0.00E+00	6.23E+07	0.00E+00	8.45E+07	0.00E+00	1.25E+08	3.57E-06
3.87E+07	0.00E+00	6.23E+07	0.00E+00	9.18E+07	7.14E-06	1.25E+08	0.00E+00
4.28E+07	1.19E-06	6.23E+07	3.57E-06	9.18E+07	1.43E-05	1.25E+08	-7.14E-06
4.28E+07	7.14E-06	6.38E+07	0.00E+00	9.18E+07	1.07E-05	1.25E+08	3.57E-06
4.28E+07	0.00E+00	6.38E+07	7.14E-06	9.18E+07	3.57E-06	1.25E+08	-3.57E-06
4.28E+07	0.00E+00	6.38E+07	-7.14E-06	9.18E+07	1.07E-05	1.25E+08	3.57E-06
4.28E+07	7.14E-06	6.38E+07	0.00E+00	9.47E+07	3.57E-06	1.25E+08	-3.57E-06
4.28E+07	0.00E+00	6.38E+07	0.00E+00	9.47E+07	3.57E-06	1.25E+08	-3.57E-06
4.28E+07	0.00E+00	6.38E+07	7.14E-06	9.47E+07	-3.57E-06	1.27E+08	1.43E-05
4.28E+07	7.14E-06	6.38E+07	7.14E-06	9.47E+07	-7.14E-06	1.27E+08	1.43E-05
4.28E+07	0.00E+00	6.38E+07	0.00E+00	9.47E+07	-3.57E-06	1.27E+08	1.07E-05
4.62E+07	-7.14E-06	6.38E+07	0.00E+00	9.47E+07	3.57E-06	1.27E+08	0.00E+00
4.62E+07	-7.14E-06	6.87E+07	-7.14E-06	9.47E+07	7.14E-06	1.27E+08	0.00E+00
4.62E+07	0.00E+00	6.87E+07	-3.57E-06	9.47E+07	-7.14E-06	1.27E+08	7.14E-06
4.62E+07	-7.14E-06	6.87E+07	0.00E+00	9.47E+07	-3.57E-06	1.27E+08	1.43E-05
4.62E+07	0.00E+00	6.87E+07	0.00E+00	9.57E+07	0.00E+00	1.27E+08	3.57E-06
4.90E+07	7.14E-06	6.87E+07	0.00E+00	9.57E+07	0.00E+00	1.27E+08	0.00E+00
4.90E+07	7.14E-06	6.92E+07	3.57E-06	9.57E+07	7.14E-06	1.42E+08	1.07E-05
4.90E+07	0.00E+00	6.92E+07	7.14E-06	9.57E+07	7.14E-06	1.42E+08	0.00E+00

Hoya SD-2 (continued)

Dose, rad	Strain	Dose, rad	Strain	Dose, rad	Strain	Dose, rad	Strain
1.42E+08	0.00E+00	1.88E+08	0.00E+00	1.94E+08	7.14E-06	2.85E+08	2.14E-05
1.42E+08	0.00E+00	1.88E+08	0.00E+00	1.94E+08	7.14E-06	2.85E+08	1.07E-05
1.42E+08	0.00E+00	1.88E+08	2.14E-05	1.94E+08	1.43E-05	2.85E+08	1.79E-05
1.42E+08	0.00E+00	1.88E+08	0.00E+00	1.94E+08	0.00E+00	2.85E+08	2.50E-05
1.42E+08	1.07E-05	1.88E+08	0.00E+00	1.94E+08	0.00E+00	2.85E+08	1.07E-05
1.47E+08	4.76E-06	1.88E+08	7.14E-06	1.94E+08	1.43E-05	2.85E+08	0.00E+00
1.47E+08	1.43E-05	1.88E+08	0.00E+00	2.13E+08	7.14E-06	2.85E+08	3.57E-06
1.47E+08	3.57E-06	1.88E+08	0.00E+00	2.13E+08	1.43E-05	2.85E+08	7.14E-06
1.47E+08	7.14E-06	1.88E+08	1.43E-05	2.13E+08	1.07E-05	2.85E+08	-3.57E-06
1.47E+08	1.43E-05	1.88E+08	0.00E+00	2.13E+08	1.43E-05	2.85E+08	1.43E-05
1.47E+08	7.14E-06	1.88E+08	7.14E-06	2.13E+08	1.43E-05	2.85E+08	1.07E-05
1.47E+08	7.14E-06	1.88E+08	7.14E-06	2.37E+08	7.14E-06	2.85E+08	7.14E-06
1.60E+08	0.00E+00	1.90E+08	2.14E-05	2.37E+08	2.14E-05	2.88E+08	1.43E-05
1.60E+08	7.14E-06	1.90E+08	1.43E-05	2.37E+08	1.79E-05	2.88E+08	1.43E-05
1.60E+08	-3.57E-06	1.90E+08	7.14E-06	2.47E+08	1.43E-05	2.88E+08	-3.57E-06
1.60E+08	0.00E+00	1.90E+08	3.57E-06	2.47E+08	1.43E-05	2.88E+08	3.57E-06
1.60E+08	-3.57E-06	1.90E+08	7.14E-06	2.47E+08	1.55E-05	2.88E+08	7.14E-06
1.67E+08	-7.14E-06	1.90E+08	1.07E-05	2.60E+08	1.07E-05	2.88E+08	1.43E-05
1.67E+08	1.43E-05	1.90E+08	2.14E-05	2.60E+08	-3.57E-06	2.88E+08	7.14E-06
1.67E+08	2.62E-05	1.92E+08	1.43E-05	2.60E+08	0.00E+00	2.88E+08	1.07E-05
1.68E+08	1.43E-05	1.92E+08	0.00E+00	2.60E+08	3.57E-06	2.88E+08	2.14E-05
1.68E+08	2.14E-05	1.92E+08	2.14E-05	2.60E+08	1.43E-05	2.88E+08	3.57E-06
1.68E+08	0.00E+00	1.92E+08	-7.14E-06	2.71E+08	1.07E-05	2.88E+08	0.00E+00
1.68E+08	1.07E-05	1.92E+08	2.86E-05	2.71E+08	0.00E+00	2.88E+08	3.57E-06
1.68E+08	0.00E+00	1.92E+08	2.86E-05	2.71E+08	-3.57E-06	2.88E+08	1.43E-05
1.68E+08	1.43E-05	1.92E+08	0.00E+00	2.71E+08	-3.57E-06	2.88E+08	1.07E-05
1.68E+08	3.57E-06	1.92E+08	7.14E-06	2.71E+08	3.57E-06	2.88E+08	7.14E-06
1.68E+08	1.43E-05	1.92E+08	7.14E-06	2.71E+08	7.14E-06	2.88E+08	1.43E-05
1.75E+08	0.00E+00	1.92E+08	7.14E-06	2.71E+08	1.43E-05	3.31E+08	1.43E-05
1.75E+08	0.00E+00	1.92E+08	-7.14E-06	2.79E+08	1.43E-05	3.31E+08	2.14E-05
1.75E+08	7.14E-06	1.92E+08	0.00E+00	2.79E+08	0.00E+00	3.31E+08	2.62E-05
1.75E+08	7.14E-06	1.92E+08	-7.14E-06	2.79E+08	1.07E-05	3.48E+08	1.43E-05
1.75E+08	0.00E+00	1.92E+08	1.43E-05	2.79E+08	-3.57E-06	3.48E+08	7.14E-06
1.77E+08	3.57E-06	1.94E+08	2.14E-05	2.79E+08	1.07E-05	3.48E+08	3.57E-06
1.77E+08	0.00E+00	1.94E+08	0.00E+00	2.79E+08	3.57E-06	3.48E+08	1.43E-05
1.77E+08	1.43E-05	1.94E+08	7.14E-06	2.79E+08	0.00E+00	3.48E+08	1.79E-05
1.82E+08	1.43E-05	1.94E+08	7.14E-06	2.79E+08	-3.57E-06	3.63E+08	1.43E-05
1.82E+08	0.00E+00	1.94E+08	0.00E+00	2.79E+08	7.14E-06	3.63E+08	7.14E-06
1.82E+08	0.00E+00	1.94E+08	2.14E-05	2.79E+08	1.43E-05	3.63E+08	7.14E-06
1.82E+08	0.00E+00	1.94E+08	1.43E-05	2.79E+08	7.14E-06	3.63E+08	1.43E-05
1.82E+08	0.00E+00	1.94E+08	2.14E-05	2.79E+08	7.14E-06	3.63E+08	7.14E-06
1.82E+08	0.00E+00	1.94E+08	2.86E-05	2.85E+08	3.57E-06	3.63E+08	1.43E-05
1.82E+08	2.14E-05	1.94E+08	7.14E-06	2.85E+08	7.14E-06	3.63E+08	2.14E-05

Hoya SD-2 (continued)

Dose, rad	Strain
3.73E+08	2.14E-05
3.73E+08	2.14E-05
3.73E+08	2.50E-05
3.74E+08	2.14E-05
3.74E+08	1.43E-05
3.74E+08	1.07E-05
3.74E+08	7.14E-06
3.74E+08	7.14E-06
3.74E+08	2.14E-05
3.74E+08	2.86E-05
3.74E+08	2.14E-05
3.74E+08	1.43E-05
3.81E+08	1.43E-05
3.81E+08	2.14E-05
3.81E+08	2.86E-05
3.81E+08	2.14E-05
3.81E+08	2.86E-05
3.81E+08	2.86E-05
3.81E+08	1.43E-05
3.81E+08	7.14E-06
3.81E+08	1.43E-05
3.81E+08	1.43E-05
3.81E+08	7.14E-06
3.81E+08	2.86E-05
3.81E+08	2.50E-05
3.81E+08	2.14E-05
3.85E+08	2.14E-05
3.85E+08	2.14E-05
3.85E+08	1.43E-05
3.85E+08	7.14E-06
3.85E+08	1.79E-05
3.85E+08	2.86E-05
3.85E+08	1.43E-05
3.85E+08	1.43E-05
3.85E+08	2.86E-05
3.85E+08	7.14E-06
3.85E+08	1.43E-05
3.85E+08	1.43E-05
3.85E+08	2.14E-05
3.85E+08	2.50E-05
3.85E+08	1.43E-05
3.85E+08	2.14E-05

APPENDIX B
Sink/float measurements

Pyrex

27 Jun 00	Sink, °C	Ref sink , °C	ΔT	α liquid	Δd/d	ΔL/L
A	32.34	32.29	0.05	8.40E-04	-4.20E-05	1.40E-05
B	32.32	32.29	0.03	8.40E-04	-2.52E-05	8.40E-06
C	31.72	32.26	-0.54	8.40E-04	4.54E-04	-1.51E-04
D	31.13	32.39	-1.26	8.40E-04	1.06E-03	-3.53E-04
E	28.33	32.19	-3.86	8.40E-04	3.24E-03	-1.08E-03
28 Jun 00						
A	32.24	32.19	0.05	8.40E-04	-4.20E-05	1.40E-05
B	32.18	32.53	-0.35	8.40E-04	2.94E-04	-9.80E-05
C	31.87	32.04	-0.17	8.40E-04	1.43E-04	-4.76E-05
D	30.84	32.35	-1.51	8.40E-04	1.27E-03	-4.23E-04
E	28.14	31.96	-3.82	8.40E-04	3.21E-03	-1.07E-03
29 Jun 00 #1						
A	32.29	32.31	-0.02	8.40E-04	1.68E-05	-5.60E-06
B	32.24	32.24	0	8.40E-04	0.00E+00	0.00E+00
C	32.02	32.39	-0.37	8.40E-04	3.11E-04	-1.04E-04
D	30.94	32.36	-1.42	8.40E-04	1.19E-03	-3.98E-04
E	28.49	32.35	-3.86	8.40E-04	3.24E-03	-1.08E-03
29 Jun 00 #2						
A	32.43	32.31	0.12	8.40E-04	-1.01E-04	3.36E-05
B	32.24	32.36	-0.12	8.40E-04	1.01E-04	-3.36E-05
C	31.89	31.98	-0.09	8.40E-04	7.56E-05	-2.52E-05
D	31	32.4	-1.4	8.40E-04	1.18E-03	-3.92E-04
E	28.65	32.12	-3.47	8.40E-04	2.91E-03	-9.72E-04
30 Jun 00 #1						
A	32.27	32.28	-0.01	8.40E-04	8.40E-06	-2.80E-06
B	32.25	32.02	0.23	8.40E-04	-1.93E-04	6.44E-05
C	31.74	31.94	-0.2	8.40E-04	1.68E-04	-5.60E-05
D	30.93	31.89	-0.96	8.40E-04	8.06E-04	-2.69E-04
E	28.26	32.36	-4.1	8.40E-04	3.44E-03	-1.15E-03
30 Jun 00 #2						
A	32.24	32.12	0.12	8.40E-04	-1.01E-04	3.36E-05
B	32.3	32.17	0.13	8.40E-04	-1.09E-04	3.64E-05
C	31.86	31.95	-0.09	8.40E-04	7.56E-05	-2.52E-05
D	31.03	31.96	-0.93	8.40E-04	7.81E-04	-2.60E-04
E	28.15	32.46	-4.31	8.40E-04	3.62E-03	-1.21E-03
AVERAGE						
A	32.30	32.25	5.17E-02	8.40E-04	-4.34E-05	1.45E-05
B	32.26	32.27	-1.33E-02	8.40E-04	1.12E-05	-3.73E-06
C	31.85	32.09	-2.43E-01	8.40E-04	2.04E-04	-6.81E-05
D	30.98	32.23	-1.25E+00	8.40E-04	1.05E-03	-3.49E-04
E	28.34	32.24	-3.90E+00	8.40E-04	3.28E-03	-1.09E-03
Standard Dev						
A	0.07	0.08	6.05E-02		5.08E-05	1.69E-05
B	0.05	0.17	2.03E-01		1.71E-04	5.69E-05
C	0.11	0.19	1.78E-01		1.49E-04	4.98E-05
D	0.10	0.23	2.47E-01		2.08E-04	6.92E-05
E	0.20	0.18	2.84E-01		2.38E-04	7.94E-05
					avg std dev	5.45E-05
					std dev of avg	2.22E-05

Hoya SD-2

5 Jul 00 #1	Sink, °C	Ref sink, °C	ΔT	α liquid	Δd/d	ΔL/L
A	22.87	22.87	0	8.40E-04	0.00E+00	0.00E+00
B	22.78	22.88	-0.1	8.40E-04	8.40E-05	-2.80E-05
C	22.66	22.76	-0.1	8.40E-04	8.40E-05	-2.80E-05
D	22.78	22.69	0.09	8.40E-04	-7.56E-05	2.52E-05
E	22.53	22.79	-0.26	8.40E-04	2.18E-04	-7.28E-05
5 Jul 00 #2						
A	22.77	22.79	-0.02	8.40E-04	1.68E-05	-5.60E-06
B	22.8	22.77	0.03	8.40E-04	-2.52E-05	8.40E-06
C	22.8	22.77	0.03	8.40E-04	-2.52E-05	8.40E-06
D	22.69	22.74	-0.05	8.40E-04	4.20E-05	-1.40E-05
E	22.52	22.66	-0.14	8.40E-04	1.18E-04	-3.92E-05
5 Jul 00 #3						
A	22.81	22.72	0.09	8.40E-04	-7.56E-05	2.52E-05
B	22.91	22.81	0.1	8.40E-04	-8.40E-05	2.80E-05
C	22.85	22.88	-0.03	8.40E-04	2.52E-05	-8.40E-06
D	22.8	22.75	0.05	8.40E-04	-4.20E-05	1.40E-05
E	22.69	22.81	-0.12	8.40E-04	1.01E-04	-3.36E-05
6 Jul 00 #1						
A	22.71	22.74	-0.03	8.40E-04	2.52E-05	-8.40E-06
B	22.66	22.68	-0.02	8.40E-04	1.68E-05	-5.60E-06
C	22.71	22.69	0.02	8.40E-04	-1.68E-05	5.60E-06
D	22.74	22.69	0.05	8.40E-04	-4.20E-05	1.40E-05
E	22.56	22.66	-0.1	8.40E-04	8.40E-05	-2.80E-05
6 Jul 00 #2						
A	22.77	22.77	0	8.40E-04	0.00E+00	0.00E+00
B	22.78	22.73	0.05	8.40E-04	-4.20E-05	1.40E-05
C	22.85	22.82	0.03	8.40E-04	-2.52E-05	8.40E-06
D	22.74	22.72	0.02	8.40E-04	-1.68E-05	5.60E-06
E	22.61	22.76	-0.15	8.40E-04	1.26E-04	-4.20E-05
6 Jul 00 #3						
A	22.71	22.7	0.01	8.40E-04	-8.40E-06	2.80E-06
B	22.68	22.6	0.08	8.40E-04	-6.72E-05	2.24E-05
C	22.83	22.8	0.03	8.40E-04	-2.52E-05	8.40E-06
D	22.68	22.68	0	8.40E-04	0.00E+00	0.00E+00
E	22.61	22.68	-0.07	8.40E-04	5.88E-05	-1.96E-05
AVERAGE						
A	22.77	22.77	8.33E-03	8.40E-04	-7.00E-06	2.33E-06
B	22.77	22.75	2.33E-02	8.40E-04	-1.96E-05	6.53E-06
C	22.78	22.79	-3.33E-03	8.40E-04	2.80E-06	-9.33E-07
D	22.74	22.71	2.67E-02	8.40E-04	-2.24E-05	7.47E-06
E	22.59	22.73	-1.40E-01	8.40E-04	1.18E-04	-3.92E-05
Standard Dev						
A	0.06	0.06	4.26E-02	0.00E+00	3.58E-05	1.19E-05
B	0.09	0.10	7.34E-02	0.00E+00	6.17E-05	2.06E-05
C	0.08	0.06	5.28E-02	0.00E+00	4.43E-05	1.48E-05
D	0.05	0.03	4.84E-02	0.00E+00	4.07E-05	1.36E-05
E	0.06	0.07	6.54E-02	0.00E+00	5.50E-05	1.83E-05
					avg std dev	1.58E-05
					std dev of avg	6.46E-06

REFERENCES

Chapter 1

1.1 J. Kenneth Shultis and Richard E. Faw, *Radiation Shielding*, Prentice-Hall, 1996, p. 56
1.2 Corning Incorporated, Corning, NY, 14831
1.3 Hoya Corporation, 2-7-5 Naka-Ochiai, Shinjuku-ku, Tokyo 161-8525 Japan
1.4 J.E. Shelby, "Effect of radiation on the physical properties of borosilicate glasses," Journal of Applied Physics, **51** (5), May 1980, p. 2561-65
1.5 S.L. Conners, "Effects of Gamma Radiation on the Structure and Properties of Borosilicate Glasses", M.S. Thesis, 1992, Alfred University, Alfred, New York
1.6 S. Sato, "Radiation Effect of Simulated Waste Glass Irradiated with Ion, Electron, and γ-Ray," Nuclear Instruments and Methods in Physics Research, **B1** (1984), p. 534-537
1.7 W.A. Zdaniewski, T.E. Easler, and R.C. Bradt, "Gamma Radiation Effects of the Strength of a Borosilicate Glass," Journal of the American Ceramic Society, **66** (5), May 1983, p. 311-313
1.8 J. Paymal, "Quelques Effets des Réactions (n, alpha) dans les Verres," Verres et Réfractaires, No 5, Sept-Oct 1961, p. 259-269
1.9 ibid, No 6, Nov-Dec, 1961, p. 341-351
1.10 ibid, No 1, Jan-Feb 1962, p.20-30
1.11 ibid, No 2, Mar-Apr 1962, p.100-113
1.12 W. Primak, "Fast-Neutron-Induced Changes in Quartz and Vitreous Silica," Physical Review, 110 (6), June 15, 1958, p. 1240-1254
1.13 N.E. Moyer and R.C. Buschert, "X-Ray Lattice Parameter Studies of Electron-Irradiated Silicon," Radiation Effects in Semiconductors, Plenum, NY, 1968, p. 444-451

Chapter 2

2.1 R. Zallen, *The Physics of Amorphous Solids*, John Wiley & Sons, Inc., 1983, p. 6
2.2 W.H. Zachariasen, "The Atomic Arrangement in Glass," Journal of the American Chemical Society, **54**, 1932, p. 3841
2.3 Y.-M. Chiang, D.P. Birnie III, and W.D. Kingery, *Physical Ceramics*, John Wiley & Sons, Inc., 1997, p. 89
2.4 N.R. Moody, S.L. Robinson, J.P. Lucas, J. Handrock, and R.Q. Hwang, "Effects of Radiation and Hydrogen on the Fracture Resistance of Borosilicate Glasses," Journal of the American Ceramic Society, **78** (1), 1995, p. 114-120
2.5 H.A. El-Batal, "Effect of Thermal Neutrons on Thermal Expansion of some Ternary Borate Glasses," Nuclear Instruments and Methods in Physics Research, **B88**, 1994, p.411-417
2.6 W.J. Weber, R.C. Ewing, C.A. Angell, G.W. Arnold, A.N. Cormack, J.M. Delaye, D.L. Griscom, L.W. Hobbs, A. Navrotsky, D.L. Price, A.M. Stoneham, M.C. Weinberg, "Radiation Effects in Glasses Used for Immobilization of High-Level Waste and Plutonium Disposition," Journal of Materials Research, **12** (8), August 1997, p. 1946-1975
2.7 J.H. Crawford, Jr., "Radiation Damage in Solids: A Survey," Ceramic Bulletin, **44** (12), 1965
2.8 C.S. Marians and L.W. Hobbs, Journal of Non-Crystalline Solids, **119**, 1990, p. 269

2.9 F.M. Ezz-Eldin and H.A. El-Batal, "Radiation Effects on Thermal Expansion of Some Ternary Alkali-Silicate Glasses," Journal of Non-Crystalline Solids, **152**, 1993, p. 195-200
2.10 J.B. Bates et al., Journal of Chemical Physics, **61**, 1974, p. 4163
2.11 L.W. Hobbs, "Network topology in aperiodic networks," Journal of Non-Crystalline Solids, **192 & 193**, 1995, p. 79-91
2.12 J. Paymal, "Quelques Effets des Réactions (n, alpha) dans les Verres," Verres et Réfractaires, No 5, Sept-Oct 1961, p. 259-269
2.13 ibid, No 6, Nov-Dec, 1961, p. 341-351
2.14 ibid, No 1, Jan-Feb 1962, p.20-30
2.15 ibid, No 2, Mar-Apr 1962, p.100-113
2.16 J.E. Shelby, "Effect of radiation on the physical properties of borosilicate glasses," Journal of Applied Physics, **51** (5), May 1980, p. 2561-65
2.17 S.L. Conners, "Effects of Gamma Radiation on the Structure and Properties of Borosilicate Glasses", M.S. Thesis, 1992, Alfred University, Alfred, New York
2.18 S. Sato, "Radiation Effect of Simulated Waste Glass Irradiated with Ion, Electron, and γ-Ray," Nuclear Instruments and Methods in Physics Research, **B1** (1984), p. 534-537
2.19 W.A. Zdaniewski, T.E. Easler, and R.C. Bradt, "Gamma Radiation Effects of the Strength of a Borosilicate Glass," Journal of the American Ceramic Society, **66** (5), May 1983, p. 311-313
2.20 P.L. Higby, E.J. Friebele, C.M. Shaw, and M. Rajaram, "Radiation Effects on the Physical Properties of Low-Expansion-Coefficient Glasses and Ceramics," Journal of the American Ceramic Society, **71** (9), 1988, p. 796-802
2.21 W. Primak and R. Kampwirth, "The Radiation Compaction of Vitreous Silica," Journal of Applied Physics, **39** (12), 1968, p. 5651-58
2.22 W. Primak, "Fast-Neutron-Induced Changes in Quartz and Vitreous Silica," Physical Review, 110 (6), June 15, 1958, p. 1240-1254
2.23 Evans East, 104 Windsor Center, Suite 101, East Windsor, New Jersey, 08520
2.24 Corning Incorporated, Corning, NY, 14831
2.25 Schott Corporation, 3 Odell Plaza, Yonkers, NY, 10701
2.26 Hoya Corporation, 2-7-5 Naka-Ochiai, Shinjuku-ku, Tokyo 161-8525 Japan

Chapter 3

3.1 J.F. Ziegler, IBM-Research, 28-0, Yorktown, NY, 10598, e-mail: Ziegler@Watson.IBM.Com
3.2 J. Paymal, "Quelques Effets des Réactions (n, alpha) dans les Verres," Verres et Réfractaires, No 5, Sept-Oct 1961, p. 259-269
3.3 ibid, No 6, Nov-Dec, 1961, p. 341-351
3.4 ibid, No 1, Jan-Feb 1962, p.20-30
3.5 ibid, No 2, Mar-Apr 1962, p.100-113
3.6 J. Kenneth Shultis and Richard E. Faw, *Radiation Shielding*, Prentice-Hall, 1996, p. 56
3.7 J.F. Ziegler and J.M. Manoyan,The Stopping of Ions in Compounds, Nuclear Instruments and Methods in Physics Research, **B35** (1988) p. 215-228
3.8 Chr. Lehmann, *Interaction of Radiation with Solids and Elementary Defect Production*, North-Holland, 1977, p. 88
3.9 V. McLane, C.L. Dunford, P.F. Rose, *Neutron Cross Sections, Vol 2, Neutron Cross Section Curves*, National Nuclear Data Center, Brookhaven National Laboratory, Academic Press,Inc., 1981

3.10 J.E. Shelby, "Effect of Radiation on the Physical Properties of Borosilicate Glasses," Journal of Applied Physics, **51** (5), May 1980, p. 2561-2565
3.11 S.F. Mughabghab, M. Divadeenam, N.E. Holden, *Neutron Cross Sections, Vol 1, Neutron Resonance Parameters and Thermal Cross Sections*, National Nuclear Data Center, Brookhaven National Laboratory, , Academic Press, Inc., 1981

Chapter 4

4.1 Far West Technology, Inc., 330 D South Kellog, Goleta, California 93117
4.2 J.H. Hubbell and S.M. Seltzer, "Tables of X-Ray Mass Energy-Absorption Coefficients," NIST Physics Laboratory online database, URL: http://www.physics.nist.gov/PhysRefData/XrayMassCoef/intro.html [cited 12 July 2000]
4.3 T.B. Metcalfe, *Radiation Spectra of Radionuclides*, Noyes Data Corporation, Park Ridge, New Jersey, 1976
4.4 P.R. Bevington, *Data Reduction and Error Analysis in the Physical Sciences*, McGraw-Hill Book Company, New York, 1969, p.313
4.5 J.E. Shelby, "Effect of radiation on the physical properties of borosilicate glasses", Journal of Applied Physics, **51** (5), May 1980, p. 2561-65
4.6 S.L. Conners, "Effects of Gamma Radiation on the Structure and Properties of Borosilicate Glasses", M.S. Thesis, 1992, Alfred University
4.7 S. Sato , H. Furuya, K. Asakura, and K. Ohta, "Radiation Effect of Simulated Waste Glass Irradiated with Ion, Electron, and γ-Ray," Nuclear Instruments and Methods in Physics Research, B1 (1984), p. 534-537
4.8 C. Lehmann, *Interaction of Radiation with Solids*, North-Holland Publishing Company, New York, 1977, p. 90
4.9 N.E. Moyer and R.C. Buschert, "X-Ray Lattice Parameter Studies of Electron-Irradiated Silicon," Radiation Effects in Semiconductors, Plenum, NY, 1968, p. 444-451
4.10 A. Cozma and B. Puers, "Characterization of the electrostatic bonding of silicon and Pyrex glass," Journal of Micromechanical Microengineering, **5** (1995), p. 98-102
4.11 P. Nitzsche, K. Lange, B. Schmidt, S. Grigull, and U. Kreissig, "Ion Drift Processes in Pyrex-Type Alkali-Borosilicate Glass during Anodic Bonding," Journal of the Electrochemical Society, **145** (5), May 1998, p. 1755-1762
4.12 E. Snoeks and A. Polman, "Densification, anisotropic deformation, and plastic flow of SiO_2 during MeV heavy ion irradiation," Applied Physics Letters, **65** (19), November 1994, p. 2487-2489
4.13 S. Klaumünzer, L. Changlin, S. Löffler, M. Rammensee, and G. Schumacher, "Plastic Flow of Vitreous Silica and Pyrex During Bombardment with Fast Heavy Ions," Nuclear Instruments and Methods in Physics Research, **B39** (189), p. 665-669
4.14 S. Klaumünzer, "Ion-Beam-Induced Plastic Deformation: A Universal Phenomenon in Glasses," Radiation Effects and Defects in Solids, 1989, vol. 110, p. 79-83

Chapter 5

5.1 J. Paymal, "Quelques Effets des Réactions (n, alpha) dans les Verres," Verres et Réfractaires, No 5, Sept-Oct 1961, p. 259-269
5.2 ibid, No 6, Nov-Dec, 1961, p. 341-351
5.3 ibid, No 1, Jan-Feb 1962, p.20-30

5.4 ibid, No 2, Mar-Apr 1962, p.100-113
5.5 M.A. Knight, "Glass Densities by Settling Method," The Journal of the American Ceramic Society, **28** (11), Nov 1945, p. 297-302
5.6 J.E. Shelby, "Radiation Effects in Hydrogen-Impregnated Vitreous Silica," Journal of Applied Physics, **51** (5), May 1980, p. 2561-2565
5.7 S.L. Conners, "Effects of Gamma Radiation on the Structure and Properties of Borosilicate Glasses," M.S. Thesis, 1992, Alfred University
5.8 S. Sato, "Radiation Effect of Simulated Waste Glass Irradiated with Ion, Electron, and γ-Ray," Nuclear Instruments and Methods in Physics Research, **B1** (1984), p. 534-537
5.9 W.A. Zdaniewski, T.E. Easler, and R.C. Bradt, "Gamma Radiation Effects of the Strength of a Borosilicate Glass," Journal of the American Ceramic Society, **66** (5), May 1983, p. 311-313
5.10 J.E. Shelby, "Effect of radiation on the physical properties of borosilicate glasses," Journal of Applied Physics, **51** (5), May 1980, p. 2561-65
5.11 P.R. Bevington, *Data Reduction and Error Analysis for the Physical Sciences*, McGraw-Hill Book Company, New York, 1969, p. 73

Chapter 6

6.1 J. Paymal, "Quelques Effets des Réactions (n, alpha) dans les Verres," Verres et Réfractaires, No 5, Sept-Oct 1961, p. 259-269
6.2 ibid, No 6, Nov-Dec, 1961, p. 341-351
6.3 ibid, No 1, Jan-Feb 1962, p.20-30
6.4 ibid, No 2, Mar-Apr 1962, p.100-113

Chapter 7

7.1 C.A. Volkert and A. Polman, "Radiation-Enhanced Plastic Flow of Covalent Materials During Ion Irradiation," Materials Research Society Symposium Proceedings, **235**, 1992, p. 3-14